Available online at www.sciencedirect.com
ScienceDirect
Earth and Planetary Science Letters 257 (2007) 200–214
EPSL
www.elsevier.com/locate/epsl

Upper mantle flow in the western Mediterranean

Giuliano F. Panza [a,b,*], Reneta B. Raykova [c,1], Eugenio Carminati [d], Carlo Doglioni [d]

[a] Dipartimento di Scienze della Terra, Università degli Studi di Trieste, Via E. Weiss 4, 34127 Trieste, Italy
[b] The Abdus Salam International Centre for Theoretical Physics, Earth System Physics Section, strada Costiera 11, 34014 Trieste, Italy
[c] Geophysical Institute of BAS, Acad. G. Bonchev str. blok 3, 1113 Sofia, Bulgaria
[d] Dipartimento di Scienze della Terra, Università La Sapienza, P.le Aldo Moro 5, 00185 Roma, Italy

Received 20 July 2006; received in revised form 18 January 2007; accepted 18 February 2007
Available online 27 February 2007
Editor: R.D. van der Hilst

Abstract

Two cross-sections of the western Mediterranean Neogene-to-present back-arc basin are presented, in which geological and geophysical data of the TRANSMED Project are tied to a new shear-wave tomography. Major results are i) the presence of a well stratified upper mantle beneath the older African continent, with a marked low-velocity layer between 130–200 km of depth; ii) the dilution of this layer within the younger western Mediterranean back-arc basin to the north, and iii) the easterly raising of a shallower low-velocity layer from about 140 km to about 30 km in the Tyrrhenian active part of the back-arc basin. These findings suggest upper mantle circulation in the western Mediterranean back-arc basin, mostly easterly-directed and affecting the boundary between upper asthenosphere (LVZ) and lower asthenosphere, which undulates between about 180 km and 280 km.

Keywords: shear-wave velocity model; back-arc basin; mantle flow; Mediterranean geodynamics; mantle stratification

1. Introduction

There usually is a gap between surface geology and mantle tomography. Since the Mediterranean is one of the most studied areas in the world, we try to integrate the deep structure of the Mediterranean along two TRANSMED sections [1], i.e., II [2] and III [3] (Fig. 1). The Mediterranean has been shaped by a number of subduction zones since the Cretaceous, where segments of the Tethyan oceanic or thinned continental lithosphere have been recycled into the mantle. The present geodynamic setting is characterized by the widespread Neogene-to-Present back-arc basin in the western Mediterranean in the hanging-wall of the westerly-directed Apennines–Maghrebides subduction, and the northeasterly directed Dinaric–Hellenic subduction in the eastern Mediterranean. In this study we focus mainly on the western side of the basin, comparing superficial geological and geophysical constraints (Figs. 4a and 5a) with a new shear-wave tomography of the area (Figs. 4b and 5b).

The back-arc spreading in the western Mediterranean developed since 30 Ma and gradually shifted from west to east, moving from the Provençal, Valencia and Alboran basins, to the Algerian and Tyrrhenian basins,

* Corresponding author. Dipartimento di Scienze della Terra, Università degli Studi di Trieste, Via E. Weiss 4, 34127 Trieste, Italy. Tel.: +39 040 5582117; fax: +39 040 5582111.
E-mail addresses: panza@dst.units.it (G.F. Panza), rraykova@geophys.bas.bg, rraykova@bo.ingv.it (R.B. Raykova), eugenio.carminati@uniroma1.it (E. Carminati), carlo.doglioni@uniroma.it (C. Doglioni).
[1] At present: Istituto Nazionale di Geofisica e Vulcanologia-sezione Bologna, Via D. Creti 12, 40128 Bologna, Italy.

0012-821X/$ - see front matter © 2007 Elsevier B.V. All rights reserved.
doi:10.1016/j.epsl.2007.02.032

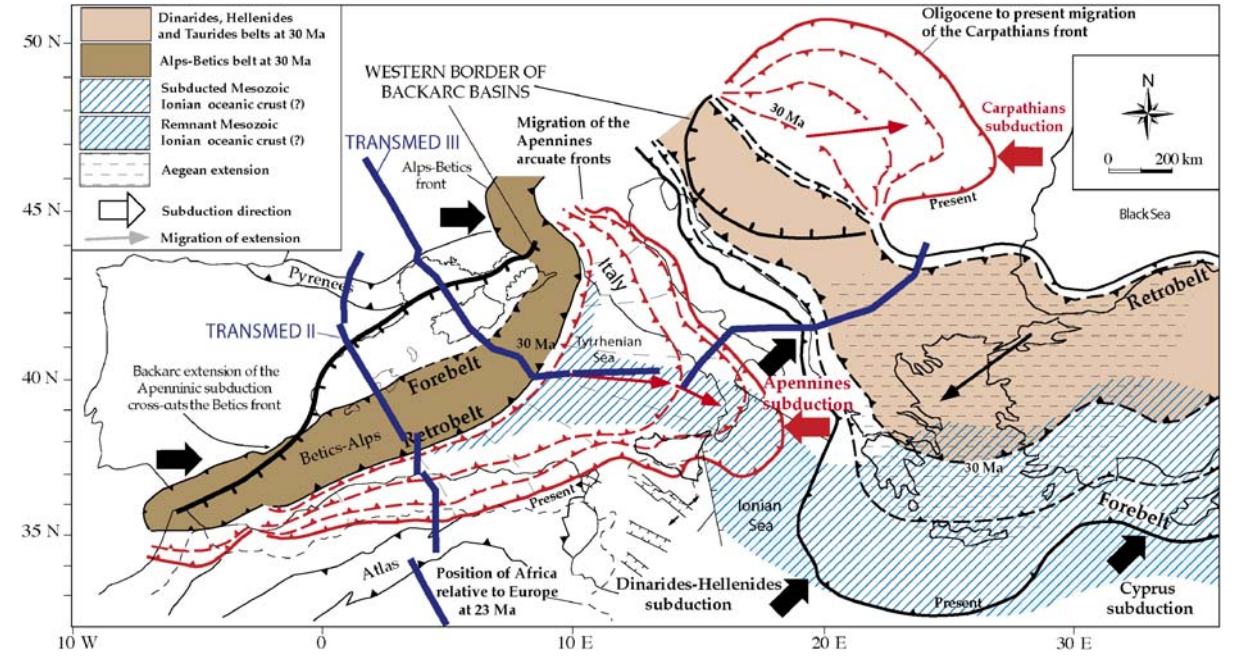

Fig. 1. Simplified tectonic map of the western–central Mediterranean and adjoining regions (after [5]). The positions through time of the subduction zones active in the last 45 Ma are shown. The position of the geological and tomographic transects discussed in the paper are shown as well.

[e.g., 4,5]. The rifting accompanied the "eastward" retreat of the subduction zone, and the slab retreat kinematically requires a contemporaneous "eastward" mantle flow, regardless this is the cause or a consequence of the retreat [6]. However a number of controversies still exist in the geodynamic reconstruction of this area.

We contribute to this debate with a set of shear-wave velocity (V_s) models of the lithosphere–asthenosphere system along the two sections. The two sections run respectively from south France, through Pyrenees, Valencia basin, to north Algeria into the Sahara platform (II), and from central France, through the Gulf of Lion, Sardinia, southern Apennines, Albania, Balkans and the Moesian platform in Bulgaria (III) (Figs. 4a and 5a).

The V_s structure of the very upper mantle, in the central western Mediterranean, is obtained by non-linear inversion of surface waves dispersion curves obtained from a tomographic analysis of regional and global dispersion data. The local dispersion curves are assembled in the period range 5–150 s, combining regional group velocity measurements and published Rayleigh wave dispersion data. The resolution of the tomography data is improved using a priori information about the shallow crustal velocity structure. Local Smoothness Optimization (LSO) is applied to select the representative cellular structures and the three-dimensional model. The lithosphere–asthenosphere velocity structure is reliably reconstructed to depths of about 300 km and highlights some new features along the TRANSMED sections, which largely fit the superficial information.

The comparison of the superficial geological and geophysical constraints with the new V_s tomography of the area results is a new model of the mantle flow in a back-arc setting.

2. Evolution of the Western Central Mediterranean and of the Balkan area

Although a detailed analysis of the tectonic and geodynamic evolution of the area is beyond the scope of this paper, a brief description of the evolution sketched in Fig. 1 will be provided. For a more complete discussion the reader is referred to [2,3,4,7].

Traces of pre-Cenozoic deformations are widespread in the Western–Central Mediterranean area and adjoining regions. However, the present crustal and lithospheric geometry of the region developed mostly since the Cenozoic. For this reason the description of the evolution will range from Eocene to Recent times.

Paleomagnetic studies [8] evidenced an anticlockwise rotation of the Corsica–Sardinia block between 19 Ma and 16 Ma (Burdigalian). In the Middle Eocene (45 Ma), after the restoration of the Corsica–Sardinia block at their position prior to rotation, the Alps were probably linked to the Betics through Alpine Corsica

and the Balearic promontory to form a double vergent belt related to a south-eastward subduction of Neotethyan oceanic and European continental lithosphere underneath an intervening microplate between the European and African plates [6]. Contemporaneous shortening occurred in the Pyrenees (until ~24.7 Ma according to a magnetostratigraphic study [9]) driving to the complete inversion of a basin intervening between Iberia and Eurasia.

At about 30 Ma ago, the west directed Apennines–Maghrebides subduction started, nucleating along the Alps–Betics retrobelt and possibly triggered by the occurrence, in the foreland east of the Alpine belt, of oceanic or thinned continental lithosphere [6].

The Apennines–Maghrebides subduction zone was characterized, since the beginning, by fast radial eastward rollback, as evidenced by the migration of the subduction related calkalcaline volcanism and of the compressional front which induced widespread extensional tectonics accompanied by alkaline volcanism in the backarc (Gulf of Lions and Provençal Basin, in the Catalan Coastal Ranges area, in Sardinia, still attached to Iberia, in the Valencia trough and in the Algerian Basin). In the Provençal and in the Algerian Basins, continental crust stretching evolved into oceanization in the Lower–Middle (?) Miocene, coeval with the counter-clockwise rotation of the Corsica–Sardinia block. Large portions of the Alps–Betics orogen located in the back-arc area were disarticulated and spread-out into the western Mediterranean (e.g., the metamorphic slices of Kabylie in northern Algeria, and Calabria in southern Italy). The Apennines and Maghrebides fold-and-thrust belt developed on top of the retreating subduction and the deformation front migrated to the east in the Apennines and to the South in the Maghrebides, following the slab roll-back [10]. It has been proposed that, in the Langhian, continental collision was followed by slab breakoff along the northern African margin, as suggested by tomographic models, by the occurrence of bimodal volcanism and by uplift along the African margin [7]. This hypothesis was accepted by [2] and no subducting slab is imaged beneath northern Africa in the TRANSMED II section. However, along this section, the slab could alternatively be missing because stretched and shifted eastward during the rollback.

A shift of active extension from west to east of Sardinia occurred in the Langhian (ca. 15 Ma) as testified by the Middle Miocene to present opening of the Tyrrhenian Basin.

The extension affecting most of the western Mediterranean in the Tertiary developed in a context of relative convergence between Africa and Europe. However, the maximum amount of N–S Africa/Europe relative motion in the last 23 Ma was about 135 km at the Tunisia longitude, whereas the eastward migration of the Apennines arc exceeded 700 km during the same time span (Fig. 1). As a consequence, the eastward migration of the Apennines–Maghrebides arc cannot be considered as a consequence of the relative N–S Africa/Europe convergence but it is rather a consequence of the Apennines–Maghrebides subduction rollback [6].

The Balkan area is characterized by the occurrence of a polyphased orogenic belt named differently in different areas: Dinarides, Hellenides and Taurides. This double vergence orogen is the result of at least two or three subduction zones since Mesozoic times, as testified by the occurrence of two distinct oceanic sutures (Vardar and Sub-Pelagonian ophiolites), representing one or two (contrasting reconstructions) branches of the Mesozoic Tethyan ocean, plus the oceanic part of the present day subduction of the Ionian Sea. In the Vardar ocean, the northeast-directed subduction is dated Jurassic–Early Cretaceous and deformation did not significantly involve the shelf margin of the Adriatic plate. The east-northeast dipping subduction of the Adriatic lithosphere beneath the Dinarides started in the Mesozoic and in the Cenozoic it became the main process acting in the area. The main structuration of the Dinarides occurred progressively from the latest Maastrichtian, with climax between the Oligocene and earliest Miocene.

3. The geological cross-sections

3.1. Sources of information

A detailed description of sources of information used to constrain the geological sections of Figs. 4a and 5a is in [2,3]; we summarize in the following the data used to constrain only the geometry of the base of crust and lithosphere, since these are the main features that can be compared with tomographic data. Extended references are given in [2,3].

3.1.1. TRANSMED II section

In the Aquitaine Basin–Pyrenees and in the Ebro basin–Catalan Coastal Ranges, the crustal geometry was constrained by the ECORS-Central Pyrenees deep seismic reflection profile [11] and by the ESCI-Catalanides deep seismic reflection profile [12] respectively and by refraction and gravimetric data, e.g. [13], by wide-angle reflection data [14], by magnetotelluric modelling [15] as well as by seismic tomography data [16]. The lithosphere–asthenosphere boundary was

drawn from integrated lithospheric models combining topography, gravity, and heat flow [17].

In the València Trough and Balearic promontory, the Moho depth was based on the interpretation of the ESCI-València trough deep seismic reflection profile [14] but regional refraction and gravimetric data [12,13] were also taken in account. The lithospheric mantle thickness was derived from both gravimetric and geoid anomaly models [18] and from the integrated model of [17] and from an integrated model by [2].

The oceanic nature of the Algerian Basin crust and its thickness were constrained by seismic refraction results [19] and by aeromagnetic data [20]. The lithosphere–asthenosphere boundary was calculated specifically for the TRANSMED Project [2] by integrated lithospheric modeling combining thermal, gravity, and local isostasy analysis.

In the Kabylies–Tell–Atlas and in the Saharan portions of the transect, the Moho depth was drawn according to the results of gravity models [21] whereas the lithospheric thickness and geometry was based on an original integrated model [2].

3.1.2. TRANSMED III section

In the Massif Central, the Moho was drawn from refraction data [22], while lithospheric geometries were based on tomography results [23] and on the results of mantle thermal modelling [24]. The structure of the Moho below the Gulf of Lion platform and slope was based on deep seismic reflection data [25] and gravity modelling [26].

In the Provençal Basin and in the western continental shelf of Sardinia, the Moho depth was mainly based on the ECORS and CROP deep seismic reflection profiles [27] and by seismic refraction results [25]. The base of the lithosphere was drawn from the gravity models of [28].

Below Sardinia, Moho depth and lithospheric thickness were drawn according to the results of [29,30] and on the results of the European Geotraverse project [31]. The asymmetric lithosphere boundary under Sardinia was based on the gravity modelling of [28].

In the Tyrrhenian Sea, the depth of the Moho was derived from [29] partly modified by Carrara (2002, unpublished results), while the geometry of the lithosphere–asthenosphere boundary was based on the models of [30,32].

In the continental Italy and Adriatic portions of the transect, running through the southern Apennines and the Apulian foreland, the geometry of the Moho and of the lithosphere–asthenosphere boundary was based on the studies of [29,30,32]. The location of the Apenninic subducting slab (subcrustal seismicity is rare), constrained by the studies of [33,34], is consistent with the occurrence of positive Bouguer anomalies (up to 120 mGal or more [35]) and very high heat flow values (up to 140 mW/m^2 or more [36]) along the Tyrrhenian margin and in the adjacent Tyrrhenian Sea. Moreover, the occurrence of hot asthenospheric material at relatively shallow depth below the western portion of the Southern Apennines is consistent with shear waves attenuation [37] and geochemical studies [38].

Below the Albanian Dinarides, the Moho depth was constrained by gravimetric data [39]. The geometry of the slab subducting beneath Albania (subcrustal seismicity is also absent) was constrained by tomographic studies showing a clear and fast velocity body (interpreted as the evidence of the active subduction process) under the Albanian Dinarides [40].

Below the Macedonian Balkanides, the depth of Moho discontinuity was both based on two deep seismic profiles and on magnetic [41] and gravity [42] models. More to the east, in the Bulgarian Balkanides and in the Moesian platform, the Moho discontinuity and the base of the lithosphere were deduced from gravimetric and seismic data [43,44].

3.2. Description of the geological cross-sections

3.2.1. TRANSMED II section

In its northernmost part, the transect crosses the northern foreland basin of the Pyrenees (the Aquitaine basin), which rests on a 35 km thick crust and 110 km thick lithosphere. More to the south, the Pyrenees, an orogenic belt which developed between the late Senonian (Late Cretaceous) and the mid-Oligocene times, characterized by a doubling of the crust which reaches depths of 70 km, whereas the base of the lithosphere is at 150 km. To the south, the crust and the lithospheric mantle (LID) gradually thin reaching below the southern foreland basin of the Pyrenees (the Ebro basin) thicknesses comparable to those of the Aquitaine basin.

The continental crust and the LID continue to thin below the Catalan Coastal Ranges, reaching minimum values (of 15–20 and 55 km respectively) below the Valencia trough, an extensional basin developed during the Oligocene–Lower Miocene. The Valencia trough is bordered to the south by the Balearic Promontory, characterized in the Tertiary by both compressional and extensional tectonics [45] and underlined by relatively thicker continental crust (25 km) and lithosphere (90 km).

South of the Balearic Islands the lithosphere thins quite abruptly, leading to the Algerian basin [46], a Miocene basin floored by 10 km thick oceanic crust and 50 km thick lithosphere. The crust and lithosphere thicken again rather continuously below northern Africa where the transect crosses the Tell–Maghrebides fold-and-thrust belt and reach maximum thicknesses of 40 km and 170–180 km, respectively, below the Sahara Atlas (an intraplate right-lateral transpressive inversion structure) and the Saharan platform.

3.2.2. TRANSMED III section

At its northwestern end the section crosses the French Massif Central, where 30 km continental crust deformed during the Variscan orogeny outcrop. The lithospheric base, generally around 80–90 km deep, is interpreted to be much shallower (around 50 km) below the Cenozoic Massif Central alkaline volcanic province. Since the crust is not thinned accordingly, the volcanism and the asthenosphere upwelling are interpreted in literature as a thermal effect due to the upwelling of a mantle plume [23], but its deep origin is still under debate.

The continental crust and lithosphere thin first progressively below the Gulf of Lions continental margin, and then abruptly below the Provençal Basin, floored by Neogene oceanic crust, where they reach thicknesses of 10–15 km and 25 km, respectively. A rather progressive increase of crustal and lithospheric thickness occurs below the thinned continental lithosphere of the western Sardinia margin and below the continental swell of the Corsica–Sardinia block, which was structured during the Variscan and older orogenic cycles, and was later dissected by Neogene–Quaternary extensional tectonics. The Sardinia crust and lithosphere have maximum thicknesses of 30 and 70 km, respectively. Gravity modelling [28,47] suggests an asymmetric morphology of the lithospheric roots across Sardinia. Maximum lithospheric thicknesses are shifted to the east with respect to highest topography. Below the western Sardinian margin the increase of the lithospheric thickness toward the centre of the Island is less abrupt than below the eastern Sardinia margin.

East of Sardinia the lithosphere thins again progressively, reaching its minimum thicknesses (less than 20 km) in the Tyrrhenian Sea, a basin partly floored by oceanic crust formed mainly from the Tortonian to the Present. Farther east (crossing the Campania continental margin) the crust and lithosphere gradually thicken, reaching thicknesses of 30 km and 40 km, respectively, below the Southern Apennines, a Neogene fold-and-thrust belt, dissected by Late Neogene to Present extensional tectonics. This belt developed in the hanging-wall of a west-directed subduction zone, where the, up to 80–100 km thick, continental lithosphere of the Adriatic microplate steeply sinks to the west.

To the east, the Apennines foreland (partly in continental Italy and partly in the southern Adriatic Sea) rests on the about 100 km thick continental lithosphere of the Adriatic microplate, thinned during the Mesozoic rifting. The crustal thickness is around 30 km. In the eastern southern Adriatic Sea, the transect crosses the foreland basin of the Albanian Dinarides, an orogen associated with the east-northeastward subduction of the Adriatic lithosphere. Due to subduction related flexure, the base of crust and lithosphere reach depths of 40 km and 120 km below the foreland basin and even deeper depths below the Dinarides. Further to the east, the complex multistage Dinarides–Hellenides orogen is crossed together with its conjugate retrobelt, i.e., the Balkans. The transect ends in the Moesian platform, which is the undeformed foreland of the Balkans. The whole region was affected by Eocene and Neogene-to-Present extensional tectonics. In these areas the lithosphere is continental and generally thickened (about 40 km thick crust and 120–130 km thick lithosphere), but local thinning occurs in correspondence of the Sofia graben.

4. The seismic cross-sections

4.1. Seismic data processing and methods

This study is a part of a series of regional tomography investigations made in the Mediterranean area [34,48,49,50] (unpublished results of Raykova, 2004 and Farina, 2006). We use surface waves since, in the period range considered (about 5–150 s), they sample the elastic properties of the crust and upper mantle and this kind of waves is particularly suitable to investigate regions where a velocity inversion (decrement of velocity with increasing depth) can be present. The regionalization of the dispersion of surface waves by 2D tomography and the inversion of local dispersion curves by non-linear “hedgehog” method, taking into account the detailed information available about the structure of the upper layers of the crust, is a very perspective procedure to obtain high-resolution shear-wave velocity models, and their uncertainties, of the crust and upper mantle. Our model supplies a due revision of the results by [51] who have produced a tomographic S-wave model for the same region that is biased by a methodological problem, discussed in detail by [52].

All relevant group velocity measurements available in the literature for different study areas, like Spain [53], Italy [32,49], Greece [54], Alps [55], and Balkan

Peninsula [50,56], have been considered. In addition many pertinent seismic records from VBB and BB stations available on-line at data centres as IRIS (www.iris.washington.edu), ORFEUS (orfeus.knmi.nl), GEOFON (www.gfz-potsdam.de/geofon), GEOSCOPE (www.geoscope.ipgp.jussieu.fr), MEDNET (mednet.ingv.it), GRNS (www.szgrf.brg.de), and CRSN (www.ig.ca.cz) have been processed. The hypocentre information for the analysed events is taken from on-line bulletins of NEIC (neic.usgs.gov) and ISC (www.isc.ac.uk). The location of stations and earthquake epicentres are selected in order to have as homogenous as possible path coverage of the area under investigation. The length of paths-considered does not exceed 2500 km in order to have as much as possible usable measurements of group velocity at short periods. The regional group velocity measurements of Rayleigh wave fundamental mode are obtained by frequency–time analysis (FTAN) [57] (and references therein). More than 1000 records are analysed to assemble the data set of about 800 dispersion curves, which ensures, in the period range from 5–10 to 50–80 s, a relatively good coverage of the study region. One example of such measurements by FTAN is given in Fig. 2.

To increase the penetration depth of the inverted data set we consider published phase velocity measurements (extended references can be found in [49,53,58]) for Rayleigh waves with periods from about 15–20 s to about 150 s.

A surface-wave tomography method [59,60] is applied to estimate lateral variations in group- and phase-velocities at properly chosen set of periods (5–80 s for group velocities and 15–150 s for phase velocities). The method also evaluates the resolution of the data, defined as the average size of the equivalent smoothing area and its elongation [60] and hence it is not necessary to perform check board or similar tests. The results of tomography (path, group-velocity and resolution distributions) for Rayleigh wave fundamental mode, at a period of 20 s, is shown in Fig. 3. The lateral resolution of our tomography varies between 120 km (periods from 15 to 25 s) to about 400 km (periods from 50 to 80 s) for group velocities and between about 200 km (periods from 20–35 s) to about 600 km for phase velocities (periods from 100 to 150 s). The resolution of dispersion measurements is only indirectly connected with the lateral variations of the structural models and areas with similar dispersion properties do not necessarily have laterally homogeneous structures. Therefore the introduction of a priori independent information about the crustal parameters [58,61] significantly improves the resolving power of the tomography data also at mantle depths, even if some smearing cannot be excluded at the greatest depths.

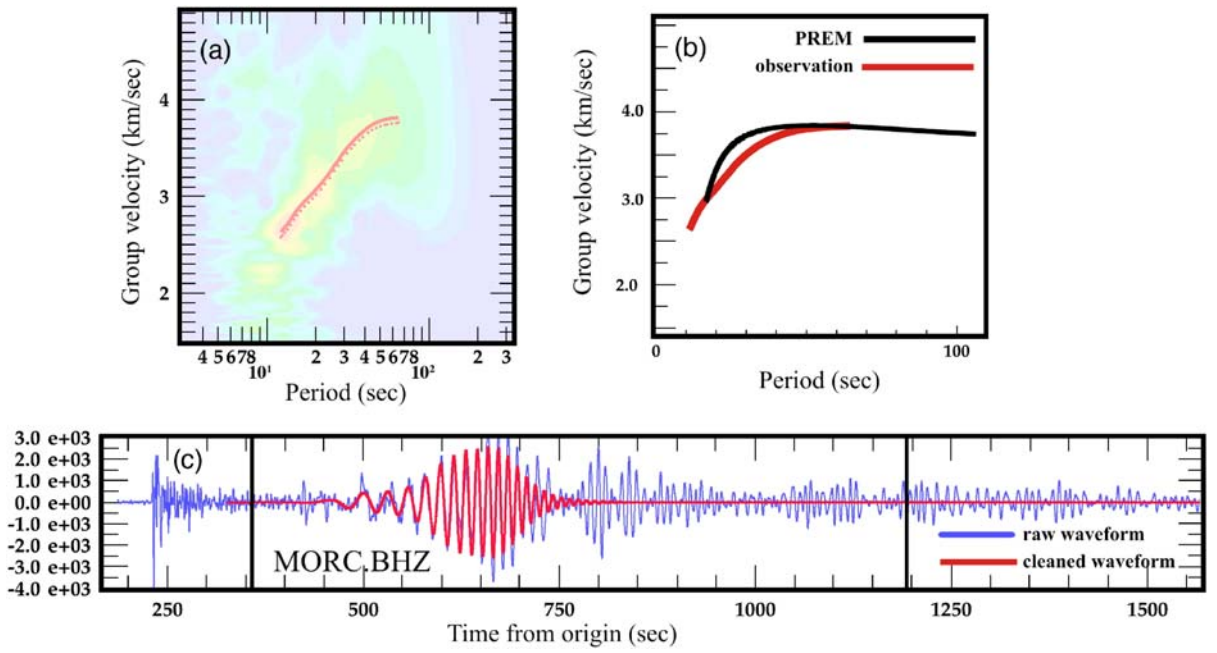

Fig. 2. Example of FTAN analysis of a seismogram recorded at station MORC (CZ) for an earthquake that occurred in Algeria (36.6° N 4.77° E10, November 2000, mb magnitude 5.8 by ISC): (a) FTAN diagram of the "raw" waveform; (b) comparison between observed (red line) and predicted by PREM model (black line) group velocity dispersion curve of the Rayleigh wave; (c) comparison between raw waveform (blue line) and extracted waveform of fundamental Rayleigh wave (red line), which corresponds to the dispersion curve that will be used in the 2D tomography.

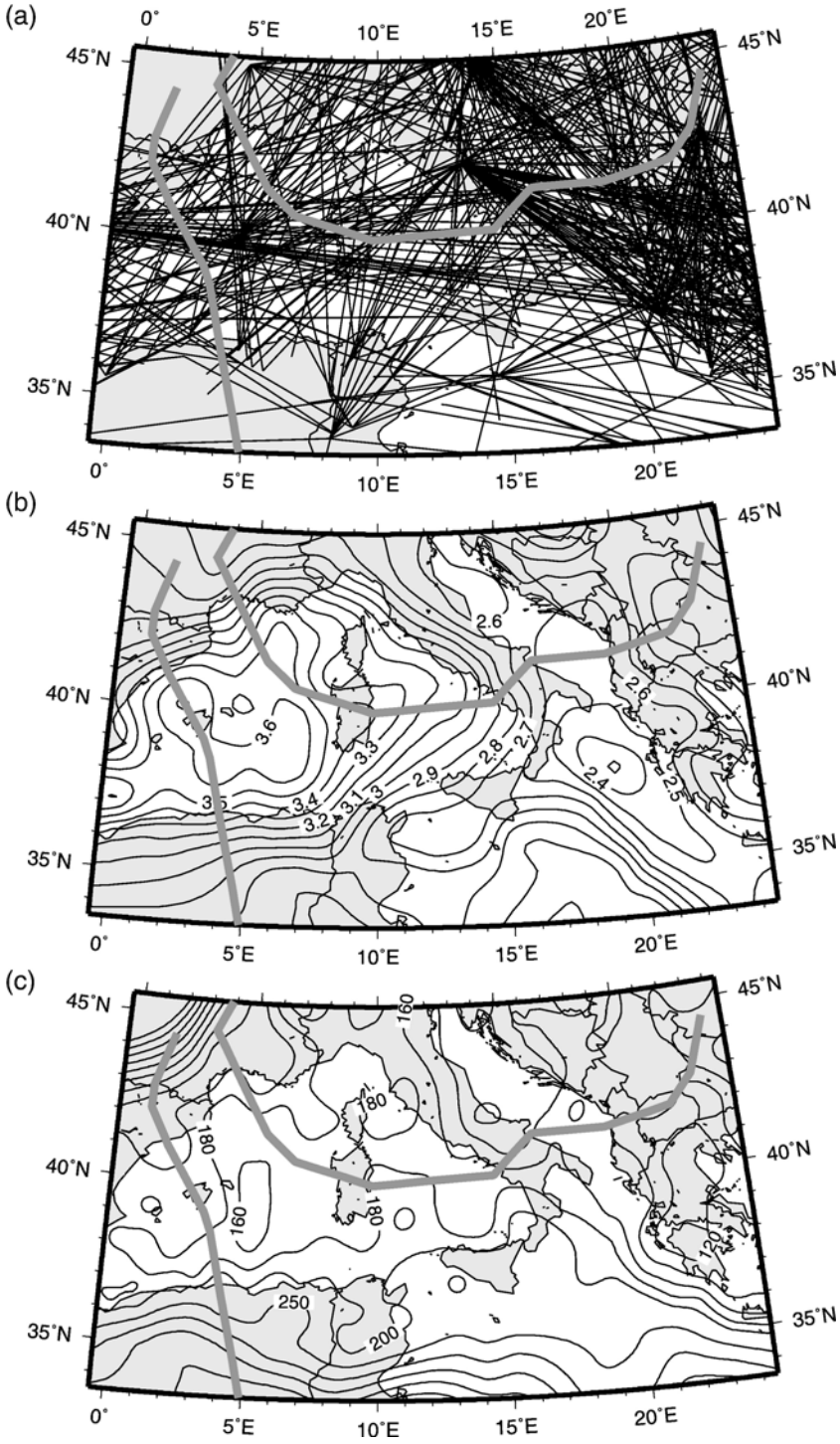

Fig. 3. Results of Rayleigh waves tomography for period 20 s: (a) station-to-epicentre paths; (b) group velocity distribution in km/s; (c) data resolution distribution as mean size of averaging area in km. TRANSMED II and TRANSMED III are denoted by thick grey lines.

The local values of group and phase velocity are calculated on a predetermined grid of $1° \times 1°$, according to the lateral resolution of our data set and a priori independent constraints deduced from existing literature. The local dispersion curves are assembled at each grid point and group velocity dispersion curves are

extended to 150 s, using data from global studies [62]. The cellular dispersion curve is calculated as the average of the local curves at the four corner grid points of each cell, and the standard deviation at selected periods is estimated. The period range of the cellular dispersion curve varies according to data coverage and resolution at the specified period.

We make an inversion of the dispersion data for 15 cells along TRANSMED II and 28 cells along TRANSMED III.

From the cellular dispersion curves, V_s models are retrieved employing the non-linear inversion method known as "hedgehog" [63] (and references therein). One of the key parameters in the inversion is the absolute value of the single point error at each specified period and the r.m.s. value for the whole dispersion curve, estimated as 65% of average single error determined for all selected periods [48,49]. The value of the group velocity at 80 s is calculated as an average between our tomography results and data from published global tomography [62] with resulting average standard deviation of 0.03 km/s. In order to optimize the horizontal resolution of the data, the physical properties of the layers down to depths of about 6–8 km are fixed according to a priori and independent information, wherever it is available, like seismic, geophysical and geological data, derived from previous studies in the region. When the cell is located in a sea region, the thickness of the water layer is defined (data from NGDC, www.ngdc.noaa.gov) as a weighted average of all bathymetric measurements inside the area of the cell. The thickness of the sediments is defined, in a similar way, from the map of [64] or the data in [65]. The properties of the remaining upper crustal layers are taken from published information and some extended references are given in [32,48,49,50,53,56]. This information is used also in the parameterization of the velocity structures (such as range of the Moho depth, range of the shear-wave velocity in crustal and mantle layers) in the depth range from 6–8 km to 350 km, in agreement with the vertical sensitivity of our data set, estimated from the depth distribution of the partial derivative [66] of the group and phase velocity curves with respect to V_s. The deeper structure is fixed accordingly with the model published in [67].

For each cell, because of the well-known non-uniqueness of the inverse problem, a set of models fits the dispersion data, all with similar levels of reliability. The tested model is accepted as a solution if the differences of the measured and theoretical velocity values are less than the single error at specified periods and the r.m.s. value for the whole dispersion curve. The inversion procedure tests about 30 000 models per cell and, on average, 10 structures are accepted as the cellular solutions.

An optimized smoothing method [48,49] (Farina, 2006, unpublished results) is used to define the representative cellular model by a formalized criterion, based on operational research theory [68,69]. LSO fixes the cellular model as the one that has minimal divergence in velocity between neighbouring cells [48].

The models selected by LSO are appraised according to known geophysical constraints, since the non-linear inversion and the smoothing algorithm give us only a mathematical solution. The results of the non-linear inversion and LSO are shown in Figs. 4b and 5b as a mosaic of the chosen models in each cell: the value of V_s is colour coded for easier visualization of the velocity structure. The range of variability of the interfaces (the boundaries between layers can well be transition zones in their own right) and the velocity and its range of variability is given for most of the parameterized layers (some values are omitted for graphical reasons).

4.2. Description of the tomographic cross-sections

The V_s structure along TRANSMED sections II and III is shown in Figs. 4b and 5b, where the regional seismicity (International Seismological Centre, on-line bulletin from 1904 to 2004, $M \geq 3.0$) is plotted as dots. The main features of the cross-sections can be summarized as follows.

4.2.1. TRANSMED II section

Cells from 1 to 5 have a typical continental structure with the average velocity in the mantle about 4.35–4.40 km/s; the structure of cell 6 corresponds to the rift zone in the region, the velocity in the mantle varies slowly down to about 200 km of depth and it is relatively low (4.25–4.35 km/s); the cell 10 (central Algerian basin) with thin lid (15–20 km) and low velocity asthenosphere (4.10–4.15 km/s) has an oceanic signature; cells 7 in the Valencia trough and 11 in the southern Algerian basin have transitional character, suggesting to be thin continental lithosphere; the lid under Balearic islands is thin and fast (10–15 km and velocity 4.70–4.80 km/s) the lithosphere beneath north Africa is faster than in the Mediterranean (4.40–4.55 km/s), and its thickness is about 120 km; there is a large contrast in lithospheric thickness (between cells 11 and 12) in north Africa; in the cells 12 to 15 the thick lid is overlying a very low velocity zone that evidences the presence of a well-developed asthenospheric channel; there is no striking evidence for a continuous

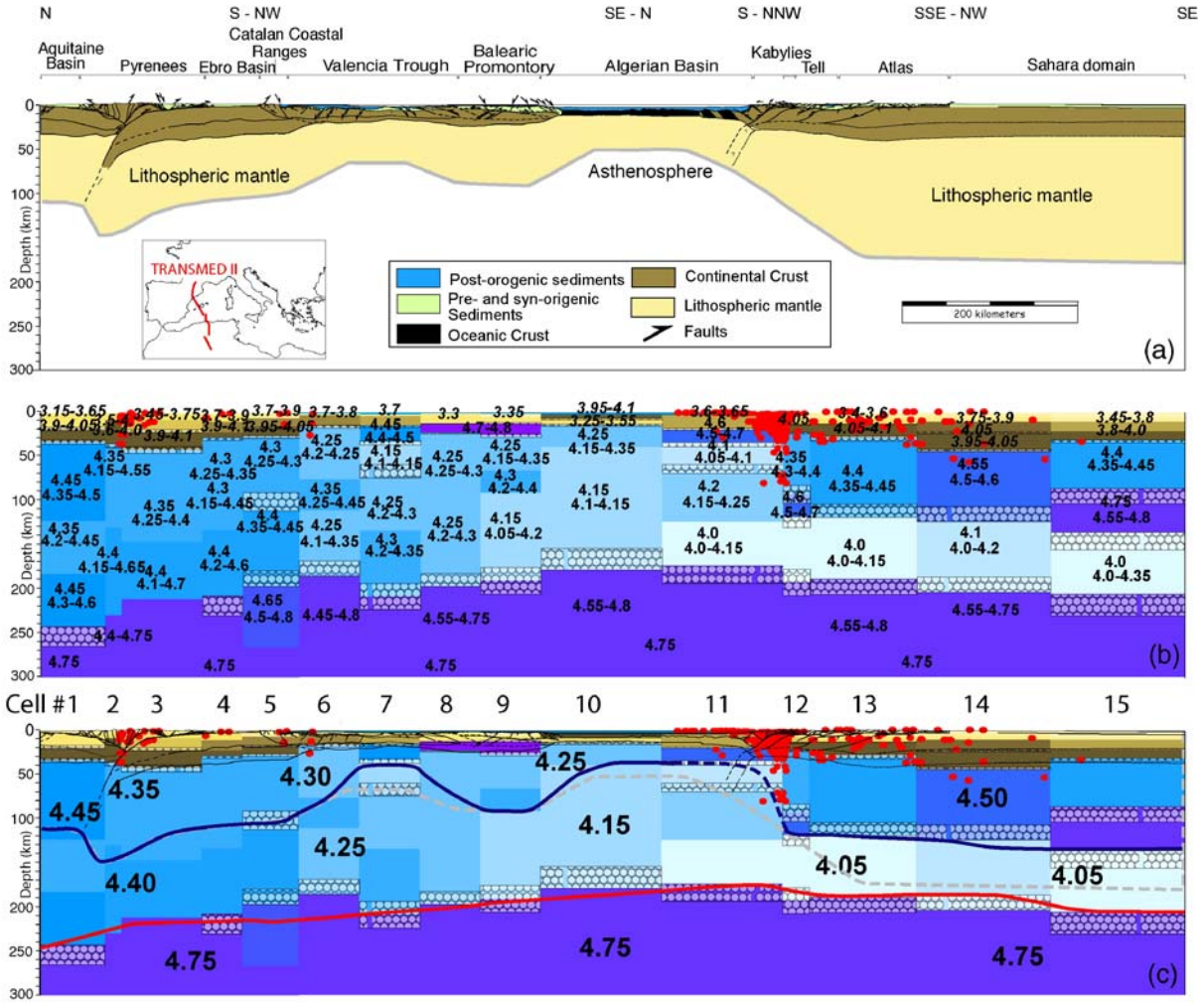

Fig. 4. (a) Lithospheric scale cross-sections simplified and redrawn from the TRANSMED II geotraverse [2]. (b) Lithosphere–asthenosphere system along the trace of the TRANSMED II geotraverse: the tomographic cross-section was obtained from selected solutions and related seismicity (body waves magnitude greater or equal to 3.0). The chosen shear velocity and its range of variability in km/s are printed on each layer. When the velocity ranges of vertically adjacent layers do not overlap, a hatched rectangle outlines the range of variability of their thicknesses. Numbers in *Italic* denote the velocities in the crustal layers. The hypocentres are denoted by red dots. (c) Overlap between the TRANSMED II regional cross-sections and the V_s tomography; only a few average representative values of V_s are reported to avoid overcrowding of characters; the dashed line reproduces the lithosphere–asthenosphere boundary given in part (a), while the new geometry of the base of the lithosphere (blue) and of the limit between upper and lower asthenosphere (red) are shown by continuous lines. A well-developed low velocity layer under Africa is visible to the right.

slab below northern Africa for depths greater than 100–120 km.

4.2.2. TRANSMED III section

Cells 1 and 2 have thick lithosphere with respect to the next cells: about 200 km with V_s velocity 4.40–4.50 km/s; the cells from 1 to 4 have higher velocities in the mantle with respect to the following cells and represent the NW continental part of the section; it is clearly visible in a low velocity channel under all the Mediterranean from cell 5 to cell 18, at depths from 20 km to about 150 km; in the cell 16 a low velocity hot mantle reservoir is well visible, that can be interpreted as the shallow asthenosphere in the back-arc basin, and sourcing the oceanic crust flooring the Tyrrhenian basin; there is no evidence for deep hot mantle plume under the Tyrrhenian sea; the mantle, consistent with the presence of a continental lithosphere under cells 20, 21, and 22, is quite different from that of North Africa, as seen along TRANSMED II in cells from 11 to 15 (Fig. 4); in cell 23, more or less coincident with a local maximum of the heat flow (85 kW/m^2 and more in [70]), there is a relatively low velocity layer centred at about 100 km of depth, very likely a remnant of the Mesozoic rifting; in

cells from 24 to 28 the velocity inversion in the upper mantle is very gentle if not absent and they are consistent with a continental structure, where the lithosphere is quite thick. Seismicity and high velocities correlate quite well in the Apennines and in the Dinaric subduction zone.

5. Discussion

The new tomography highlights several important issues: i) the African lithosphere, shows a well-developed, about 50–70 km thick, sandwiched low-velocity layer (4.0–4.3 km/s) between 120–200 km of depth (Fig. 4); ii) this layer, that seems to be a general feature of the North-Central Pan–African Orogenic block [71], is missing or diluted within the back-arc basin to the north, where the fast African lid (4.4–4.6 km/s, cells 13 to 15, Fig. 4) is missing, and V_s spreads in the range 4.1–4.3 km/s in the Algerian basin (cells 10–11) and iii) the recent easternmost back-arc basin, i.e., the Tyrrhenian sea, is characterized by sub-Moho V_s as low as 3.85 km/s (Fig. 5); this low velocity layer raises from west to east from a depth of about 60 km–100 km (cells 5 to 13, Fig. 5) to about 25 km–30 km (cell 16, Fig. 5), where it matches with the northern prolongation of the Marsili basin, which is one of the easternmost active parts of the back-arc spreading and it is characterized by even lower velocities [34,49]. These anomalously low velocities can be even smaller in the north–south direction if the east–west anisotropy inferred by [72,73] is taken into account.

In cell 16 (Ischia–Neaples), the crust–mantle transition is rather complex and seems to be consistent with a lithospheric doubling where the deeper Moho is at about 20 km and sits on soft mantle, or with the presence of a shallow layer of consolidated magma reservoir. Alternatively the crust–mantle transition can be very shallow, with a ~7 km thick crust overlying a ~5 km thick mantle layer, with V_s around 4.40 km/s, sitting on a ~10 km thick very low-velocity mantle, with V_s around 3.50 km/s, or a thin continental crust is intruded by a 5 km thick layer of consolidated magma. The former interpretation turns out to be consistent with long wavelength Bouguer anomaly modelling [49].

At the discontinuity between the upper (low-velocity layer) and the lower asthenosphere, the velocity rapidly increases from about 4.4 km/s to about 4.7 km/s. The boundary is undulated, ranging between 180 km–250 km in section II (Fig. 4), and slightly deeper, between 220 km–300 km in section III (Fig. 5). The deepest depression of this discontinuity partly coincides with the overlying Tyrrhenian basin (cells 13 to 16, Fig. 5). The swell of this boundary occurs beneath the Algerian basin (cells 9 to 11, Fig. 4), beneath the Provençal basin (cells 5 to 9, Fig. 5) and along the Apennines and Dinaric subduction zones (cells 17 to 20 and 23–27, Fig. 5).

No evidences of low velocity "fingers" traceable to those reported by [74] in the quality factor are seen beneath the Massif Central (cell 1–2, Fig. 5), but this is not surprising since their size is far below the resolving power of our data and the lack of uncertainty estimates about their size makes any comparison very difficult.

6. Conclusions

Beneath the tectonically stable and old Africa plate, the mantle shows a stratification which may represent chemical and physical variations such as fluids concentration and partial melting in the low-velocity zone (LVZ) in the upper asthenosphere (Fig. 6), or phase transition [75] or variation of the Mg/Fe ratio in the lower asthenosphere and upper mantle in general [76], where the velocity increases below about 200 km–250 km. Moving into the younger and active back-arc basin of the western Mediterranean, the mantle appears more chaotic, and the 150–200 km deep LVZ is less evident (Fig. 4). There is a much shallower layer, between 30–100 km deep, raising from west to east, right beneath the central part of the easternmost back-arc basin (Fig. 5, Tyrrhenian Sea). The presence of such a layer suggests sizeable shallow partial melting, which is feeding the new oceanic crust in the Marsili basin and the related volcano south of the section [49]. No evidence of a deeply rooted plume occurs beneath the back-arc basin. The retreat of a slab implies that the upper mantle fills the space left by the removed lithosphere along W-directed subduction zones [10]. This is in agreement with reconstructions of the mantle structure in the Mediterranean [34,37,77,78] showing a very thin lithospheric mantle in the hanging-wall of the subduction zone, low Q factor, low seismic velocities and high heat flow [47,79]. The mantle wedge above the slab is inferred to be asthenosphere replacing the subducted lithosphere. Therefore, the "eastward" retreat of the slab should predict a contemporaneous flow in the mantle along the same trend (Fig. 6), regardless this flow is generating the retreat or it is a consequence of it [6]. Therefore, according to the kinematic reconstruction and the new tomography shown here, the upper asthenosphere (LVZ), which is well stratified and confined beneath the old northern Africa continental lithosphere at about 130–200 km, it is rather dispersed in the back-arc of the Apennines subduction, having a thicker section between 40–200 km. This setting possibly generated a dilution of the LVZ, and the slower

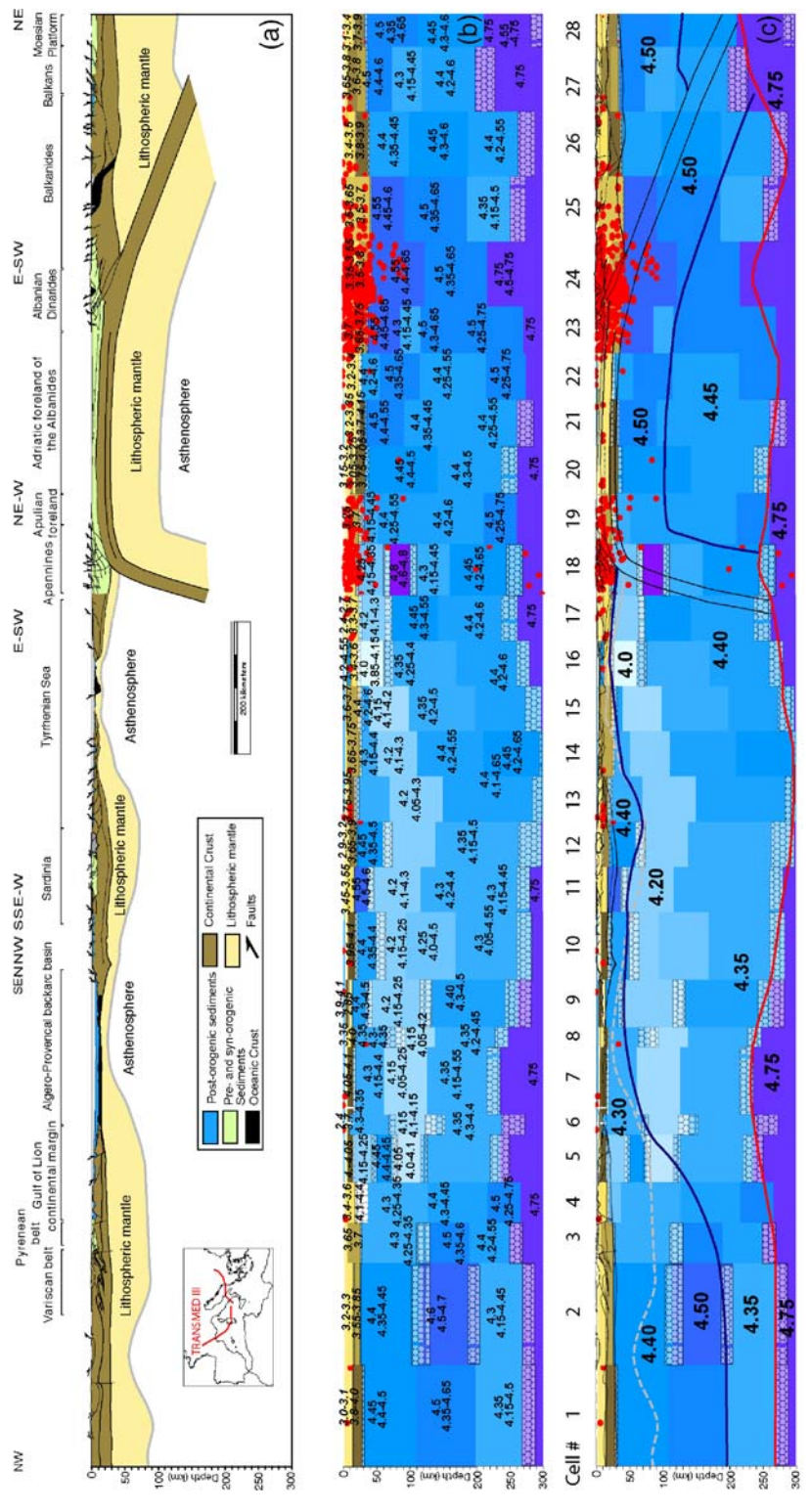

Fig. 5. (a) Lithospheric scale cross-sections simplified and redrawn from the TRANSMED III geotraverse [3]. (b) Lithosphere–asthenosphere system along the trace of the TRANSMED III geotraverse: the tomographic cross-section was obtained from selected solutions and related seismicity (body waves magnitude greater or equal to 3.0). The chosen V_s and its range of variability in km/s are printed on each layer. When the velocity ranges of vertically adjacent layers do not overlap, a hatched rectangle outlines the range of variability of their thicknesses. Numbers in *Italic* denote the velocities in the crustal layers. The hypocentres are denoted by red dots. (c) Overlap between the TRANSMED III regional cross-sections and the V_s tomography; only a few average representative values of V_s are reported to avoid overcrowding of characters; the dashed line reproduces the lithosphere–asthenosphere boundary given in part (a), while the new geometry of the base of the lithosphere (blue) and of the limit between upper and lower asthenosphere (red) are shown by continuous lines. The well-developed low velocity layer, visible under Africa in Fig. 4, is either missing or dispersed in the shallower asthenosphere, particularly in the centre of the back-arc basins.

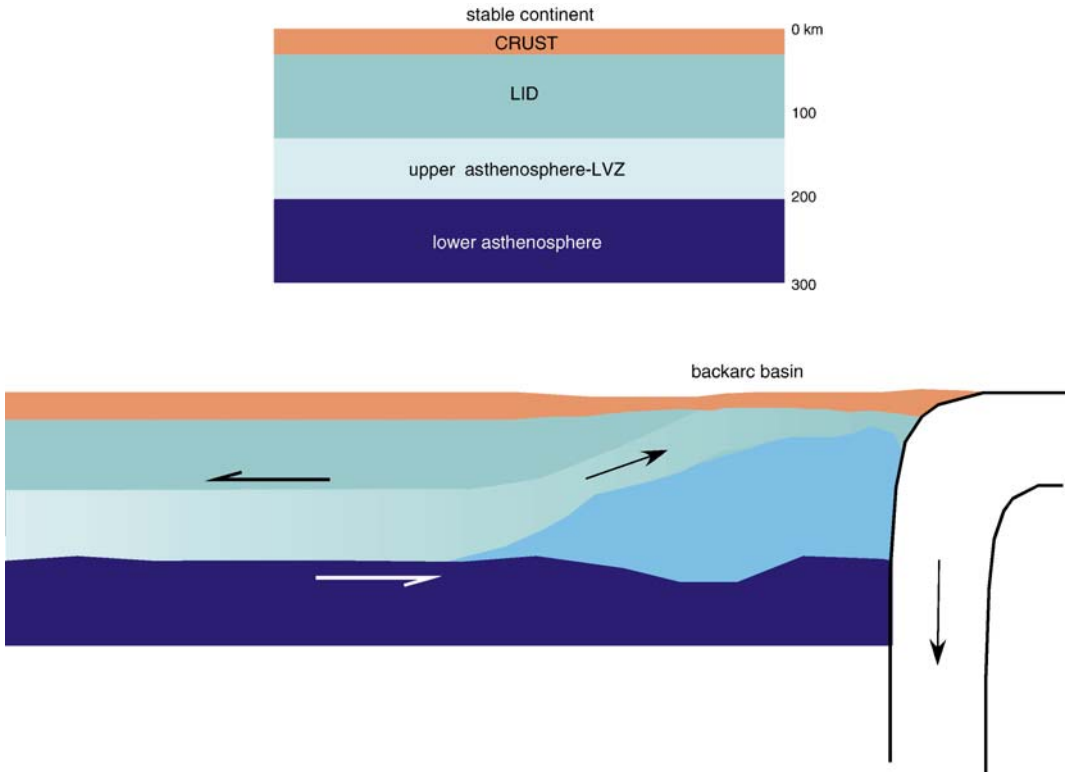

Fig. 6. Hypothetical, schematic reconstruction of the upper mantle stratification (upper section) and later mobilization and dispersion into the back-arc basin (lower section).

velocities are confined at the top of the mantle in the active backarc (Fig. 5). All these evidences are in favour of shallow upper mantle convection/circulation [80] and confirm the "west to east" flow of the mantle relative to the lithosphere, as suggested by the Apennines slab eastward retreat [4]. This flow is consistent with shear-wave splitting analysis that mostly supports an E–W upper mantle anisotropy [72,73], indicating olivine crystals preferred orientation induced by mantle flow.

Acknowledgements

We express our thanks to A. Levshin, who provided global group velocity measurements available at CIEI, University of Colorado at Boulder, to T. Yanovskaya, who provided the 2D tomography software from St. Petersburg State University. This research was sponsored by ICTP "Abdus Salam" Associates Scheme (R. Raykova) and by CEI University network project "Geodynamical model of central Europe for safe development of ground transportation systems". The manuscript was made during the stay of R. Raykova at Istituto Nazionale di Geofisica e Vulcanologia, sezione di Bologna as a post-doc SPICE researcher, supported from the European Commission's Human Resources and Mobility Programme, Marie Curie Research Training Networks. Part of this research is funded by Italian MIUR PRIN 2004: Modelling of the mantle–crust system by petrological and geophysical methods; PNRA 2.7–2.8, 2004–2006 "Sismologia a banda larga nella regione del Mare di Scotia e suo utilizzo per lo studio della geodinamica della litosfera"; ALPS-GPSQUAKENET Project (I/II/3.3/02) of the EU Interreg III-B Alpine Space Programme.

References

[1] W. Cavazza, F. Rour, W. Spakman, G.M. Stampfli, P.A. Ziegler, the TRANSMED Project Working Groups, The TRANSMED Atlas — the Mediterranean Region from Crust to Mantle, Springer, Berlin Heidelberg, 2004.

[2] E. Roca, D. Frizon de Lamotte, A. Mauffret, R. Bracène, J. Vergés, N. Benaouali, M. Fernàndez, J.A. Muñoz, H. Zeyen, TRANSMED transect II, in: W. Cavazza, F. Roure, W. Spakman, G.M. Stampfli, P.A. Ziegler (Eds.), The TRANSMED Atlas — the Mediterranean Region from Crust to Mantle, Springer, Berlin Heidelberg, 2004.

[3] E. Carminati, C. Doglioni, A. Argnani, G. Carrara, C. Dabovski, N. Dumurdzanov, M. Gaetani, G. Georgiev, A. Mauffret, S. Nazai, R. Sartori, V. Scionti, D. Scrocca, M. Séranne, L. Torelli, I. Zagorchev, TRANSMED Transect III, in: W. Cavazza,

F. Roure, W. Spakman, G.M. Stampfli, P.A. Ziegler (Eds.), The TRANSMED Atlas — the Mediterranean Region from Crust to Mantle, Springer-Verlag, Berlin, 2004, pp. 141.
[4] E. Gueguen, C. Doglioni, M. Fernandez, On the post-25 Ma geodynamic evolution of the western Mediterranean, Tectonophysics 298 (1998) 259–269.
[5] E. Carminati, C. Doglioni, Europe–Mediterranean tectonics, Encyclopedia of Geology, Elsevier, 2004, pp. 135–146.
[6] C. Doglioni, E. Gueguen, P. Harabaglia, F. Mongelli, On the origin of W-directed subduction zones and applications to the western Mediterranean, Geol. Soc. Spec. Publ. 156 (1999) 541–561.
[7] E. Carminati, M.J.R. Wortel, W. Spakman, R. Sabadini, The role of slab detachment processes in the opening of the western–central Mediterranean basins: some geological and geophysical evidence, Earth Planet. Sci. Lett. 160 (1998) 651–665.
[8] L. Vigliotti, V.E. Langenheim, When did Sardinia stop rotating? New palaeomagnetic results, Terra Nova 7 (1995) 424–435.
[9] A.J. Meigs, J. Vergés, D.W. Burbank, Ten-million-year history of a thrust sheet, Geol. Soc. Amer. Bull. 108 (1996) 1608–1625.
[10] C. Doglioni, A proposal of kinematic modelling for W-dipping subductions — possible applications to the Tyrrhenian–Apennines system, Terra Nova 3 (1991) 423–434.
[11] F. Roure, P. Choukroune, X. Berástegui, J.A. Muñoz, A. Villien, P. Matheron, M. Bareyt, M. Seguret, P. Cámara, J. Deramond, ECORS Deep Seismic data and balanced cross-sections, geometric constraints to trace the evolution of the Pyrenees, Tectonics 8 (1989) 41–50.
[12] J. Gallart, N. Vidal, J.J. Dañobeitia, the ESCI-Valencia Trough Working Group, Lateral variations in the deep crustal structure at the Iberian margin of the Valencia trough imaged from seismic reflection methods, Tectonophysics 232 (1994) 59–75.
[13] J.J. Danobeitia, M. Arguedas, F. Gallart, E. Banda, J. Makris, Deep crustal configuration of the Valencia trough and its Iberian and Balearic borders from extensive refraction and wide-angle reflection profiling, Tectonophysics 203 (1992) 37–55.
[14] N. Vidal, J. Gallart, J.J. Danobeitia, A deep seismic transect from the NE Iberian Peninsula to the Western Mediterranean, J. Geophys. Res. 103 (1998) 12381–12396.
[15] J. Ledo, C. Ayala, J. Pous, P. Queralt, A. Marcuello, J.A. Muñoz, New geophysical constraints on the deep structure of the Pyrenees, Geophys. Res. Lett. 27 (2000) 1037–1040.
[16] A. Souriau, H. Pauchet, A new synthesis of Pyrenean seismicity and its tectonics implications, Tectonophysics 290 (1998) 221–244.
[17] H. Zeyen, M. Fernàndez, Integrated lithospheric modelling combining thermal, gravity, and local isostasy analysis: application to the NE Spanish geotransect, J. Geophys. Res. 99 (1994) 18089–18102.
[18] C. Ayala, M. Torne, et al., The lithosphere–asthenosphere boundary in the western Mediterranean from 3D joint gravity and geoid modelling: tectonic implications, Earth Planet. Sci. Lett. 209 (2003) 275–290.
[19] K. Hinz, Crustal structure of the Balearic Sea, Tectonophysics 20 (1973) 295–302.
[20] A. Galdeano, J.C. Rossignol, Assemblage à altitude constante de cartes d'anomalies magnétiques couvrant l'ensemble du bassin occidental de la Méditerranée, Bull. Soc. Géol. Fr. 7 (1977) 461–468 (in French).
[21] K. Mickus, C. Jallouli, Crustal structure beneath the Tell and Atlas mountains (Algeria and Tunisia) through the analysis of gravity data, Tectonophysics 314 (1999) 373–385.
[22] M. Sapin, A. Hirn, Results of explosion seismology in the southern Rhone valley, Ann. Geophys. 30 (1974) 181–202.
[23] M. Granet, G. Stoll, J. Dorel, U. Achauer, G. Poupinet, K. Fuchs, Massif Central (France): new constraints on the geodynamical evolution from teleseismic tomography, Geophys. J. Int. 121 (1995) 33–48.
[24] S. Sobolev, H. Zeyen, H. Stoll, F. Werling, R. Altherr, K. Fuchs, Upper mantle temperatures from teleseismic tomography of French Massif Central including effects of composition, mineral reactions, anharmonicity, anelasticity and partial melt, Earth Planet. Sci. Lett. 139 (1996) 147–163.
[25] G. Pascal, A. Mauffret, P. Patriat, The ocean–continent boundary in the Gulf of Lion from analysis of expanding spread profiles and gravity modeling, Geophys J. Int. 113 (1993) 701–726.
[26] N. Chamot-Rooke, F. Jestin, J.M. Gaulier, Constraints on Moho depth and crustal thickness in the Liguro–Provençal Basin from a 3D gravity inversion: geodynamic implications, Rev. Inst. Fr. Pét. 52 (1997) 557–583.
[27] B. De Voogd, R. Nicolich, J.L. Olivet, F. Fanucci, J. Burrus, A. Mauffret, G. Pascal, A. Argnani, J.M. Auzende, M. Bernabini, C. Bois, L. Carmingani, A. Fabri, I. Finetti, A. Galdeano, C.Y. Gorini, P. Labaume, D. Lajat, P. Patriat, B. Pinet, J. Ravat, F. Ricci Lucchi, S. Vernassa, First deep seismic reflection transect from the gulf of Lions to Sardinia (ECORS-CROP profiles in western Mediterranean), in: American Geophysical Union (Ed.), Continental Lithosphere: Deep Seismic Reflections, Geodynamics, vol. 22, 1991, pp. 265–274.
[28] F. Cella, S. de Lorenzo, M. Fedi, M. Loddo, F. Mongelli, A. Rapolla, G. Zito, Temperature and density of the Tyrrhenian lithosphere and slab and new interpretation of gravity field in the Tyrrhenian Basin, Tectonophysics 412 (2006) 27–47.
[29] R. Nicolich, G.V. Dal Piaz, Moho Isobaths, in: G. Bigi, D. Cosentino, M. Parrotto, R. Sartori, P. Scandone (Eds.), Structural model of Italy, Scale 1:500.000, C.N.R. Progetto Finalizzato Geodinamica, 1990.
[30] G.F. Panza, P. Scandone, G. Calcagnile, St. Mueller, P. Suhadolc, The lithosphere–asthenosphere system in Italy and surrounding regions, in: G. Bigi, D. Cosentino, M. Parrotto, R. Sartori, P. Scandone (Eds.), Structural model of Italy, Scale 1:500.000, C.N.R. Progetto Finalizzato Geodinamica, 1990.
[31] J. Ansorge, D. Blundell, St. Mueller, Europe's lithosphere–seismic structure, in: D. Blundell, R. Freeman, St. Mueller (Eds.), A Continent Revealed: the European Geotraverse, Cambridge Univ. Press, 1992, pp. 33–70.
[32] A. Pontevivo, G.F. Panza, Group velocity tomography and regionalization in Italy and bordering areas, Phys. Earth Planet. Inter. 134 (2002) 1–15.
[33] G. Chimera, A. Aoudia, A. Sarao', G.F. Panza, Active tectonics in Central Italy: constraints from surface wave tomography and source moment tensor inversion, Phys. Earth Planet. Inter. 138 (2003) 241–262.
[34] G.F. Panza, A. Pontevivo, G. Chimera, R.B. Raykova, A. Aoudia, The lithosphere–asthenosphere: Italy and surroundings, Episodes 26 (2003) 169–174.
[35] G. Bigi, D. Cosentino, M. Parotto, R. Sartori, P. Scandone, Structural Model of Italy, Scale 1/500.000, Sheets 3–6, CNR, P.F. Geodinamica, SELCA, Florence.
[36] B. Della Vedova, S. Bellani, G. Pellis, P. Squarci, Deep temperatures and surface heat flow distribution, in: G.B. Vai, I.P. Martini (Eds.), Anatomy of an Orogen: the Apennines and Adjacent Mediterranean Basins, Kuwler Academic Publishers, Dordrecht, The Netherlands, 2001, pp. 65–76.
[37] G. Mele, A. Rovelli, D. Seber, M. Baranzagi, Shear wave attenuation in the lithosphere beneath Italy and surrounding

regions: tectonic implications, J. Geophys. Res. 102 (1997) 11863–11875.
[38] F. Italiano, M. Martelli, G. Martinelli, P.M. Nuccio, Geochemical evidence of melt intrusions along lithospheric faults of the Southern Apennines, Italy; geodynamic and seismogenic implications, J. Geophys. Res. 105–13 (2000) 569–578.
[39] A. Frasheri, P. Nishani, S. Bushati, A. Hyseni, Relationship between tectonic zones of the Albanides, based on results of geophysical studies, in: P.A. Ziegler, F. Horvath (Eds.), Peri-Tethys Memoir 2. Structure and Prospects of Alpine Basins and Forelands, Mém. Mus. Natl. Hist. Nat., 170 (1996) 485–511.
[40] C. Piromallo, A. Morelli, P-wave tomography of the mantle under the Alpine–Mediterranean area, J. Geophys. Res. 108 (B2: 2065) (2003), doi:10.1029/2002JB001757.
[41] Stojkovic et al., Explanatory note of the Magnetic map of SFRJ, 1:500 000, 1976.
[42] P. Bilibajkic, M. Mladenovic, S. Mujagic, N. Rimac, Explanatory note of the Gravimetry Map of SFRJ – Bouguer anomalies, 1:500 000, Savezni Geol. zav., Beograd, 1979 (in Serbian-Croatian).
[43] V. Babushka, J. Plomerova, E. Spasov, Lithosphere thickness beneath the territory of Bulgaria — a model derived from teleseismic P-residuals, Geol. Balc. 16 (1986) 51–54.
[44] A. Boykova, Moho discontinuity in central Balkan Peninsula in the light of the geostatistical structural analysis, Phys. Earth Planet. Inter. 114 (1999) 49–58.
[45] C. Doglioni, E. Gueguen, F. Sabat, M. Fernandez, The western Mediterranean extensional basins and the Alpine orogen, Terra Nova 9 (1997) 109–112.
[46] A. Mauffret, D. Frizon de Lamotte, S. Lallemant, C. Gorini, A. Maillard, E–W opening of the Algerian Basin (Western Mediterranean), Terra Nova 16 (2004) 257–264.
[47] F. Cella, M. Fedi, G. Flori, A. Rapolla, Gravity modelling of the litho-asthenosphere system in the Central Mediterranean, Tectonophysics 287 (1998) 117–138.
[48] R.B. Raykova, G.F. Panza, Surface wave tomography and non-linear inversion in the southeast Carpathians, Phys. Earth Planet. Inter. 157 (2006) 164–180.
[49] G.F. Panza, A. Peccerillo, K. Aoudia, B. Farina, Geophysical and petrological modelling of the structure and composition of the crust and upper mantle in complex geodynamic settings: the Tyrrhenian sea and surroundings, Earth Sci. Rev. 80 (2007) 1–46.
[50] R. Raykova, S. Nikolova, Tomography and velocity structure of the crust and uppermost mantle in southeastern Europe obtained from surface wave analysis, Stud. Geophys. Geod. 51 (2007) 166–184.
[51] F. Marone, S. van der Lee, D. Giardini, Three-dimensional upper-mantle S-velocity model for the Eurasia–Africa plate boundary region, Geophys. J. Int. 158 (2004) 109–130.
[52] Z. Du, G.F. Panza, Amplitude and phase differentiation of synthetic seismograms: a must for waveform inversion at regional scale, Geophys. J. Int. 136 (1999) 83–98.
[53] J. Badal, V. Corchete, G. Payo, L. Pujades, J. Canas, Imaging of shear-wave velocity structure beneath Iberia, Geophys. J. Int. 124 (1996) 591–611.
[54] E.E. Karagianni, D.G. Panagiotopoulos, G.F. Panza, P. Suhadolc, C.B. Papazachos, B.C. Papazachos, A. Kiratzi, D. Hatzfeld, K. Makropoulos, K. Priestley, A. Vuan, Rayleigh wave group velocity tomography in the Aegean area, Tectonophysics 358 (2002) 187–209.
[55] G.F. Panza, R. Raykova, G. Chimera, A. Aoudia, Multiscale surface wave tomography in the Alps, Mem. Sci. Geol. 54 (2002) 55–56.
[56] R. Raykova, S. Nikolova, Anisotropy in the Earth's crust and the uppermost mantle in the Southeastern Europe obtained from Rayleigh and love surface waves, J. Appl. Geophys. 54 (2003) 247–256.
[57] A.L. Levshin, T.B. Yanovskaya, A.V. Lander, B.G. Bukchin, M.P. Barmin, L.I. Ratnicova, E.N. Its, Surface Seismic Waves in Laterally Inhomogeneous Earth, in: V.I. Keilis-Borok (Ed.), Kluiwer Publ. House, Dordrecht, 1989.
[58] A. Pontevivo, G.F. Panza, The lithosphere–asthenosphere system in the Calabrian Arc and surrounding seas — Southern Italy, Pure Appl. Geophys. 163 (2006) 1617–1659.
[59] T.B. Yanovskaya, P.G. Ditmar, Smoothness criteria in surface-wave tomography, Geophys. J. Int. 102 (1990) 63–72.
[60] T.B. Yanovskaya, Resolution estimation in the problems of seismic ray tomography, Izv. Phys. Solid Earth 33 (9) (1997) 762–765.
[61] G.F. Panza, A. Pontevivo, The Calabrian Arc: a detailed structural model of the lithosphere–asthenosphere system, Rendiconti Accademia Nazionale della Scienze detta dei XL, Mem. Sci. Fis. Nat. 2 (122) (2004) 51–88.
[62] M.H. Ritzwoller, A.L. Levshin, Eurasian surface wave tomography: group velocities, J. Geophys. Res. 103 (1998) 4839–4878.
[63] G.F. Panza, The resolving power of seismic surface waves with respect to crust and upper mantle structural models, in: R. Cassinis (Ed.), The Solution of the Inverse Problem in Geophysical Interpretation, Plenum Publ. Corp., 1981, pp. 39–77.
[64] M. Gennesseaux, P. Burollet, E. Winnock, Thickness of the Plio–Quaternary sediments (IBCM-PQ), Boll. Geofis. Teor. Appl. 39 (1998) 243–284.
[65] G. Laske, G. Masters, A global digital maps of sediment thickness, Eos, Trans. - Am. Geophys. Union 78 (1997) F483.
[66] L. Urban, A. Cichowicz, F. Vaccari, Computation of analytical partial derivatives of phase and group velocities for Rayleigh waves respect to structural parameters, Stud. Geoph. Geod. 36 (1993) 14–36.
[67] Z.J. Du, A. Michelini, G.F. Panza, EurID: a regionalized 3D seismological model of Europe, Phys. Earth Planet. Inter. 106 (1998) 31–62.
[68] A.E. Bryson, Y.-C. Ho, Applied Optimal Control: Optimization, Estimation, and Control, Hemisphere Publishing Corporation, New York, 1975.
[69] C. De Groot-Hedlin, S. Constable, Occam's inversion to generate smooth, two-dimensional models from magnetotelluric data, Geophysics 55 (1990) 1613–1624.
[70] E. Hurtig, V. Cermak, R. Haenel, V. Zui (Eds.), Geothermal Atlas of Europe, Hermann Haack Verlag, Gotha, 1992.
[71] S.E. Hazler, A.F. Sheehan, D.E. McNamara, W.R. Walter, One-dimensional shear velocity structure of Northern Africa from Rayleigh wave group velocity dispersion, Pure Appl. Geophys. 158 (2001) 1475–1493.
[72] L. Margheriti, F.P. Lucente, S. Pondrelli, SKS splitting measurements in the Apenninic–Tyrrhenian domain (Italy) and their relation with lithospheric subduction and mantle convection, J. Geophys. Res. 108 (2003), doi:10.1029/2002JB001793.
[73] G. Barruol, A. Deschamp, O. Coutant, Mapping upper mantle anisotropy beneath SE France by SKS splitting indicates Neogene asthenospheric flow induced by Apenninic slab roll-back and deflected by the deep Alpine roots, Tectonophysics 394 (2004) 125–138.
[74] J.R.R. Ritter, U.R. Christensen, U. Achauer, K. Bahr, M. Weber, Search for a mantle plume under Central Europe, EOS 79 (1998) 420.

[75] K.N. Matsukage, Y. Nishihara, S.-I. Karato, Seismological signature of chemical differentiation of Earth's upper mantle, J. Geophys. Res. 110 (2005), doi:10.1029/2004JB003504.
[76] G. Scalera, G. Calcagnile, G.F. Panza, On the "400-Kilometers" discontinuity in the Mediterranean Area, in: R. Cassinis (Ed.), The Solution of the Inverse Problem in Geophysical Interpretation, Plenum Publishing Co., New York, 1981, pp. 335–339.
[77] G.F. Panza, St. Mueller, The plate boundary between Eurasia and Africa in the Alpine Area, Mem. Soc. Geol. Ital. 33 (1978) 43–50.
[78] G. Calcagnile, G.F. Panza, The main characteristics of the lithosphere–asthenosphere system in Italy and surrounding regions, Pure Appl. Geophys. 119 (1981) 865–879.
[79] G. Zito, F. Mongelli, S. de Lorenzo, C. Doglioni, Geodynamical interpretation of the heat flow in the Tyrrhenian Sea, Terra Nova 15 (2003) 425–432.
[80] C. Faccenna, L. Jolivet, C. Piromallo, A. Morelli, Subduction and the depth of convection in the Mediterranean mantle, J. Geophys. Res. 108 (2003), doi:10.1029/2001JB001690.

Rendiconti Lincei 19, 291 – 309 (2008)
DOI: 10.1007/s12210-008-0020-x

Angelo Peccerillo · Giuliano F. Panza · Abdelkrim Aoudia · Maria Luce Frezzotti

Relationships between Magmatism and Lithosphere-Asthenosphere Structure in the Western Mediterranean and Implications for Geodynamics

Received: 06 April 2008 / Accepted: 24 July 2008 – © Springer-Verlag 2008

Abstract Shear-wave (V_S) tomography along transects across the Western-Central Mediterranean area reveals heterogeneous lateral and vertical physical characteristics in the lithosphere-asthenosphere system (LAS). A 50 km thick low velocity layer (LVL), with $V_S \sim 4.0$–4.2 km/sec, typical of low rigidity fluid-bearing mantle material, is observed at a depth of about 70–120 km from offshore Provence, to Sardinia and the Central Tyrrhenian Sea. This LVL, enclosed between higher velocity mantle rocks, rises to a depth of less than 30 km below the recent and active volcanoes of Central Italy and the Southern Tyrrhenian Sea, where a maximum in the heath flow is observed. The LVL is absent beneath Southeastern France and the northern border of the African foreland.

In the Balearic Sea-Sardinia-Central Tyrrhenian section, the depth of LVL corresponds to pressure conditions of minimum temperature of peridotite+CO_2+H_2O solidus, consistent with conditions where fluid loss from the slab and mantle flow over the subducting plate favor significant melt generation above steep, west-dipping subduction zones. It is suggested that LVL

A. Peccerillo (✉)
Dipartimento di Scienze della Terra, Università degli Studi di Perugia, Perugia, Italy
Fax: +390755852603, E-mail: pecceang@unipg.it

G.F. Panza
Dipartimento di Scienze della Terra, Università degli Studi di Trieste, Trieste, Italy
Fax: +390405582111, E-mail: panza@dst.units.it

A. Aoudia
The Abdus Salam International Centre for Theoretical Physics, Earth System Physics Section, Trieste, Italy
Fax: +3904022407833, E-mail: aoudia@ictp.it

M.L. Frezzotti
Dipartimento di Scienze della Terra, Università degli Studi di Siena, Siena, Italy
Fax: +390577233938, E-mail: frezzottiml@unisi.it

in the Balearic-Tyrrhenian domains is the result of mantle contamination and melting left behind by the eastward retreating Adriatic-Ionian subducting plates from Oligo-Miocene to present. This layer also marks a discontinuity between the lithospere and underlying mantle behind the subduction zone, favoring detachment and westward drift of the lithosphere, and consequent opening of backarc basins.

These data support the hypothesis that the orogenic Oligocene to Quaternary volcanism in the Western Mediterranean area is the effect of shallow mantle processes, and argue against the presence of deep mantle plumes. A shallow-mantle origin is also suggested for the EM1-type Plio-Quaternary anorogenic magmatism in Sardinia and for the FOZO-DMM-type magmatism on the northern margin of the African foreland.

Keywords Upper mantle, S-wave tomography, magmatism, Western Mediterranean, geodynamics

Subject codes G14003, G18009, G17002

1 Introduction

Oligocene to present magmatism in the Western Mediterranean area (Fig. 1) shows extremely variable trace element and radiogenic isotope (i.e. Sr, Nd, Pb, Hf) signatures (Peccerillo 2005; Lustrino and Wilson 2007). Based on trace element abundances and ratios in primitive mafic rocks (MgO > 7 wt%, Ni > 200–300 ppm, Cr > 400–500 ppm), two broad groups of magmas have been recognized. One shows relative depletion in Rb and Cs, and enrichments in High Field Strength Elements (HFSE: Ta, Nb, Zr, Hf, Ti) with positive spikes of Ta and Nb in their mantle normalized patterns (Lustrino and Wilson 2007). These are akin to volcanic suites erupted in intraplate settings, and are referred to as *anorogenic* suites. Other rocks are relatively depleted in HFSE and enriched in several Large Ion Lithophile Elements (LILE: Rb, K, Th, U, Pb etc.), resembling volcanic suites erupted at converging plate boundaries. These are generally referred to as *orogenic* rocks (Fig. 2). Large petrological, geochemical and isotopic variations are observed within the two broad groups of orogenic and anorogenic magmas. Orogenic rocks consist of arc tholeiites, calcalkaline, shoshonitic and ultrapotassic suites. Anorogenic magmas range from tholeiite to Na-alkaline and nephelinite compositions.

Compositional complexities in the Western Mediterranean magmas have been explained as the interplay of various factors, including mantle contamination by different types of crustal material via subduction and crust delamination, passive uprise of uncontaminated asthenosphere, and either fossil or active deep mantle plumes (e.g. Vollmer 1976; Hoernle et al. 1995; Gasperini et al. 2000, 2002; Peccerillo and Lustrino 2005; Rotolo et al. 2006).

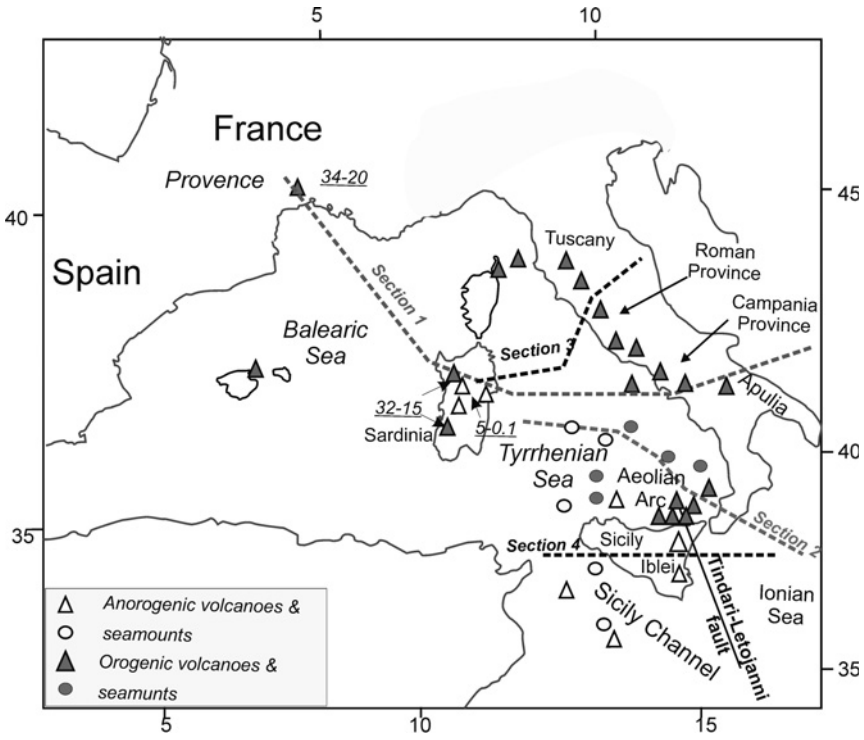

Fig. 1 Schematic distribution of orogenic and anorogenic volcanism (ages are in Ma) in the Balearic-Provençal-Tyrrhenian area. Lines represent tracks of sections reported in Figs. 3 and 4.

The Western Mediterranean is a highly studied area. Therefore, it represents a key place where geophysical and geochemical data can be combined to test the relationships between magmatism and mantle structure (Peccerillo and Panza 1999; Panza et al. 2007a), and to place constraints on the roles of shallow-mantle vs. deep plumes in the genesis of the magmatism and in the geodynamic evolution of the area.

In this paper, we report on V_S data for the lithosphere-asthenosphere system (LAS) along four key sections across the Western-Central Mediterranean area (Fig. 1). Based on these data and on the main characteristics of the magmatism, we discuss the possible origin of geophysical characteristics of LAS and the implication for magmatism and geodynamics.

2 Geodynamic setting

The Oligocene to present evolution of the Western-Central Mediterranean area has been characterized by the opening of the Ligurian-Provençal (about 32 to 15 Ma), Algerian, and Valencia basins, separation of the Corsica-Sardinia block from the Southern European plate, and by the opening of the Tyrrhenian

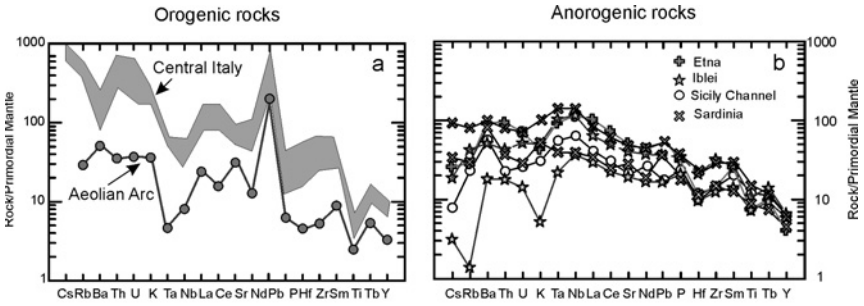

Fig. 2 Mantle-normalized incompatible element patterns for representative primitive (MgO > 7 wt%) orogenic and anorogenic rocks in the Tyrrhenian Sea area. A. Calc-alkaline basalt from the Aeolian arc and ultrapotassic leucite tephrites from Central Italy. B. Tholeiitic to Na-alkaline basalts from Iblei, Etna and Sardinia (data from Peccerillo 2005 and references therein).

Sea (about 15 Ma to present) and counter-clockwise rotation of the Apennines (e.g. Savelli and Gasparotto 1994; Carminati et al. 1998; Doglioni et al. 1998, 1999; Faccenna et al. 2001). Orogenic, mainly calcalkaline, magmatism took place in Provence (∼ 30–24 Ma), the Baleric area and Sardinia (∼ 30–15 Ma), and migrated to the Tyrrhenian Sea and the Italian peninsula (mostly 7 Ma to present), becoming progressively enriched in potassium with time (see Lustrino et al. 2004; Peccerillo 2005; Peccerillo and Lustrino 2005 for a review). The presently active orogenic volcanism in the Southern Tyrrhenian Sea and in the Campanian province (Ischia, Campi Flegrei, Vesuvio) ranges from calcalkaline to ultrapotassic, and is associated with deep-focus seismic activity defining a steep and narrow NW-dipping Benioff plane, going from Calabria and the Eastern Aeolian arc to Campania (Panza et al. 2003; De Astis et al. 2006).

During the Tyrrhenian Sea opening, there was rifting and anorogenic magmatism in Sardinia and MORB-OIB activity in the Tyrrhenian Sea (e.g. Argnani and Savelli 1999; Lustrino et al. 2000, 2004; Peccerillo 2005). Miocene to present anorogenic magmatism also took place in the Sicily Channel and the Pelagian Block (Ferdinandea-Graham Island, Linosa, Pantelleria, Iblei, Etna), situated in the northern margin of the African plate. Opening of the Tyrrhenian Sea resulted in longitudinal stretching of the Apennines, with formation of several arc sectors separated by important transverse tectonic lines (e.g. 41° parallel line, Tindari-Letojanni fault, etc.; Locardi 1988; Turco and Zuppetta 1998; Rosenbaum et al. 2008). Some of these faults are associated with deep tear-off zones of the Adriatic-Ionian subducted slab, along which asthenospheric mantle material can feed the volcanism (Rosenbaum et al. 2008).

3 S-wave velocities across key sections in the Western Mediterranean

V_S tomography along the investigated sections is shown in Figs. 3 and 4. Section 1 is reported schematically in Fig. 3 whereas sections 2, 3 and 4 are shown

in Fig. 4. Section 1 has been already published and discussed by Panza et al. (2007b). It goes from Provence to Central Sardinia, the Campanian province (Vesuvio, Campi Flegrei, Ischia), up to the Balkan peninsula, running along the 41° Parallel Line in its central segment. Section 2 runs from offshore Southern Sardinia to the Aeolian arc and Calabria following an E-W and then NW-SE direction. This matches the direction of maximum extension during the last 5 Ma, according to Sartori (2003). Section 3 is located in the Central-Northern Tyrrhenian Sea and goes through the Roman magmatic province. Finally, Section 4 runs from the Sicily Channel to the Ionian Sea, along the northern border of the African foreland and crosses the Tindari-Letojanni fault system, i.e. the boundary between the Pelagian Block to the west, a promontory of the African plate, and the Ionian plate to the east. Quaternary anorogenic magmatism took place in this area, notably at Pantelleria, Linosa, Graham-Ferdinandea Island, Etna, Iblei. Detailed information about the data, path coverage, resolution, etc. is provided in Panza et al. (2007a,b) and Boyadzhiev et al. (2008). The V_S and thickness ranges of variability of the cells from 1 to 10 of Section 1 are reported in Table 1.

Section 1 (Fig. 3) shows that the distribution of S-wave velocities in the upper mantle beneath Provence (cell# 1–4) is rather homogeneous ($V_S \sim 4.30$–4.50 km/sec) down to 250 km depth. Starting from off-coast Provence (cell# 5), the upper mantle structure changes significantly because of the presence of a layer with quite low S-wave velocities (V_S = 4.00–4.10) at a depth of about 70–120 km. This well developed Low Velocity Layer (LVL) is delimited, at the top and at the bottom, by high-velocity material having $V_S \sim 4.30$–4.50 km/s,

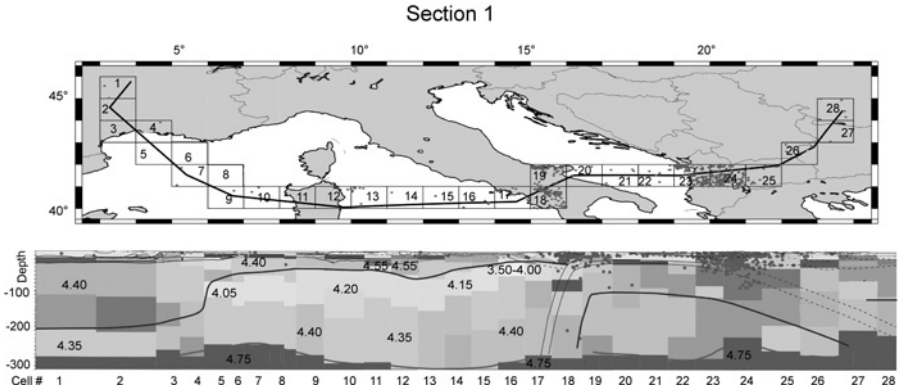

Fig. 3 V_S tomography and the lithosphere-asthenosphere system along the TRANSMED III geotraverse (Carminati et al. 2004), modified after Panza et al. (2007b), and reported in the text as "Section 1". The geometry of the base of the lithosphere is indicated by the blue line while in red is reported the limit between upper and lower asthenosphere. Only a few average representative values of V_S are reported. The V_S and thickness ranges of variability of the cells from 1 to 10 are reported in Table 1. Data for the remaining cells are reported in Panza et al. (2007a).

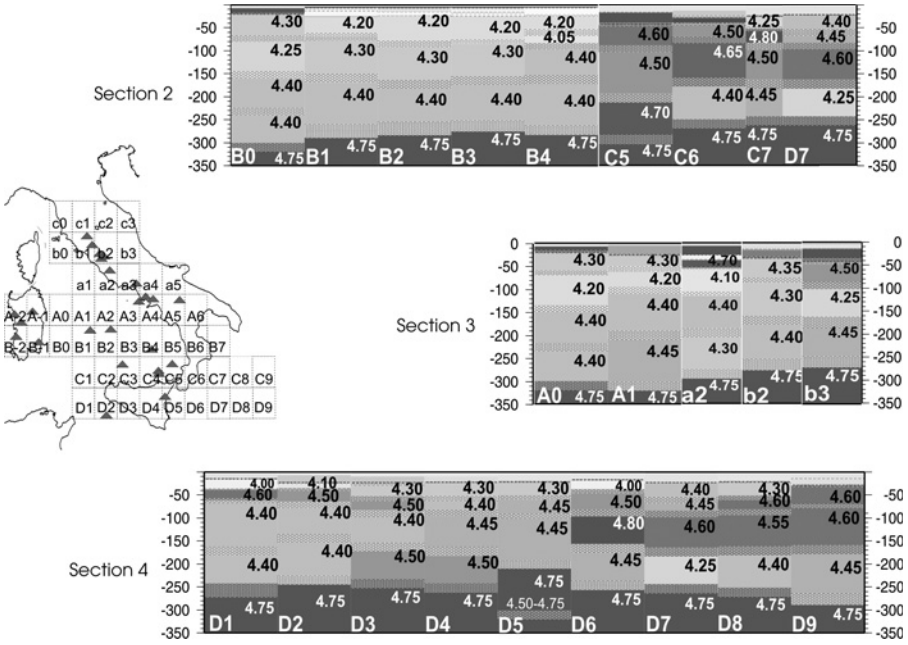

Fig. 4 V_S tomography along Section 2, 3 and 4, retrieved from the cellular V_S model of the Tyrrhenian Sea and surroundings (Panza et al. 2007a) as shown in the inset (red triangles are recent and active volcanoes). In each labelled cell, the chosen shear velocity is reported on each layer where the hatched zone stands for the thickness variability. The V_S ranges of variability are reported in Panza et al. (2007a).

and extends eastward to the Central Tyrrhenian Sea (Magnaghi and Vavilov basins), keeping almost constant thickness, V_S and depth. The LVL rises to a shallower level beneath the Pontine Islands and Campania (cell# 15–17), with a decrease of V_S to less than 4.0 km/s (for details see Panza et al. 2007b).

Other interesting features revealed by Section 1 are a very high velocity lid beneath Sardinia (cell# 11–12; V_S = 4.45–4.55 km/s), which is not found elsewhere in the investigated area (Panza et al. 2007a,b). LVL beneath the Western Mediterranean area was also detected by P-wave tomography (see Hoernle et al. 1995) and was interpreted as an isolated portion of a large scale mantle upwelling affecting the Western Atlantic and Central-Southern Europe.

In Section 2 (Fig. 4), the LAS is somewhat different than along Section 1. The LVL is still present but it lies at a much shallower depth, being detected at 30 to 70 km and rising to 20–30 km beneath the Eastern Aeolian volcanoes. An almost vertical seismically active high-velocity body with V_S from 4.50 to 4.80 km/s likely representing the descending Ionian slab (Panza et al. 2003), interrupts the LVL beneath Calabria (cell# C5, C6).

Table 1 Ranges of variability of the parameters h (thickness) and Vs for each layer of the chosen solution for the cells from 1 to 10 reported in Fig. 3. Similar data for the remaining cells (Fig. 3) are reported in Panza et al. (2007a).

cell 1, e-7 (45.5, 3.5)		cell 2, d-7 (44.5,3.5)		cell 3, c-7 (43.5,3.5)		cell 4, c-6 (43.5, 4.5)	
VS (km/s)	h (km)	VS (km/s)	h (km)	VS (km/s)	h (km)	VS (km/s)	H (km)
1.39	1.8	1.39	1.8	1.39	1.8	1.50	1.0
3.01	1.0	3.06	1.0	3.06	1.0	1.85	1.0
3.12	3.2	3.18	3.2	3.18	3.2	2.66	1.0
–	–	–	–	–	–	3.24	2.0
–	–	–	–	–	–	–	–
3.00–3.10	7–9	3.20–3.30	8–10	3.55–3.75	9.5–12	3.40–3.60	12–14.5
3.80–4.00	13–17	3.55–3.85	10.5–11.5	3.55–3.85	7–9.5	4.10–4.40	20–30
4.40–4.50	65–95	4.35–4.45	75–105	4.25–4.35	85–105	4.25–4.35	75–90
4.35–4.65	75–90	4.50–4.70	72–90	4.35–4.60	60–80	4.30–4.45	75–90
4.15–4.50	70–90	4.15–4.45	65–82	4.20–4.55	60–80	4.25–4.75	50–70
4.75	*	4.75	*	4.75	*	4.75	*
cell 5, b-6 (42.5,4.5)		cell 6, b-5 (42.5,5.5)		cell 7, a-5 (41.5,5.5)		cell 8, a-4 (41.5,6.5)	
VS (km/s)	h (km)	VS (km/s)	h (km)	VS (km/s)	h (km)	VS (km/s)	h (km)
0.0	1.4	0.0	2.1	0.0	2.5	0.0	2.6
1.16	0.6	1.16	0.9	0.16	0.5	1.22	0.2
1.59	1.0	1.39	1.0	1.39	1.0	1.86	0.5
2.40	1.5	2.19	0.5	2.57	1.0	2.30	1.1
3.18	1.5	–	–	2.89	1.0	2.84	0.6
4.00–4.05	8–11	2.30–2.50	1.5–2	4.05–4.10	7.5–12.5	3.25–4.45	6–8
4.15–4.25	28–36	3.55–3.85	2–2.5	4.15–4.40	25–35	3.90–4.10	5–7
4.40–4.45	25–35	4.30–4.35	60–75	4.15–4.40	20–32.5	4.30–4.35	45–75
4.00–4.10	40–50	4.10–4.15	45–75	4.05–4.25	65–82.5	4.05–4.20	60–77.5
4.30–4.40	105–135	4.30–4.40	100–135	4.15–4.55	90–110	4.20–4.45	90–100
4.75	*	4.75	*	4.75	*	4.75	*
cell 9, A-4 (40.5,6.5)		cell 10, A-3 (40.5,7.5)					
VS (km/s)	h (km)	VS (km/s)	h (km)				
0.0	2.7	0.0	2.2				
1.16	0.1	1.39	1.5				
1.78	0.2	1.85	0.5				
–	–	2.60	1.8				
–	–	2.66	1.0				
3.90–4.10	4–5	3.95–4.10	9–15				
2.75–2.95	6–7	4.35–4.40	30–45				
4.30–4.50	20–30	4.15–4.25	45–60				
4.15–4.25	77.5–95	4.00–4.50	57.5–75				
4.30–4.50	110–150	4.05–4.55	92.5–115				
4.75	*	4.75	*				

Section 3 cuts the central Tyrrhenian Sea and the Roman magmatic province. In its western segment, it is characterized by a LVL with V_S = 4.1–4.2 km/s at about 50–120 km depth, and becomes somewhat shallower in the Roman province (cell a2).

Section 4 reveals very different characteristics for the upper mantle, as compared with the other investigated sections. Basically, no LVL is found, except for a shallow thin lens occurring at a depth of 20–30 km offshore South-Western Sicily approximately beneath the active Ferdinandea-Graham volcanic area (cells D1, D2), and another small lens east of Etna (cell D6). The latter, however, is an area where no recent volcanism has been detected. Notably, east of the Tindari-Letojanni fault, at about 100–150 km depth, a very high velocity layer ($V_S \sim$ 4.5–4.8 km/s) is encountered. This becomes shallower going eastward and can be related to the Ionian lithosphere dipping north-westward beneath the Southern Tyrrhenian Sea.

4 Characteristics of the magmatism

Orogenic magmatic centers with variable ages occur along Sections 1, 2, and 3 (Fig. 1). The Oligo-Miocene magmatism in Sardinia and Provence is mainly calcalkaline with some arc tholeiites, whereas Plio-Quaternary volcanoes of the Aeolian arc and along the Tyrrhenian border of the Italian peninsula range from calcalkaline and shoshonitic to ultrapotassic. Trace element compositions and radiogenic isotopes (Figs. 2–5) are variable, with enrichment in LILE and radiogenic Sr increasing from calcalkaline to potassic and ultrapotassic rocks (e.g. Vollmer 1976; Hawkesworth and Vollmer 1979; Peccerillo 2003, 2005 and references therein).

Anorogenic magmatic centers are also present in the investigated areas. They range from tholeiitic to Na-alkaline and nephelinitic and occur in Sardinia (5 to 0.1 Ma, but with first occurrence at about 12 Ma; Lustrino et al. 2007a), at several places in the Tyrrhenian basin (e.g., Ustica and some seamounts; age from 7 to 0.1 Ma), along the Sicily Channel (Miocene to present), at Etna (0.5 Ma to present) and Iblei Mts. (discontinuously from Cretaceous to Quaternary). When occurring in the same area, such as in Sardinia, anorogenic rocks show a younger age than orogenic magmas (e.g., Lustrino et al. 2007a,b). Notably, anorogenic rocks in Sardinia have intermediate values of key element ratios (e.g. Ba/Nb, Ce/Pb) between typical anorogenic (e.g. Sicily) and orogenic compositions (Lustrino et al. 2004, 2007b).

Sr and Nd isotopic ratios of mafic anorogenic rocks are moderately variable ($^{87}Sr/^{86}Sr \sim$ 0.7030–0.7045; $^{143}Nd/^{144}Nd \sim$ 0.5130–0.5125), whereas radiogenic Pb isotopic ratios show a wide range of values (e.g. $^{206}Pb/^{204}Pb \sim$ 20.00–17.50). Anorogenic mafic rocks in Sicily and the Sicily Channel have poorly radiogenic Sr isotopic signatures and moderately variable Pb isotopic

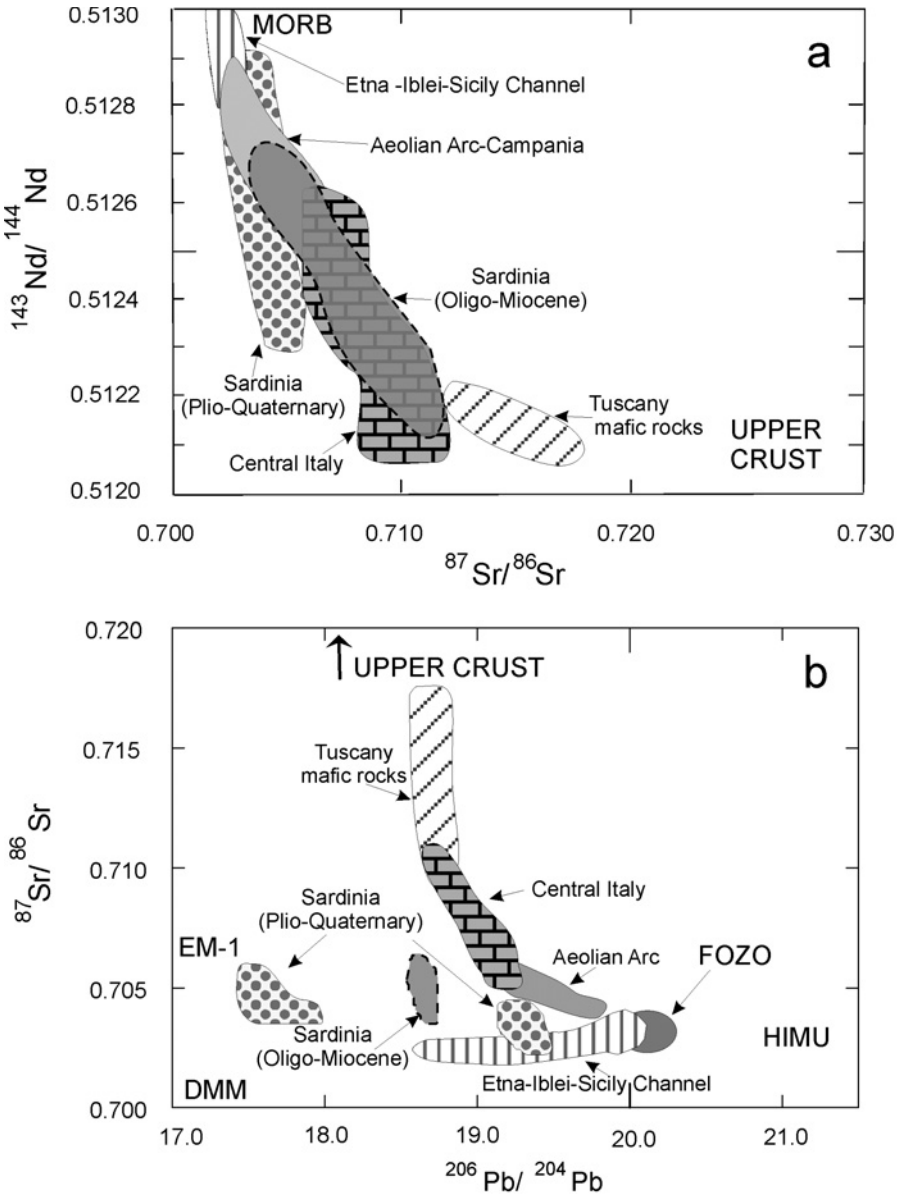

Fig. 5 Sr-Nd-Pb isotopic variations for volcanic rocks in Central-Southern Italy. Modified after Peccerillo (2005). Upper crustal and some mantle end-member compositions (FOZO, HIMU, DMM, EM1) are shown. For explanation, see text.

ratios (Fig. 5), overall defining a trend between FOZO (Focus Zone) or HIMU (High-μ, where μ is U/Pb ratio) towards DMM (Depleted MORB-type Mantle) (e.g. Esperança and Crisci 1995; Hoernle et al. 1996; Civetta et al. 1998). There is much controversy about the significance of these compositions, which

are found at a global scale for mantle-derived magmas (e.g. Hofmann 1997). Some authors believe they represent physically distinct mantle reservoirs, such as lithosphere (DMM) and deep mantle plumes (HIMU and FOZO). Others believe they simply reveal smaller scale compositional heterogeneities occurring within the mantle source of basaltic magma as a consequence of continuous crustal recycling (see Stracke et al. 2005 and references therein; Foulger et al. 2005 and the web-site http://www.mantleplumes.org/; Lustrino and Carminati, 2007). The intermediate compositions between DMM and FOZO-HIMU in eastern Sicily and the Sicily Channel have been interpreted either as generated by mixing between distinct mantle reservoirs (i.e. deep mantle plume and lithospheric mantle; e.g. Hoernle et al. 1995, 1996; Civetta et al. 1998) or as the effect of metasomatic events which occurred on resident lithospheric mantle rocks in a zone of long-lived extension (Esperança and Crisci 1995; Di Bella et al. 2008 and references therein).

Anorogenic rocks in Southern Sardinia resemble closely Sicily volcanics. In contrast, rocks from Central-Northern Sardinia have moderately radiogenic Sr and Nd, but low Pb isotopic ratios ($^{206}Pb/^{204}Pb \sim 17.7$) close to values of the so called Enriched Mantle-1 (EM1; Lustrino et al. 2007b and references therein). These isotopic signatures are unique in the Mediterranean and in Europe and are observed in some oceanic volcanoes such as Kerguelen and Walvis Ridge, which are believed to sample deep mantle sources (see Hofmann 1997).

5 Relationships between magmatism and upper mantle structure and heath flow

The data summarized above reveal interesting relationships between the nature of the magmatism and the structure of the Lithosphere-Asthenosphere System as indicated by V_S tomography. LVL is restricted to areas where Oligocene to present orogenic volcanism has occurred. In contrast, no LVL is observed in zones, such as the Sicily Channel, where only anorogenic volcanism is present. The interpretation of the causal reasons of these relationships is critical for our understanding of magmatism and geodynamics in the Tyrrhenian area and surroundings, especially concerning the long-lived controversy regarding the role of shallow- vs. deep-mantle processes (see Peccerillo and Lustrino 2005 and references therein).

Some authors suggest that the ascent of deep mantle plume had an important role in the magmatism and the geodynamic evolution of the Western Mediterranean and Western-Central Europe (e.g. Vollmer 1976; Hoernle et al. 1995; Gasperini et al. 2002; Piromallo et al. 2008). According to these authors (e.g. Gasperini et al. 2000, 2002) the FOZO or HIMU-type magmas of Etna and the EM1-type magmas in Sardinia represent almost pure though

distinct plume materials. The hyperbolic isotopic trends observed by orogenic rocks (Fig. 5) would be the result of the interaction between plume-related FOZO material and subduction-related crustal components (e.g. Gasperini et al. 2002). The low-velocity material detected in the upper mantle by seismic wave tomography (Hoernle et al. 1995) was interpreted as a deep plume. This would be part of a larger plume emplaced beneath the Eastern Atlantic and Central Europe, even though, on account of the resolution involved ($\sim 0.4\%$ variation of P-wave velocity), its deeper part (below ~ 300 km) is barely distinguishable from normal mantle. However, the low-velocity layer beneath the Western Mediterranean is isolated from the main low-velocity zone of the Eastern Atlantic and such a feature is explained as an effect of detachment from the main plume during emplacement (Hoernle et al. 1995).

Other authors suggest that basin opening, migration of the compression front (Apennines to Maghrebian belt) and the bulk of orogenic magmatism in the Western-Central Mediterranean area may be related to the migration of the Africa-Europe subduction processes from the Southern France-Western Iberian peninsula to its present position in the Southern Tyrrhenian Sea (e.g. Carminati et al. 1998; Doglioni et al. 1999; Faccenna et al. 2001). Orogenic magmatism was the result of introduction of fluids and melts of slab origin above the eastward retreating subduction zone. By contrast, the anorogenic magmatism is suggested as either related to backarc mantle decompression melting or to local melting events along rifting zones at the margin of the African plate where extensional tectonic regime occurs (see Corti et al. 2006 and references therein). FOZO-type isotopic compositions of anorogenic magmas in Sicily are interpreted as indicating resident material evolved in situ, as suggested by Esperança and Crisci (1995). EM1 isotopic composition of Central-Northern Sardinia volcanic rocks is believed to represent lithospheric compositions affected by contamination by delaminated lower crustal during Hercynian or older collisional events (Lustrino et al. 2007b). Interaction between resident mantle and crustal material brought into the upper mantle by Oligocene to present subduction process would be responsible for isotopic trends of orogenic magmas around the Tyrrhenian Sea (e.g. Peccerillo 2003, 2005 and references therein).

S-wave tomography data discussed in this paper provide important new constraints to help interpreting mantle processes and geodynamics in the Tyrrhenian Sea. As pointed out earlier, V_S data show that the LVL beneath the Western Mediterranean occurs exclusively in zones that have been affected by orogenic magmatism from Oligocene to present. This continuous LVL may represent a track of mantle anomalies (i.e. related to fluids and/or melts released from the slab) left behind by the Oligocene to present rollback of the Adriatic-Ionian slab. The occurrence of this layer may have significant effects on the geodynamic evolution of areas behind volcanic arcs. Entering of fluids into the mantle is able to produce a drastic decrease of the viscosity in the low-velocity

layer (Manea and Gurnis 2007), allowing a much faster decoupling between the upper plate and the underlying mantle. This favors detachment and westward drift of the lithosphere and consequent opening of Balearic-Provençal and Tyrrhenian basins.

The nature of the fluid phases occurring in the mantle and generating low V_S values (fluids, silicate melts, carbonate melts or a combination of these) is hard to constrain. The LVL lies at a depth of about 70–120 km between South-Eastern Provence and Central Tyrrhenian Sea (Panza et al. 2007b). This corresponds to a pressure of about 2–4 GPa, a pressure range of minimum solidus temperature for peridotite + CO_2, where carbonatitic liquids are stable. On the other hand, depths of about 60–120 km have been suggested to be the site where abundant silicate arc magmas form within the mantle wedge above subduction zones with dipping angles of about 45° (Schmidt and Poli 1998).

It must be recalled that the nature of the undergoing slab, and consequently the type of fluids/melts released into the mantle wedge, may have changed significantly from Oligocene to present. Early stages of subduction beneath Southern France, Spain and Sardinia took place by consumption of oceanic-type crust (e.g. Carminati et al. 1998). Metasomatic modification of the mantle wedge and magmatism were likely provided by aqueous fluids. In contrast, the latest stages of subduction along the Italian peninsula involved a thinned continental-type crust with large amounts of marls and other carbonate-rich sediments being brought into the upper mantle (e.g. Peccerillo 1999). The role of marly sediments in the generation of geochemical anomalies in the upper mantle beneath the Italian peninsula has long been suggested and modelled (Peccerillo et al. 1988). Their involvement in the mantle contamination during the latest stages of Adriatic plate subduction is able to account for several geochemical and isotopic characteristics of ultrapotassic magmas, but also provides an explanation for intense CO_2 degassing along the Italian peninsula (Frezzotti et al. 2008). Whatever the nature of the fluid phases within the LVL, its occurrence in areas of orogenic volcanism clearly speaks in favor of a close genetic relationship among subduction, arc magmatism and low anomalous V_S mantle material.

The uprise of the LVL to shallow depths beneath Campania and Southern Tyrrhenian Sea volcanic areas may be related to eastward mantle flow against the immerging Ionian-Adriatic slab (Panza et al. 2007b). This could explain, among others, the occurrence of a thin high-velocity layer beneath Ischia (cell# 17; see detailed section in Panza et al. 2007a,b), which had been interpreted as massive intrusions by Panza et al. (2007a) but may, in fact, represent a rigid block of mantle lid that has been lifted to shallow depths by the mantle flow. Such a hypothesis is supported by the anomalous heat flow occurring regionally in the Southern Tyrrhenian area (Fig. 6; Della Vedova et al. 2001), where large scale thermal anomalies could be related to passive

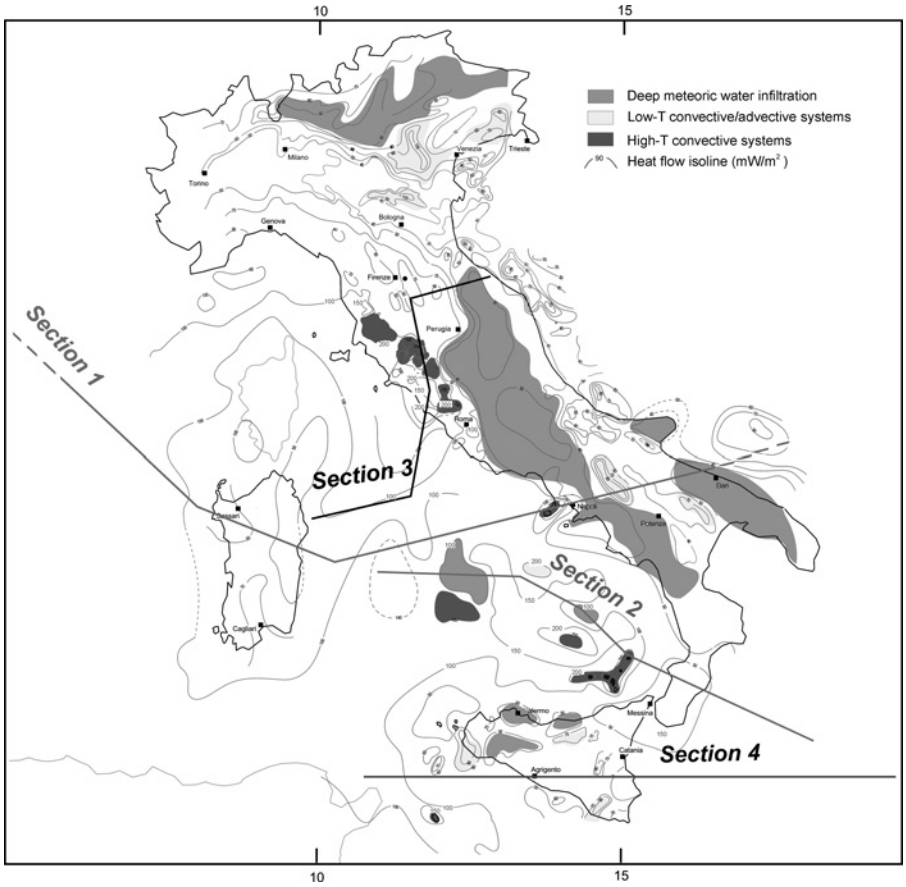

Fig. 6 Heat flow map of Italy and location of the cross sections shown in Fig 3 and 4, simplified after Della Vedova et al. (2001).

upwelling of partially molten mantle material in a region characterized by a strong Plio-Quaternary extensional regime.

The shallow depth and thin LVL beneath Tuscany and Roman regions could also depend on eastward mantle flow against the Adriatic subducting plate. However, a passive ascent of low-density metasomatized peridotite could be envisaged. Geochemical and petrological data have shown that mafic mantle-derived magmatism in Tuscany and in the Roman provinces is the effect of a double metasomatic process, which occurred during Alpine (pre-Oligocene) and Apennine (Oligocene to present) subduction (Peccerillo 2005; Peccerillo and Martinotti 2006). This generated an anomalous mantle whose overall composition and mechanical characteristics were modified profoundly. It is likely, therefore, that ascent of the LVL beneath the Roman area might be related to the low density mantle whose physical characteristics had been extensively modified by multiple metasomatic events.

The heath flow anomaly in the Tuscany-Roman volcanic region, is not apparently related to the presence of a shallow LVL but rather to ponding of large amounts of magmas coming from the mantle. In fact, the anomalous heath flow zone is located along a narrow belt parallel to the Tyrrhenian Sea border. This is also the place where the large multicenter volcanic complexes of the Roman province and the young intrusive magmatism of Southern Tuscany occur (Fig. 6). Therefore, it is likely that the thermal anomalies reflect the occurrence of magmas ponding within the crust or at the Moho. It has to be noted that the overall amount of ultrapotassic magmas emplaced in Central Italy must be much larger than the already huge volumes of products erupted at the surface. Except for a few districts (e.g. Ernici; Frezzotti et al. 2007), lavas and pyroclastic rocks cropping out in the Roman province are, in fact, almost completely formed by evolved magmas (trachytes, phonolites, tephriphonolites, etc.), which represent derivative melts formed by at least 50–60% fractional crystallisation of mafic parents (basanites and trachybasalts). The obvious implication is that very large amounts of mafic parental magmas were generated inside the upper mantle and they are likely stored and cooling at depth in large magma chambers, which representing a suitable source of thermal anomalies.

6 Implications for magmatism and geodynamics

LVL within the upper mantle in the Western Mediterranean has been reliably detected by S-wave tomography. Its occurrence in areas that were affected by Oligocene to present orogenic magmatism, as well as its absence along the northern African margin, support the hypothesis that the low velocities are the effect of fluids/melts related to subduction processes. Moreover, there is little if any geophysical evidence for the ascent of deep mantle plumes beneath the lithosphere in the investigated area, and no geophysical anomalies are detected beneath the anorogenic volcanoes of Sicily and the Sicily Channel. This implies that both the orogenic and anorogenic magmatism may be related to shallow mantle processes, without any need of deep mantle material.

Anorogenic volcanism in the Sicily Channel, Etna and Iblei has been long hypothesised to have sampled deep mantle material with a HIMU or FOZO composition. However, there is no evidence of low-velocity mantle material in this zone from our data. The only lens of soft mantle has been found beneath Ferdinandea-Graham (Fig. 3; cell# D1, D2) and east of Etna. Such a limited extent of soft material might be consistent with a moderate degree of partial melting locally occurring within the mantle beneath Ferdinandea-Graham. This suggests that magmatism along the northern margin of the African plate could be the effect of decompression melting of the upper mantle in extensional setting along the northen margin of the African plate (Grasso 2001; Corti et al. 2006). Obviously, ascent of thin finger-like bodies of mantle material from

the deeper mantle (see Wilson & Patterson 2001) or from the transition zone (Montelli et al. 2004; Cadoux et al. 2007) cannot be excluded by our data but remains highly speculative.

The Plio-Quaternary anorogenic magmatism of Sardinia, however, represents a main problem. It occurs in an area affected by extension behind an eastward migrating subduction zone. The structure of the asthenosphere beneath this island (Fig. 3; cell# 11, 12) is not much different from that of the Balearic Sea and Tyrrhenian basin. Yet, the EM1-type isotopic signatures of the large majority of outcropping rocks are very particular and suggest a different origin with respect to the rest of the anorogenic magmatism of the entire circum-Mediterranean area. We believe that the particular characteristics of the Sardinian Plio-Quaternary rocks can be explained by assuming a generation of magmas within the lithospheric mantle. Note that the Sardinia lid shows very high seismic wave velocities (V_S = 4.40–4.60) that are not found in the lithosphere of other volcanic areas in the region (see also Panza et al. 2007a,b). The unique EM1-type isotopic signatures of Sardinian rocks would, therefore, relate to the particular structure of the lithosphere in this area.

Lustrino et al. (2000, 2007b) suggested that a geochemically anomalous lithospheric mantle is present beneath Sardinia. The process responsible for such an anomaly dates back to Hercynian or pre-Hercynian times when lower crust delamination and foundering within the upper mantle generated low U/Pb and Th/Pb melts that were added to local peridotite. Aging of this material stored for long times in the lithosphere would give EM1-type isotopic signatures. The occurrence of particular mechanical characteristics of the lid accompanied by particular isotopic characteristics of the Plio-Quaternary magmatism strongly supports such a hypothesis.

7 Conclusions

The integrated study of seismic wave velocities and nature of magmatism along some key transects across the Western Mediterranean allow placement of constraints on some of the most debated issues on geodynamics and magmatism in this region.

Low S-wave velocity mantle layers (LVL) are restricted to areas affected by Oligocene to Quaternary volcanism. This supports the hypothesis that mantle seismic anomalies are generated by subduction processes, rather than by plumes ascending from the deep mantle.

The LVL across the Mediterranean lies at depths of about 70–120 km, corresponding to pressures at which carbonatitic magmas are stable and H_2O-C_2O-bearing peridotite shows a minimum in the solidus temperature. This suggests that the LVL developed in the mantle wedge above the subduction of the Adriatic-Ionian plate by melting processes induced by fluid release from

the slab and inflow of hot asthenosphere into the mantle wedge. Uprise of the LVL to shallow depths in the Southern Tyrrhenian Sea is attributed to mantle flow against westward dipping Adriatic-Ionian plates and/or to passive ascent of intensively metasomatized low-density mantle material.

Plio-Quaternary anorogenic volcanism in Sardinia has particular isotopic characteristics (unradiogenic Pb isotopic ratios and moderately radiogenic Sr-Nd), whose significance has been long debated (e.g. Gasperini et al. 2000; Lustino and Dallai 2004; Lustrino et al. 2004, 2007b). S-wave tomography revealed that the mechanical features of the asthenosphere beneath Sardinia is similar to that in the Provençal basin and Central Tyrrhenian Sea, where magmatism does not show the isotopic particularities observed in Sardinia. This rules out an asthenospheric origin of the anorogenic volcanicm in Sardinia. By contrast, a rigid lithospheric mantle with high values of S-wave velocities (V_S = 4.40–4.60) is observed, a feature that is not observed in other volcanic areas in the region. The parallelism between particular isotopic signature of recent magmatism and unique rigid structure of the lithosphere strongly supports the hypothesis of a lithospheric origin for anorogenic Plio-Quaternary magmatism in Sardinia.

Finally, the magmatism at Etna and along the northern border of the African plate has been considered as representative of either pure plume material (FOZO at Etna) or as a mixture between plume and lithosphere. The absence of significant geophysical anomalies in this area argues against the presence of large active mantle plumes. The small scale low-velocity observed at restricted areas (e.g. beneath the active Ferdinandea-Graham Island) could well reveal local melting events occurred in an extensional setting developed at the collision zone between Africa and Europe.

Acknowledgements. This research is funded by the Italian MIUR PRIN 2004 project (Modelling of the mantle-crust system by petrological and geophysical methods), the SISMA – Italian Space Agency project, University of Perugia, University of Siena and the Italian Presidenza del Consiglio dei Ministri – Dipartimento della Protezione Civile (project S1 of Convenzione DPC-INGV 2007–09) Thorough and constructive reviews by C. Doglioni and M. Lustrino, Università La Sapienza, Rome, are gratefully acknowledged.

References

1. Argnani A, Savelli C (1999) Cenozoic volcanism and tectonics in the southern Tyrrhenian Sea: space-time distribution and geodynamic significance. Geodynamics 27: 409–432
2. Boyadzhiev G, Brandmayr E, Pinat T, Panza GF (2008) Optimization for nonlinear inverse problem. Rendiconti Lincei 19: 17–43. DOI: 10.1007/s12210-008-0002-z
3. Cadoux A, Blichert-Toft J, Pinti DL, Albarède F (2007) A unique lower mantle source for Southern Italy volcanics. Earth and Planetary Science Letters 259: 227–238
4. Carminati E, Wortel MJR, Spakman W, Sabadini R (1998) The role of slab detachment processes in the opening of the western-central Mediterranean basins: some geological and geophysical evidence. Earth and Planetary Science Letters 160: 651–665

5. Carminati E, Doglioni C, Carrara G, Dabovski C, Dumurdjanov N, Gaetani M, Georgiev G, Mauffret A, Sartori R, Seranne M, Scrocca D, Scionti V, Torelli L, Zagorchev I, Argnani A (2004) Transmed: section III. IGC Florence, CD-rom
6. Civetta L, D'Antonio M, Orsi G, Tilton GR (1998) The geochemistry of volcanic rocks from Pantelleria Island, Sicily Channel: petrogenesis and characteristics of the mantle source region. Journal of Petrology 39: 1453–1491
7. Corti G, Cuffaro M, Doglioni C, Innocenti F, Manetti P. (2006) Coexisting geodynamic processes in the Sicily Channel. In: Y. Dilek & S. Pavlides (Eds), Postcollisional tectonics and magmatism in the Mediterranean region and Asia. Geological Society of America Special Paper 409: 83–96
8. De Astis G, Kempton PD, Peccerillo A, Wu TW (2006) Trace element and isotopic variations from Mt. Vulture to Campanian volcanoes: constraints for slab detachment and mantle inflow beneath southern Italy. Contributions to Mineralogy and Petrology 151: 331–351, DOI: 10.1007/s00410-006-0062-y
9. Della Vedova B, Bellani S, Pellis G, Squarci P (2001) Deep temperatures and surface heat flow density distribution. In: Vai GB, Martini P (eds) Anatomy of an orogen: the Apennines and adjacent Mediterranean Basins, Kluwer Academic Publishers, Dordrecht, Netherlands: 65–76
10. Di Bella M, Russo S, Petrelli M, Peccerillo A (2008) Origin and evolution of the Pleistocene Magmatism of Linosa Island (Sicily Channel, Italy). European Journal of Mineralogy 20: in press
11. Doglioni C, Mongelli F, Pialli G (1998) Boudinage of the Alpine belt in the Apenninic back-arc. Memorie Società Geologica Italiano 52: 457–468
12. Doglioni C, Harabaglia P, Merlini S, Mongelli F, Peccerillo A, Piromallo C (1999) Orogens and slabs vs. their direction of subduction. Earth Science Reviews 45: 167–208.
13. Esperança S, Crisci GM (1995) The island of Pantelleria: a case for the development of DMM-HIMU isotopic compositions in a long-lived extensional setting. Earth and Planetary Science Letters 136: 167–182
14. Faccenna C, Becker TW, Lucente FP, Jolivet L, Rosseti F (2001) History of subduction and back-arc extension in the Central Mediterranean. Geophysical Journal International 145: 809–820
15. Foulger GR, Nathland JH, Presnall DC, Anderson DL (eds) Plates, plumes and paradigms. Geological Society of America Special Publication 388, 881 pp
16. Frezzotti ML, De Astis G, Dallai L, Ghezzo C (2007) Coexisting calc-alkaline and ultrapotassic magmatism at Monti Ernici, Mid Latina Valley (Latium, Central Italy). European Journal of Mineralogy 19: 479–497
17. Frezzotti ML, Peccerillo A, Panza G (2008) CO_2 lithosphere-asthenosphere degassing beneath the western Mediterranean: an integrated model arising from petrological and geophysical data. Submitted to Chemical Geology
18. Gasperini D, Blichert-Toft J, Bosch D, Del Moro A, Macera P, Télouk P, Albaréde F (2000) Evidence from Sardinian basalt geochemistry for recycling of plume heads into the Earth's mantle. Nature 408: 701–704
19. Gasperini D, Blichert Toft J, Bosch D, Del Moro A, Macera P, Albaréde F (2002) Upwelling of deep mantle material through a plate window: evidence from the geochemistry of Italian basaltic volcanics. Journal of Geophysical Research 107, B12, 2367, DOI: 10.1029/2001JB000418
20. Grasso M (2001) The Apenninic-Maghrebian orogen in Southern Italy, Sicily and adjacent areas. In: Vai GB, Martini PI (eds) Anatomy of an Orogen. The Apennines and adjacent Mediterranean basins. Kluwer, Dordrecht: 255–286
21. Hawkesworth CJ, Vollmer R (1979) Crustal contamination vs. enriched mantle: $^{143}Nd/^{144}Nd$ and $^{87}Sr/^{86}Sr$ evidence from the Italian volcanics. Contributions to Mineralogy and Petrology 69: 151–165

22. Hoernle K, Zhang YS, Graham D (1995) Seismic and geochemical evidence for large-scale mantle upwelling beneath the eastern Atlantic and western and central Europe. Nature 374: 34–112
23. Hoernle K, Behncke B, Schmincke H-U (1996) The geochemistry of basalt from the Iblean Hills (Sicily) and the Island of Linosa (Strait of Sicily): evidence for a plume from the lower mantle. Goldschmidt Conf, J Conf Abstr 1: 264; www.the-conference.com/JConfAbs/1/264.html
24. Hofmann AW (1997) Mantle geochemistry: the message from oceanic volcanism. Nature 385: 219–229
25. Locardi E (1988) The origin of the Apenninic arc. Tectonophysics 146: 105–123.
26. Lustrino M, Dallai L (2004) On the origin of EM-I end-member. Neues Jahrbuch für Mineralogie Abhandlungen 179: 85–100
27. Lustrino M, Carminati E (2007) Phantom plumes in Europe and the circum-Mediterranean region. In: Foulger G.R. and Jurdy D.M. (eds) Plates, plumes, and planetari processes. Geological Society of America Special Publication 430: 723–746
28. Lustrino M, Wilson M (2007) The circum-Mediterranean anorogenic Cenozoic Igneous Province. Earth Science Reviews 81: 1–65
29. Lustrino M, Melluso L, Morra V (2000) The role of lower continental crust and lithospheric mantle in the genesis of Plio-Pleistocene volcanic rocks from Sardinia (Italy). Earth Planetary Science Letters 180: 259–270
30. Lustrino M, Morra V, Melluso L, Brotzu P, D'Amelio F, Fedele L, Lonis R, Franciosi L, Petteruti Liebercknect AM (2004) The Cenozoic igneous activity in Sardinia. Periodico di Mineralogia 73: 105–134
31. Lustrino M., Morra V., Fedele L., Serracino M. 2007a. The transition between "orogenic" and "anorogenic" magmatism in the western Mediterranean area: the middle Miocene volcanic rocks of Isola del Toro (SW Sardinia, Italy). Terra Nova 19: 148–159
32. Lustrino M., Melluso L., Morra V. 2007b. The geochemical peculiarity of "Plio-Quaternary" volcanic rocks of Sardinia in the circum-Mediterranean area. In: Beccaluva L., Bianchini G. and Wilson M. (eds) Cenozoic volcanism in the Mediterranean area. Geological Society of America Special Publication 418: 277–301
33. Manea V, Gurnis M (2007) Subduction zone evolution and low viscosity wedges and channels. Earth Planetary Science Letters 264: 22–45
34. Montelli R., Nolet G., Dahlen F.A., Masters G., Engdahl E.R., Hung S.H. 2004. Finite-frequency tomography reveals a variety of plumes in the mantle. Science 303: 338–343
35. Panza GF, Peccerillo A, Aoudia A, Farina B (2007a) Geophysical and petrological modeling of the structure and composition of the crust and upper mantle in complex geodynamic settings: The Tyrrhenian Sea and surroundings. Earth Science Reviews 80: 1–46
36. Panza GF, Raykova R, Carminati E, Doglioni C (2007b) Upper mantle flow in the western Mediterranean. Earth Planetary Science Letters 257: 200–214
37. Panza GF, Pontevivo A, Chimera G, Raykova R, Aoudia A (2003) The lithosphere-asthenosphere: Italy and surroundings. Episodes 26: 169–174
38. Peccerillo A (1999) Multiple mantle metasomatism in central-southern Italy: geochemical effects, timing and geodynamic implications. Geology 27: 315–318
39. Peccerillo A (2003) Plio-Quaternary magmatism in Italy. Episodes 26: 222–226
40. Peccerillo A (2005) Plio-Quaternary volcanism in Italy. Petrology, geochemistry, geodynamics. Springer, Heidelberg, 365 pp
41. Peccerillo A, Panza GF(1999) Upper mantle domains beneath Central-Southern Italy: petrological, geochemical and geophysical constraints. Pure Applied Geophysics 156: 421–443
42. Peccerillo A, Lustrino M (2005) Compositional variations of the Plio-Quaternary magmatism in the circum-Tyrrhenian area: deep- vs. shallow-mantle processes. In: Foulger GR,

Nathland JH, Presnall DC, Anderson DL (eds) Plates, plumes and paradigms. Geological Society of America Special Publication 388: 421–434
43. Peccerillo A, Martinotti G (2006) The Western Mediterranean lamproitic magmatism: origin and geodynamic significance. Terra Nova 18: 109–117
44. Peccerillo A, Poli G, Serri G (1988) Petrogenesis of orenditic and kamafugitic rocks from Central Italy. Canadian Mineralogist 26: 45–65
45. Piromallo C, Gasperini D, Macera P, Faccenna C (2008) A late Cretaceous contamination episode of the European-Mediterranean mantle. Earth Planetary Science Letters 268, DOI: 10.1016/j.epsl.2007.12.019
46. Rosenbaum G, Gasparon M, Lucente P, Peccerillo A, Miller MS (2008) Kinematics of slab tear faults during subduction segmentation and implications for Italian magmatism. Tectonics, 27: DOI: 10.1029/2007TC002143
47. Rotolo SG, Castorina D, Cellura D, Pompilio M (2006) Petrology and Geochemistry of Submarine Volcanism in the Sicily Channel Rift. Journal of Geology 114: 355–365
48. Sartori R (2003) The Thyrrhenian backarc basin and subduction of the Ionian lithosphere. Episodes 26: 217–221
49. Savelli C, Gasparotto G (1994) Calc-alkaline magmatism and rifting of the deep-water volcano of Marsili (Aeolian back-arc, Tyrrhenian Sea). Marine Geology 119: 137–157
50. Schmidt MW, Poli S (1998) Experimentally based water budgets for dehydrating slabs and consequences for arc magma generation. Earth and Planetary Science Letters163: 361–379
51. Stracke A, Hofmann AW, Hart SR (2005) FOZO, HIMU, and the rest of the mantle zoo, Geochememistry Geophysics Geosystems 6, Q05007, DOI: 10.1029/2004GC000824
52. Turco A, Zuppetta A (1998) Kinematic model for the Plio-Quaternary evolution of the Tyrrhenian-Apenninic system: implications for rifting processes and volcanism. Journal of Volcanology and Geothermal Research 82: 1–18
53. Vollmer R (1976) Rb-Sr and U-Th-Pb systematics of the alkaline rocks for Italy. Geochimica et Cosmochimica Acta 40: 283–295
54. Wilson M, Patterson R (1991) Intraplate magmatism related to short-wavelength convective instabilities in the upper mantle: Evidence from Tertiary-Quaternary volcanic province of western and central Europe. In: Ernst RE, Buchan KL (eds) Mantle Plumes: Their Identification through time. Geological Society of America Special Publication 352: 37–58

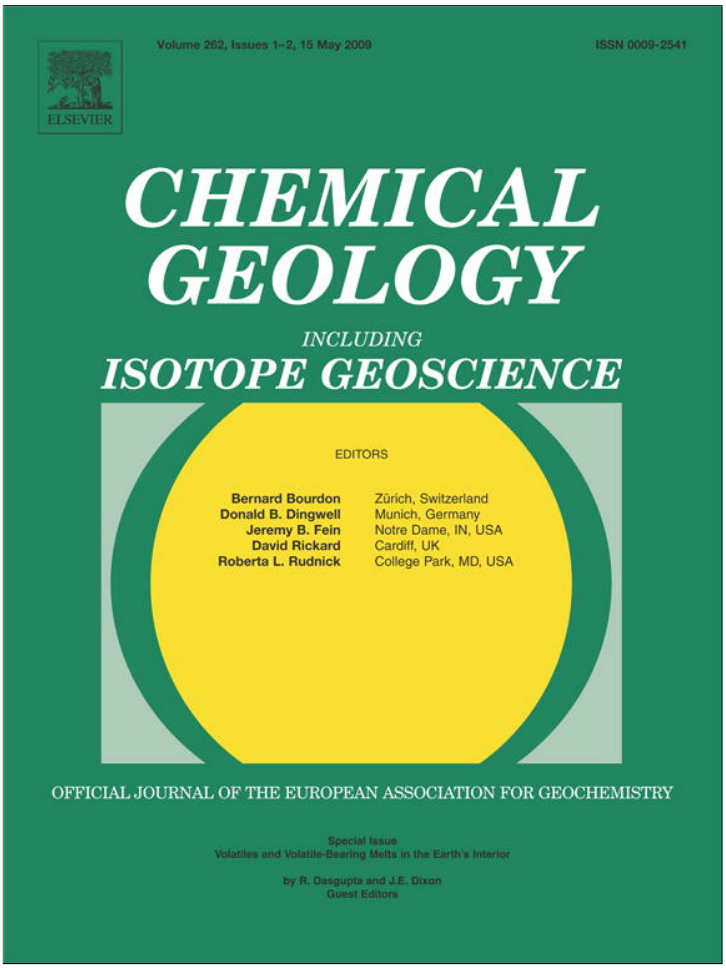

Chemical Geology 262 (2009) 108–120

Contents lists available at ScienceDirect

Chemical Geology

journal homepage: www.elsevier.com/locate/chemgeo

Carbonate metasomatism and CO_2 lithosphere–asthenosphere degassing beneath the Western Mediterranean: An integrated model arising from petrological and geophysical data

Maria Luce Frezzotti [a,*], Angelo Peccerillo [b], Giuliano Panza [c,d]

[a] Dipartimento di Scienze della Terra, Università degli Studi di Siena, Siena, Italy
[b] Dipartimento di Scienze della Terra, Università degli Studi di Perugia, Perugia, Italy
[c] Dipartimento di Scienze della Terra, Università degli Studi di Trieste, Trieste, Italy
[d] The Abdus Salam International Centre for Theoretical Physics, Trieste, Italy

ARTICLE INFO

Article history:
Accepted 24 February 2009

Keywords:
CO_2 Earth degassing
Carbonate melts
Mantle metasomatism
Magmatism
Surface-wave tomography
Western Mediterranean

ABSTRACT

We present an integrated petrological, geochemical, and geophysical model that offers an explanation for the present-day anomalously high non-volcanic deep (mantle derived) CO_2 emission in the Tyrrhenian region. We investigate how decarbonation or melting of carbonate-rich lithologies from a subducted lithosphere may affect the efficiency of carbon release in the lithosphere–asthenosphere system. We propose that melting of sediments and/or continental crust of the subducted Adriatic–Ionian (African) lithosphere at pressure greater than 4 GPa (130 km) may represent an efficient mean for carbon cycling into the upper mantle and into the exosphere in the Western Mediterranean area. Melting of carbonated lithologies, induced by the progressive rise of mantle temperatures behind the eastward retreating Adriatic–Ionian subducting plate, generates low fractions of carbonate-rich (hydrous-silicate) melts. Due to their low density and viscosity, such melts can migrate upward through the mantle, forming a carbonated partially molten CO_2-rich mantle recorded by tomographic images in the depth range from 130 to 60 km. Upwelling in the mantle of carbonate-rich melts to depths less than 60–70 km, induces massive outgassing of CO_2. Buoyancy forces, probably favored by fluid overpressures, are able to allow migration of CO_2 from the mantle to the surface, through deep lithospheric faults, and its accumulation beneath the Moho and within the lower crust. The present model may also explain CO_2 enrichment of the Etna active volcano. Deep CO_2 cycling is tentatively quantified in terms of conservative carbon mantle flux in the investigated area.

1. Introduction

The role of Earth degassing in present-day global carbon budget and consequent climate effects has been focused chiefly on volcanic emissions (e.g. Gerlach, 1991a; Varekamp and Thomas, 1998; Kerrick, 2001). The non-volcanic[1] escape of CO_2 from the upper mantle, from crustal carbonate rocks, from hydrocarbon accumulations, and from geothermal fields is not considered in the budgets of natural release processes (cf. IPCC reports). However, the impact of these processes on atmospheric CO_2 budget is relevant if considered at the regional scale.

Italy constitutes an extraordinary example of massive CO_2 subaerial fluxes in the Western Mediterranean region (e.g. Chiodini et al., 1999; Rogie et al., 2000; Chiodini and Frondini 2001; Chiodini et al., 2004; Minissale, 2004). In Italy, CO_2 emissions occur both in those areas of young or active volcanism (e.g. the Tyrrhenian border of Central Italy; Fig. 1), and at zones in which there is no evidence of magmatic activity, such as Central and Southern Apennines (Fig. 1).

Interactions between magmas and carbonate rocks at walls of magma chambers locally contribute CO_2 in some recent and active volcanic zones (e.g., Alban Hills, Mt. Ernici, Vesuvius; Federico and Peccerillo, 2002; Dallai et al., 2004; Frezzotti et al., 2007; Iacono Marziano et al., 2007a,b). However, the bulk of present-day soil degassing in Italy is a regional feature affecting both volcanic areas and zones where volcanism is unknown (e.g. Apennines). This suggests that the non-volcanic "cold" CO_2 degassing in Italy has a deep origin (i.e., upper mantle), mainly based on isotope data (e.g. $^{12}C/^{13}C$ and $^{3}He/^{4}He$; Chiodini et al., 1999; Italiano et al., 2001; Minissale, 2004; Chiodini et al., 2004; Italiano et al., 2007).

In this paper, we integrate the V_S tomography of the lithosphere–asthenosphere system along some key sections in the Western Mediterranean region, the geodynamic evolution of the study area,

* Corresponding author. Tel.: +39 0577233929; fax: +39 0577233938.
E-mail address: frezzottiml@unisi.it (M.L. Frezzotti).

[1] CO_2 that is not released from the craters and flanks of volcanoes. Although non-volcanic degassing can be associated with recent volcanism, CO_2 does not originate in magma chambers, and it is not discharged through the volcanic systems (Kerrick, 2001).

0009-2541/$ – see front matter © 2009 Elsevier B.V. All rights reserved.
doi:10.1016/j.chemgeo.2009.02.015

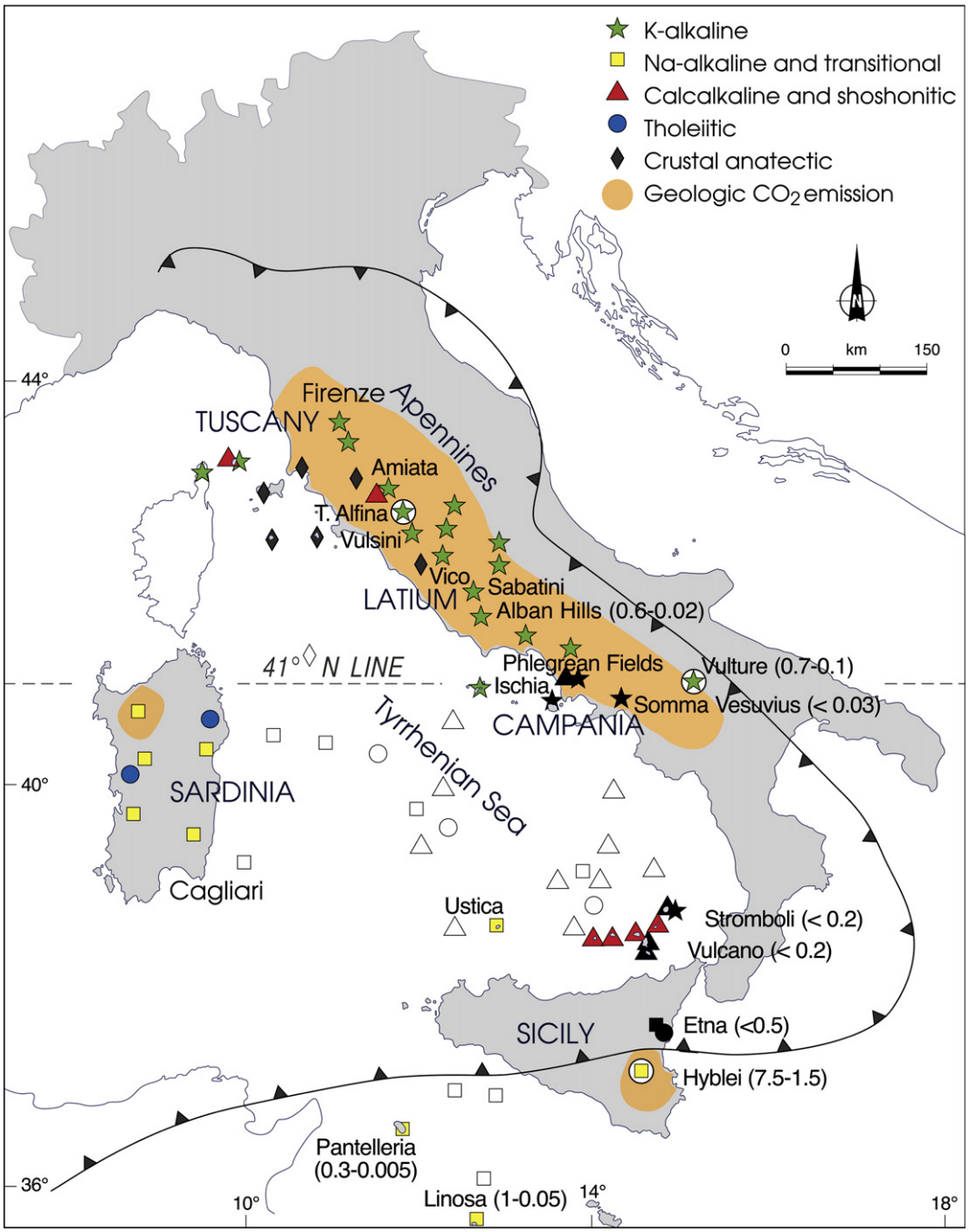

Fig. 1. Distribution of main geological CO_2 emission in Italy (gray area), as derived from the on-line catalogue of Italian gas emissions, INGV-DPCV5 project (http://googas.ov.ingv.it), and of petrochemical affinities and ages of the main Plio-Quaternary magmatic centers in Italy, modified from Peccerillo (2005). Volcanic centers marked by white circle bear peridotites. Active volcanoes are marked in black. Open symbols refer to outcrops below the sea level. Ages in parenthesis.

the properties of mantle rocks, and the timing and the nature of the magmatism to discuss a model of mantle metasomatism, which can account for deep carbon cycling and CO_2 degassing to the exosphere.

2. Nature of geologic CO_2 emission in Italy

A summary of recent CO_2 emission measurements in Italy is reported in Fig. 1 and Table 1, based on literature data. Active volcanoes represent a prominent natural source of CO_2 to the pre-industrial atmosphere in Italy, possibly since they started to build up (>0.1 Ma). At Etna (Fig. 1), CO_2 fluxes ranging from 13 to 43.8 Mt/year (average 25 Mt/year) were measured from 1976 to 1984 (Gerlach, 1991a,b; Allard et al., 1991). Lower values, between 4 and 13 Mt/year, were obtained from 1993 to 1997, due to a decrease of the CO_2 emission rate after the 1991–1993 eruption (Allard et al., 1997). At Etna, further CO_2 degassing occurs from the summit area and the lower S–SW and E flanks (1–5 Mt/year), and from ground waters (0.4 Mt/year). On average, Etna emits more CO_2 than many other volcanoes worldwide (e.g. 3.1 Mt CO_2/year from Kilauea; Gerlach et al., 2002; Table 1) and contributes about 5–10% of the total estimated global CO_2 emissions by subaerial volcanism (cf. Mörner and Etiope, 2002). Other active volcanoes (e.g., Vesuvius, Phlegrean Fields, Stromboli, Vulcano) contribute substantially to the overall atmospheric CO_2 budget in the Western Mediterranean region, which is conservatively (lower bound) estimated at about 30 Mt CO_2/year (see references in Table 1).

Table 1
Geologic CO_2 degassing in Italy.

	Output (Mt/year)
Volcanic	
Crater emission	
Etna (1976–1985)[a, b]	25.5
Etna (1993–1997)[c]	4–13
Stromboli[d]	1–2
Vulcano[e]	0.066
Ground emission	
Vulcano Fossa crater[f]	0.073
Vulcano plains[g]	0.027
Vulcano fumaroles[h]	0.088
Stromboli[i]	0.07–0.09
Vesuvius[j]	0.5
Solfatara, Phl. Fields[k]	1.8
Ischia[l]	0.14
Non-volcanic	
Regional	
Central Italy[m]	>4
Central Italy[n]	9.7–17
Central Apennines[o]	4–13.2
Tuscany and N Latium[p]	6
Campania[p]	3
Soil degassing	
Latera, Vulsini[m]	>0.07
Alban Hills[p]	0.2
Siena graben[q]	>0.5
Ustica[r]	0.02
Gas vents	
Mefite d'Ansanto[m]	0.3
Rapolano, Tuscany[o]	0.035
Mofeta dei Palici, Sicily[s]	0.091
Geothermal Fields	
Mt. Amiata, Tuscany[t]	0.5

[a] Allard et al. (1991).
[b] Gerlach (1991a,b).
[c] Allard et al. (1997).
[d] Allard et al. (1994).
[e] Baubron et al. (1990).
[f] Chiodini et al. (1996).
[g] Chiodini et al. (1998).
[h] Italiano et al. (1998).
[i] Carapezza and Federico (2000).
[j] Frondini et al. (2004).
[k] Caliro et al. (2008).
[l] Aiuppa et al. (2007).
[m] Rogie et al. (2000).
[n] Gambardella et al. (2004).
[o] Chiodini et al. (2000).
[p] Chiodini et al. (2004).
[q] Etiope (1996).
[r] Etiope (1999).
[s] De Gregorio et al. (2002).
[t] Frondini et al. (2008).

Degassing of "cold" CO_2 in areas where volcanism is not anymore active or is absent occurs via diffuse soil emission, dry gas vents, and from thermal and cold springs associated with fault and fractures often of deep origin (e.g., Chiodini et al., 1998; Chiodini et al., 1999; Etiope, 1999; Italiano et al., 2000; Rogie et al., 2000; Chiodini et al., 2000; Mörner and Etiope, 2002; Chiodini et al., 2004; Minissale, 2004; Gambardella et al., 2004) (see also Fig. 1). Regional CO_2 flux mapping for Central Italy indicates emissions of about 9.7–17 Mt CO_2/year in an area of 45,000 km^2 (Tuscany, Northern Latium geothermal fields, and Central Apennine chain; Gambardella et al., 2004, Table 1). The total budget of ground CO_2 degassing is comparable with the volcanic output (from >4 to 30 Mt/year; cf. Mörner and Etiope, 2002).

A close association between CO_2 escape and the main geological structures is evident: a CO_2 flux of 4–13 Mt/year has been estimated in the axial zones of the Apennines chain (Chiodini et al., 2004 and references therein; see also Table 1). Some 0.1 to 0.3 Mt CO_2/year are emitted from gas vents at the Mefite of the Ansanto valley (Irpinia), located in the external parts of the Apennines, right over the hypocenter of the 1980 earthquake along the deep so called *41° N parallel line* (Fig. 1; Italiano et al., 2000; Rogie et al., 2000). Focused high CO_2 fluxes are also measured in the Siena–Radicofani Graben (Tuscany), and in Sicily from mofetes distributed along two directions, corresponding to major fault systems that cut Eastern Sicily (De Gregorio et al., 2002). In Sardinia, CO_2 fluid degassing occurs, in the northern part of the Campidano Graben, from faults in the Logudoro basin (Minissale et al., 1999).

Carbon and helium isotope compositions have been used to constrain the origin of CO_2 in non-volcanic soil emissions. $^3He/^4He$ ratios from gases, summarized in Fig. 2 (R/Ra up to 4.48; Minissale, 2004), indicate an important mantle component, and are similar to R/Ra measured in lavas of Plio-Quaternary volcanoes. Chiodini et al. (2000) report that about 40% of the inorganic carbon in non-volcanic CO_2 derive from a source characterized by a $\delta^{13}C$ of −3‰, compatible with a mantle metasomatized by crustal fluids, and/or with mixed crust + mantle.

Isotope data have led most Authors (e.g., Chiodini et al., 2004; Minissale, 2004, and references therein) to propose that mantle CO_2 contributes significantly to present-day degassing processes in Central-Southern Italy. CO_2 rising from the mantle would accumulate at the Moho or within the lower crust. Namely, direct degassing of CO_2 at the surface in the zones of thinned continental crust would occur through extensional fault systems, typical of such a context. Conversely, in those areas (like some sectors of the Apennines) characterized by a thickened continental crust and little extension, mantle-derived CO_2 would remain confined in structural traps. Crustal CO_2 confinement might result in over-pressurized reservoirs, which would facilitate seismogenesis, like the Colfiorito 1997 earthquake (Chimera et al., 2003; Miller et al., 2004).

3. Overview of the geodynamic evolution

The Oligocene to present evolution of the Western-Central Mediterranean region has been characterized by the separation of

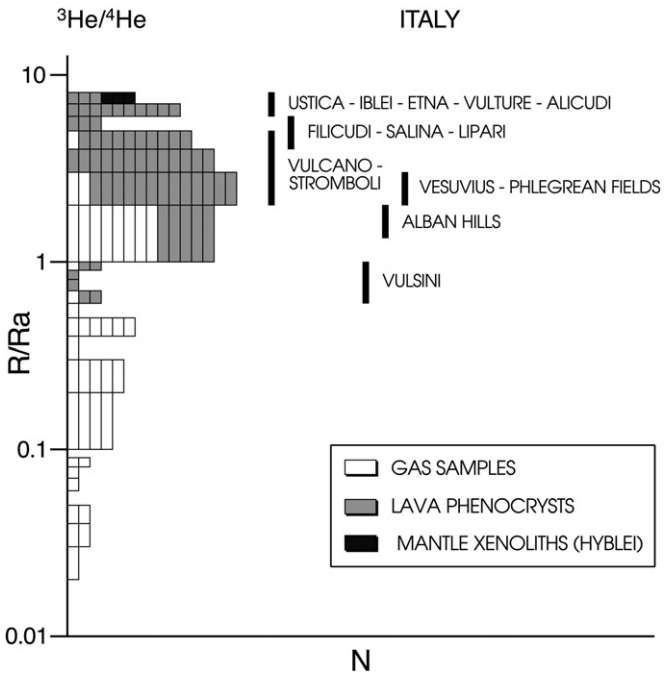

Fig. 2. Compilation of $^3He/^4He$ ratios (R/Ra), and distribution of helium isotopes in Italy, measured in gas sampled at surface, and in fluid inclusions from Plio-Quaternary magma phenocrysts (olivine and clinopyroxene) and from mantle xenoliths (Minissale, 2004; Martelli et al., 2004; 2008). *N* = number of measurements.

the Corsica–Sardinia block from the southern European margin, the opening of the Ligurian–Provençal, Algerian, and Valencia basins, and by the opening of the Tyrrhenian Sea and counter-clockwise rotation of the Italian peninsula (e.g., Doglioni et al., 1997, 1999; Carminati et al., 1998; Faccenna et al., 2001; Peresan et al., 2007). There is a general consensus that these structural modifications are related to Oligocene to Present west-dipping subduction of the African plate beneath the southern European margin, which migrated from west to east, up to its present position in the southern Tyrrhenian Sea. The Balearic–Provençal Sea opened as a back arc basin between approximately 32 to 15 Ma ago, contemporaneously with orogenic (mainly calc-alkaline) magmatism, which migrated eastward with time from Provence and Balearic Sea to Sardinia (see Lustrino et al., 2004, 2007a,b for a review). The Tyrrhenian Sea opened behind the west-dipping Adriatic–Ionian sectors of the African plate between about 15 Ma and the present, and was accompanied by the eastward migration of the orogenic magmatic activity (Savelli and Gasparotto, 1994). The average lithospheric models proposed for the two basins by Panza and Calcagnile (1979) agree with these age estimates. Parallel zones of compression (at the front) and extension (in the back arc basins) migrated towards the east, in the same direction of the magmatism (Pauselli et al., 2006).

The opening of the Tyrrhenian Sea and the counterclockwise rotation of the Italian peninsula resulted in the longitudinal stretching and fragmentation of the Apennine chain, with formation of several arc sectors separated by important transverse tectonic lines (e.g., the so called *41° N parallel line*, the Sangineto fault, the Tindari–Letojanni fault; Locardi, 1988; Turco and Zuppetta 1998; Rosenbaum et al., 2008). These structures separate crustal blocks characterized by different drifting velocity, structure of the lithosphere, and degrees of block rotation (Peresan et al., 2007), and by different compositions of the volcanism (Turco and Zuppetta 1998; Peccerillo, 1999; Peccerillo and Panza, 1999). Extensional tectonics affected the margin of the African foreland (Corti et al., 2006) where Oceanic Island Basalt (OIB)-type magmatism occurred, starting from the Miocene.

4. Overview of the magmatism

A wide variety of magma types occur in the Western Mediterranean (Fig. 3). These have been divided into two broad groups, showing distinct geological setting, incompatible element, and radiogenic isotope signatures (Peccerillo, 2005; Peccerillo and Lustrino, 2005; Lustrino and Wilson, 2007). The first group of magmas, generally referred to as "orogenic", has been erupted in Provence, Balearic Sea, Sardinia, the Southern Tyrrhenian Sea and the Italian peninsula, i.e. in zones which were affected by the Oligocene to present subduction of the African plate beneath the southern European margin. The petrochemical affinity of these magmas is mainly calc-alkaline with some arc tholeiites in Sardinia, Balearic Sea, and Provence (Lustrino et al., 2004), whereas it is calc-alkaline to shoshonitic and ultrapotassic in the Aeolian arc and in Central Italy (e.g. Francalanci et al., 1993; Peccerillo, 2003; Fig. 1). Orogenic magmas show high LILE/HFSE ratios, with negative Nb, Ta and Ti anomalies, and positive spikes of Pb in their mantle-normalized patterns, features that are typical of volcanic rocks erupted at converging plate margins.

Ages of orogenic magmas are variable. Oldest rocks occur in Provence, Balearic Sea and Sardinia (Oligo-Miocene; Fig. 3) and become younger in the Tyrrhenian Sea floor, in the Italian peninsula and the Aeolian arc (Miocene to present). The decrease in age from west to east would be related to the slab rollback and migration of the subduction zone in the same direction (Carminati et al., 1998; Doglioni et al., 1999 and references therein).

Calc-alkaline to ultrapotassic orogenic magmas along the Italian peninsula and in the Aeolian arc have variable degrees of evolution, from mafic to felsic. The most mafic rocks possess high Mg# ($Mg/(Mg+Fe^{2+})$ atomic ratios >70), Ni (>100–200 ppm) and Cr (>500 ppm), and low $\delta^{18}O$ (~+5.5 to +6.0). These are typical of mantle-derived magmas, which have suffered little or no crustal contamination during emplacement. However, these rocks also have Sr–Nd–Pb–Hf isotope compositions that are intermediate between mantle and upper crust, with crustal-like isotopic signatures

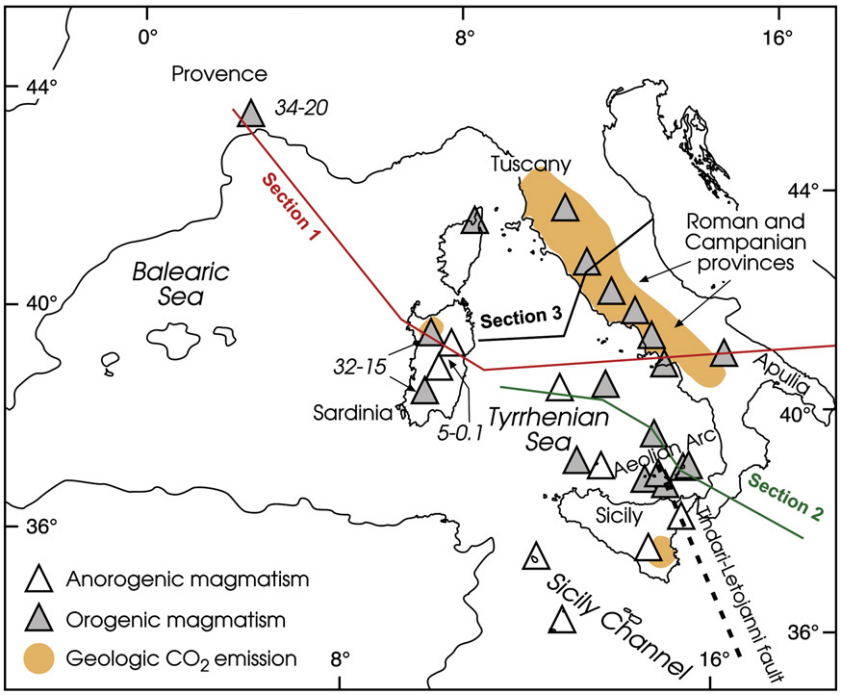

Fig. 3. Location of the orogenic and anorogenic Plio-Quaternary volcanism in the Western Mediterranean (from Peccerillo, 2003), with respect to geological CO_2 emission areas. Numbered lines represent the pathway of sections illustrated in Fig. 4.

increasing northward, where some K-alkaline basalts have radiogenic isotope ratios closer to crustal than to mantle compositions. Helium isotope composition determined on fluid inclusions in olivine and clinopyroxene phenocrysts (Martelli et al., 2008) shows a general decrease in $^{3}He/^{4}He$ moving northward (Fig. 2), which correlates with whole rock radiogenic isotopes increase in $^{87}Sr/^{86}Sr$, and decrease in $^{143}Nd/^{144}Nd$, $^{176}Hf/^{177}Hf$, and $^{206}Pb/^{204}Pb$ (Peccerillo, 2005; Martelli et al., 2008, and references therein).

These data have led several Authors (e.g., Peccerillo, 1985; Rogers et al., 1985; Conticelli et al., 2002; Peccerillo, 2005 and references therein) to conclude that mixing between upper crust and mantle components played a key role in the genesis of magmatism along the Italian peninsula and that such interaction occurred within the upper mantle. Melting of such a heterogeneously contaminated mantle generated various types of mafic melts exhibiting hybrid isotopic signatures between crust and mantle. Based on trace element and radiogenic isotope modeling, Peccerillo (1985) and Peccerillo et al. (1988) proposed that marly sediments were introduced by subduction processes into the upper mantle beneath Central-Southern Italy, generating a variably metasomatized source. The involvement of marly sediments in the mantle contamination during the latest stages of Adria plate subduction is able to account for several petrological, geochemical and isotopic characteristics of ultrapotassic magmas in Central Italy (Conticelli and Peccerillo, 1992; Conticelli et al., 2002; Schmidt, 2007).

A second group of magmas, generally referred as "anorogenic", has been erupted in back arc position and along the northern margin of the African foreland (Fig. 3). These have low LILE/HFSE ratios, generally with positive spikes of Ta and Nb, and no Pb anomalies. Sr-isotope signatures are poorly to moderately radiogenic, whereas Nd, and especially Pb isotopes are variable, and cover almost entirely the range of values shown by OIB-, and MORB-type magmas at global scale (see, Peccerillo, 2005; Stracke et al., 2005). Anorogenic magmas in the study area have been mainly erupted from 5 to 0.1 Ma ago in Sardinia, with incipient activity recently detected at about 12 Ma (Lustrino et al., 2007b), contemporaneously with the opening of the Tyrrhenian Sea (Lustrino et al., 2004), at several places in the Tyrrhenian basin (e.g., Ustica and several seamounts; Fig. 3), along the Sicily Channel (Miocene to present: Pantelleria, Linosa, and several seamounts; Calanchi et al., 1989; Rotolo et al., 2007; Di Bella et al., 2008), at Hyblei, and Etna (0.5 M.y. to present). Etna, overall showing OIB-type composition, also possesses some geochemical and isotopic signatures (e.g., relatively low Ti, high fluid-mobile element contents, relatively high $\delta^{11}B \sim -3$ to -5) that are close to arc magmas (see Schiano et al., 2001; Tonarini et al., 2001). The Tyrrhenian Sea anorogenic magmatism includes abundant MORB-type magmas forming new oceanic crust and some weakly Na-alkaline centers with an age ranging from 7 to 0.1 Ma (Peccerillo, 2005, and references therein).

5. Mantle structure beneath the Western Mediterranean

5.1. Present-day imaging: V_S tomography

Sample profiles of the three dimensional S-wave model obtained by the non-linear inversion of surface wave (Panza, 1981) tomography data in the Western Mediterranean and the Tyrrhenian Sea area are shown in Fig. 4. The complete description of the data coverage is given in Fig. 2 of Panza et al. (2007b). The detailed discussion of the lateral resolution and of the uncertainty in the models is given by Panza et al. (2007b) and Pontevivo and Panza (2006). The vertical resolution is controlled according to the results of Knopoff and Panza (1977) and Panza (1981). As a rule, the three dimensional variations evidenced satisfy the principle of maximum smoothness (Boyadzhiev et al., 2008) and are consistent with the resolving power of the used data. In Fig. 4, the central values of the V_S models are given for simplicity; details about uncertainties are given by Panza et al. (2007a,b).

Section 1 (Figs. 3, and 4a) goes from Provence to Central Sardinia and to the Campanian area, running along the *41° parallel line* in its Central and Eastern segment (Panza et al., 2007a). This section crosses the Balearic and the Tyrrhenian basins, the main extensional features in the Western Mediterranean area. Section 2 (Fig. 5b) runs from offshore southern Sardinia to the Aeolian arc and Calabria following an E–W and then NW–SE trend (Boyadzhiev et al., 2008; Peccerillo et al., 2008), along the direction of maximum extension of the Tyrrhenian basin during the last 5 Ma (Sartori, 2003). Section 3 (Fig. 4b) is located in the Central-Northern Tyrrhenian Sea and goes through the Tuscany and Roman magmatic provinces (Panza et al., 2007b), where the abundant mantle-derived ultrapotassic magmatism with crustal-like radiogenic isotope signatures reveals extremely anomalous geochemical compositions for upper mantle sources.

Section 1 (Fig. 4a) shows that the upper mantle beneath continental South-Eastern France exhibits rather homogeneous S-wave velocities ($V_S \sim 4.3$–4.5 km/s) down to 250 km of depth. Starting from the coast of Provence, the upper mantle structure changes significantly. In spite of the non-uniqueness of the inverse problem of seismological data the occurrence of a low S-wave velocity layer ($V_S = 4$–4.1 km/s) at a depth of about 60–130 km is a clear-cut feature. Such a layer is enclosed inside high-velocity material ($V_S \sim 4.3$–4.55 km/s) and extends eastward to Sardinia and the Tyrrhenian Sea, with an almost constant thickness. The low-velocity layer raises to a shallower level beneath the Campania volcanoes of Ischia, Phlegrean Fields and Vesuvius, showing a decrease of V_S to about 3.4–4.2 km/s. Note that the low-velocity layer is not limited to the underwater part of the section where young oceanic or thinned continental lithosphere is very likely present (Panza and Calcagnile, 1979), but it is also present beneath the Corsica–Sardinia block which is a fragment of the old European continental lithosphere, rotated to the East during opening of the Balearic Sea.

Section 2 (Fig. 4b), that goes from Sardinia to the Aeolian Arc and Calabria, also exhibits a low-velocity layer but it is at a much shallower depth of 30 to 70 km and rise to 0–30 km beneath the active Aeolian volcanoes. An almost vertical seismically active body with high V_S from 4.5 to 4.8 km/s likely representing the descending Ionian slab (Panza et al., 2003), cuts the low-velocity layer beneath Calabria.

Finally, Section 3 (Fig. 4b) crosses the Central Tyrrhenian Sea and the Tuscany and Roman magmatic province and the Apennines. In its Western segment, it is characterized by a low-velocity layer with $V_S = 4.1$–4.2 km/s at about 60–130 km of depth, that becomes shallower in the Roman Province (about 30–50 km).

5.2. Geochemical features: xenoliths

Spinel peridotites are present in the orogenic carbonatitic–melilitic pyroclastics of Vulture (0.2 M.y.), in the orogenic lamproitic lavas of Torre Alfina (0.9 M.y.), and in the anorogenic Miocene–Quaternary volcanics of Mt. Hyblei (South-Eastern Sicily), and of Sardinia (Fig. 1; Conticelli and Peccerillo, 1990; Jones et al., 2000; Sapienza and Scribano, 2000 and references therein).

Fig. 4. V_S models of the lithosphere–asthenosphere system along three representative sections in the Western Mediterranean. a) Section 1 — the lithosphere–asthenosphere system along the TRANSMED III geotraverse, modified from Panza et al. (2007a); the geometry of the base of the lithosphere is indicated by the blue line; the limit between upper and lower asthenosphere is indicated (red line). b) Sections 2 and 3 are built from the cellular V_S model of the Tyrrhenian Sea and surroundings given by Panza et al. (2007b). In each labeled cell, the hatched zone stands for the thickness variability, while, to avoid crowding of numbers, only the average shear velocity is reported. The V_S ranges of variability are given in Panza et al. (2007a). Red triangles indicate recent and active volcanoes. (For interpretation of the references to color in this figure legend, the reader is referred to the web version of this article.)

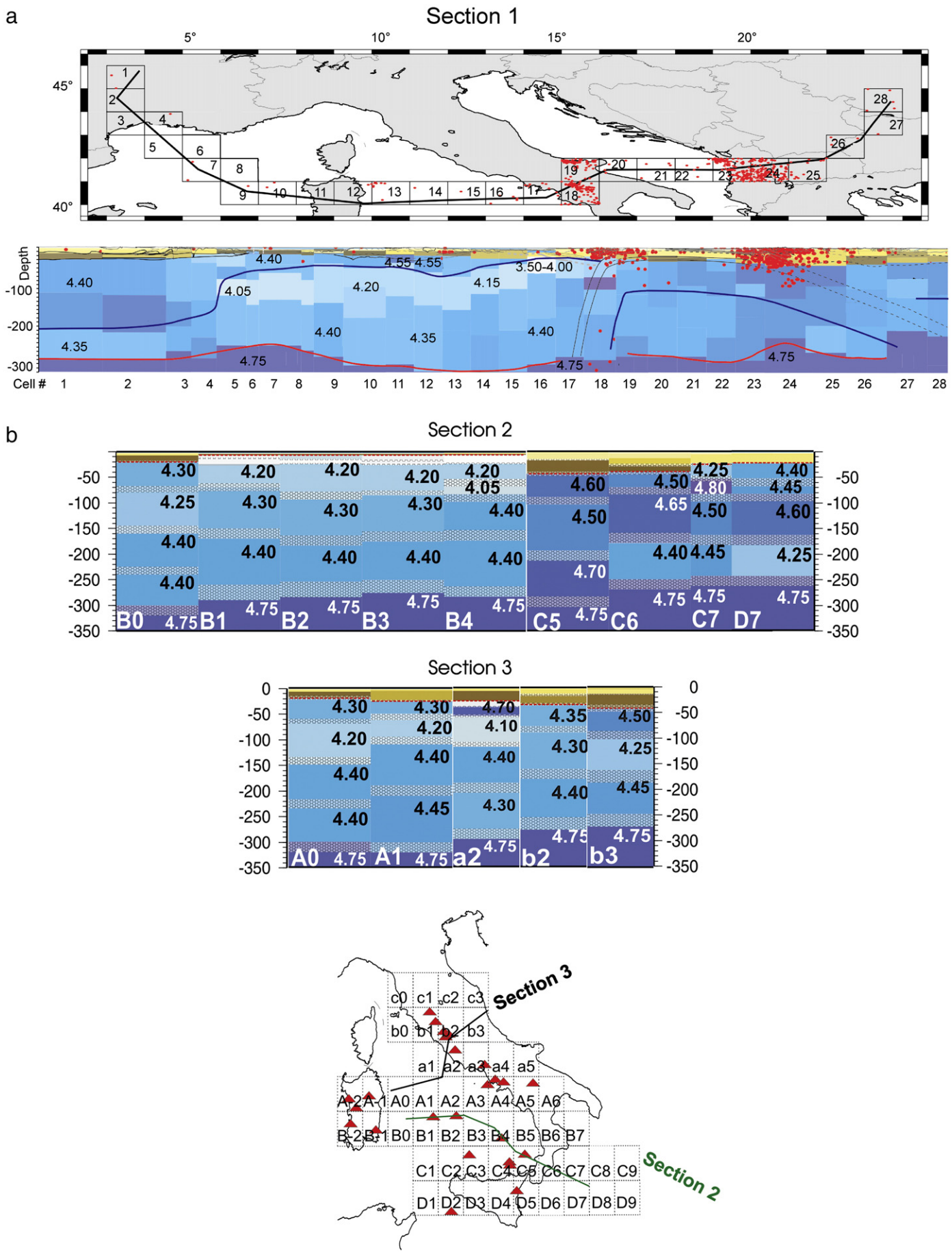

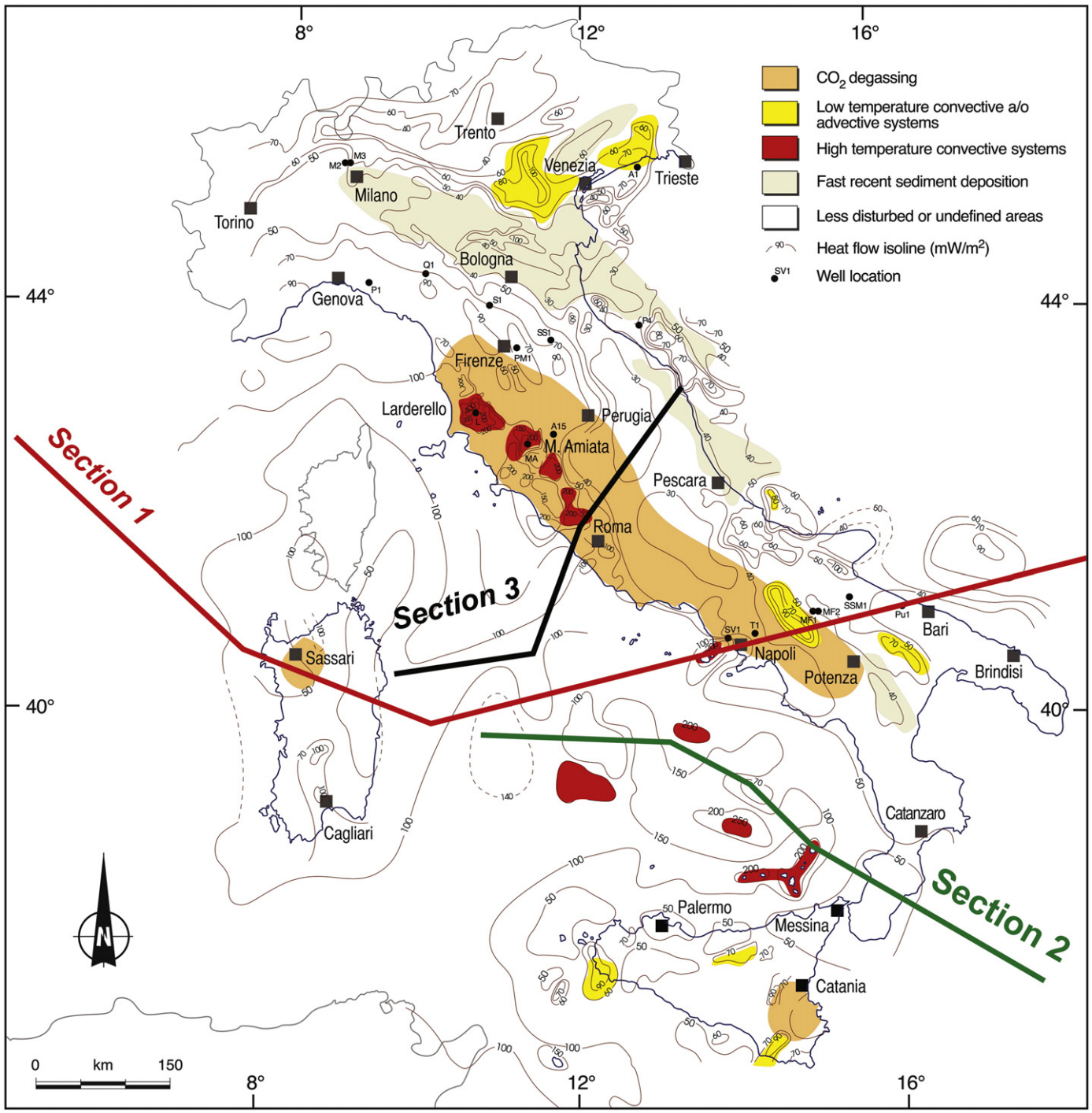

Fig. 5. Heat flow map of Italy modified after Della Vedova et al. (2001), reporting the location of major CO_2 degassing areas. Most non-volcanic CO_2 emission occurs in areas of normal heat flow. Local high heat flow is associated with subsurface magmas and includes CO_2 fluxes from major geothermal systems (Larderello and Monte Amiata, in Tuscany). Numbered lines represent the pathway of sections illustrated in Fig. 4.

At Vulture (Fig. 1), spinel peridotites consist of lherzolites and harzburgites, with subordinate dunites and wehrlites, which may contain phlogopite, amphibole, and carbonate. Downes et al. (2002) measured enriched LILE and LREE trace element patterns in clinopyroxene, associated with low HFSE contents, and proposed that metasomatic processes occurred by interaction of mantle rocks with silicate melts. Furthermore, peridotites show $^{87}Sr/^{86}Sr$ enrichment (0.7042–0.7058), higher than in most of the European continental lithosphere, and suggest that silicate-melts might have been subduction related. In these rocks, Rosatelli et al. (2007) described the existence of carbonate and silicate glasses, present as inclusions and microveins, formed by immiscibility processes from an original carbonate-rich silicate melt at pressures, *P*, of 1.8–2.2 GPa (about 50–80 km of depth). The $^{87}Sr/^{86}Sr$ ratios in metasomatic calcite are equal to $0.705816 \pm 4 \cdot 10^{-6}$, in the same range as rock $^{87}Sr/^{86}Sr$ data from Downes et al. (2002).

Torre Alfina xenoliths (Tuscany; Fig. 1) consist of spinel lherzolites and harzburgites (up to 3–4 cm in diameter) that sometimes contain phlogopite. Rare phlogopite-rich xenoliths have been found and interpreted as remnants of metasomatic veins in the upper mantle. These have Sr–Nd ($^{87}Sr/^{86}Sr \sim 0.716$–$0.717$; $^{143}Nd/^{144}Nd \sim 0.5121$) isotopic signatures close to those of the host ultrapotassic rocks

and have been suggested to represent the metasomatic veins whose melting gave ultrapotassic magmas (Conticelli, 1998).

Protogranular spinel lherzolites and harzburgites from Hyblei (Fig. 1) show whole-rock selective LREE and incompatible elements enrichments (i.e., U, La, Sr, and P; Sapienza and Scribano, 2000). They contain extremely abundant CO_2 inclusions, whose He isotope composition indicates mixing of two sources: a MORB-type mantle, and a radiogenic He enriched reservoir (Sapienza et al., 2005). He isotope data from Hyblei peridotites correlate with the He signature of Etna lavas (cf. Fig. 2).

Taken collectively, mantle xenoliths geochemical and petrological features indicate pervasive metasomatic processes in the Western Mediterranean lithosphere. Carbonate- and hydrous-silicate melts are recognized as possible metasomatic agents. Sr isotope data in mantle rocks from Vulture further suggest a subduction related origin of metasomatic melts, and the radiogenic isotopes in peridotites at Torre Alfina point to an upper crustal component in their source.

6. Carbon-cycling through subduction, mantle anomalies, and CO_2 degassing in the Western Mediterranean

The data summarized in Sections 4 and 5 highlight some remarkable relationships between the structure of the lithosphere–asthenosphere system, as indicated by V_S structural models (Fig. 4), and the main geochemical features of magmas and of mantle peridotites. The occurrence of a continuous 60–130 km deep low-velocity layer, stretching from Southern Provence to the South-Eastern Tyrrhenian Sea area and running continuously beneath both oceanic-type (e.g., Central Tyrrhenian Sea) and continental-type lithosphere (e.g., Sardinia), coincides with the zone of Oligocene to present slab rollback, and it is associated with orogenic magmatism that migrates in the same direction (Panza et al., 2007a,b; Peccerillo et al., 2008). The low-velocity layer has been interpreted as a geochemically anomalous mantle, modified by the release of "material" (i.e. fluids and/or melts of variable composition) from the retreating lithosphere, leaving a wake of physical anomalies (Peccerillo et al., 2008).

6.1. The low-velocity mantle layer: CO_2-rich fluids/melts at depth

The understanding of the nature of the low-velocity layer is crucial to have an insight into the lithosphere/asthenosphere evolution in the Western Mediterranean and to explain ongoing processes of mantle metasomatism and ultimately CO_2 degassing. Theoretically, a low-velocity layer might be induced by basaltic magmas, generated by partial mantle melting processes at high temperatures (e.g., Goes and van der Lee, 2002; Cammarano et al., 2003). Alternatively, it might correspond to a level of "fluid" enrichment (i.e., free H_2O-, CO_2-rich fluids or melts, and/or H_2O bound in mantle mineral's lattice or at grain-boundaries) which may well induce composition and density variations in the mantle (Gaetani and Grove, 1998; Jung and Karato, 2001; Presnall and Gudfinnsson, 2005; Dasgupta and Hirschmann, 2006).

It is unlikely that the low-velocity layer is related to the presence of a 70-km-thick front of basaltic magma. This would require sustained supply of significant amounts of melt (more than 1–4% in volume) through the whole mantle zone to allow migration (Hyndman and Shearer, 1989). Upward melt migration is, in fact, controlled by the supply rate from mantle melting at high temperature, and solidification of the partial melts is expected on cooling. Such a thick magma front is improbable, especially in some regions along Section 1 (Fig. 4a), such as the Provençal basin, where magmatism is not any more active at present. In addition, it would necessarily require considerably high temperatures in the mantle, which conflicts with the heat flux along the overall trajectory of Section 1 (Fig. 5).

The considerable thickness of this shallow low-velocity layer may be better justified by the presence of low fractions of volatile-rich melts, or by fluids (free or mineral-bound). Its presence in zones affected by the Oligocene to Present subduction strongly suggests that volatiles were likely released during the Eastward rollback of the West-directed Adriatic–Ionian plate. Slab dehydration, with consequent development of mantle wedge structures and volcanic fronts, has been modeled as a continuous process starting from low-grade conditions (10–20 km depth) to more than 200 km (e.g., Schmidt and Poli, 1998).

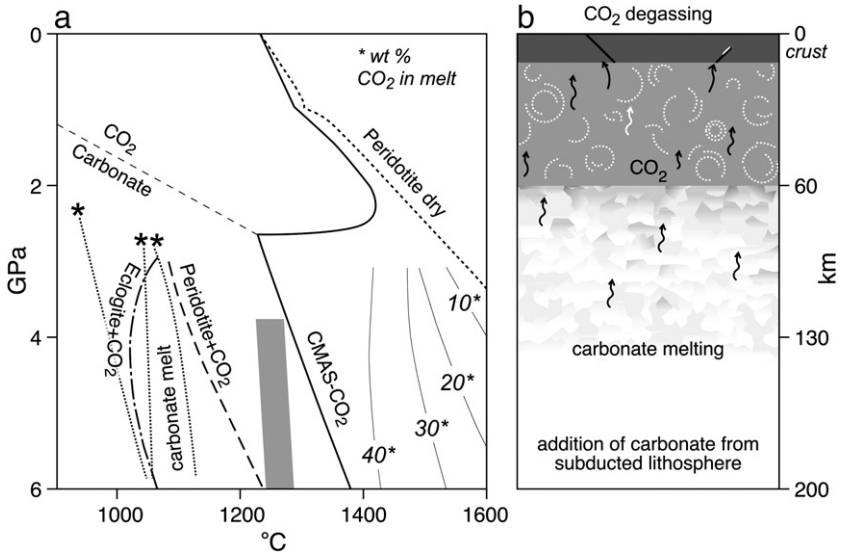

Fig. 6. Proposed evolution for lithosphere–asthenosphere degassing beneath the Western Mediterranean. a) Pressure–temperature diagram showing the effects of CO_2 on the *solidus* of carbonated lithologies in the mantle. Two different estimates of the peridotite–CO_2 *solidus* are reported: CMSA–CO_2 after Dalton and Presnall (1998), and Gudfinnsson and Presnall (2005), and peridotite–CO_2 (2.5 wt.%) from Dasgupta and Hirschmann (2006). Dry peridotite *solidus* in the CMAS system is from Gudfinnsson Presnall (2005). Eclogite–CO_2 *solidus* (dry eclogite + 5 wt.% CO_2) from Dasgupta et al. (2004). Asterisks (*) corresponds to the KNCFMASH–CO_2 *solidus* (carbonated pelite + 1.1 wt.% H_2O + 4.8 wt.% CO_2) from Thomsen and Schmidt (2008). The effect of carbonates on the composition of melts generated at increasing temperature is reported as wt.% CO_2, based on the CMSA–CO_2 system. Gray area = estimated present-day mantle temperatures at the inferred pressures (Carminati et al., 2005). b) Application of the experimentally determined melting relationships for carbonated peridotite, and crustal lithologies to illustrate present mantle processes and metasomatism beneath the Western Mediterranean. Melting of sediments and/or continental crust of the subducted Adriatic–Ionian (African) lithosphere, generates carbonate-rich (hydrous-silicate) melts at pressure >4 GPa (130 km) and T>1260 °C. Due to their low density and viscosity, such melts can migrate upward through the mantle, forming a 70 km thick carbonated partially molten CO_2-rich mantle layer recorded by tomographic images. Upwelling of carbonate-rich melts to depths less than 60–70 km, induces massive outgassing of CO_2 in the lithospheric mantle, with cessation of V_S decrement. Buoyancy forces, probably favored by fluid overpressures, and tectonics might allow further CO_2 upwelling to the Moho and the lower crust, and, ultimately, outgassing at the surface.

However, if water-rich fluids or melts were the dominant mantle modifiers, there is no explanation for the confinement of the physical modifications at $P>2$ GPa. Hydrous minerals (e.g., amphibole) are stable at $P\leq 2$ GPa in peridotites that have reacted with subduction released hydrous fluids, like in the Ulten Zone in the Eastern Alps (Scambelluri et al., 2006).

In a carbonated mantle (i.e. presence of CO_2 fluids, carbonate melts, and/or carbonates), 2 GPa represents a well recognized threshold, which corresponds to the carbonated peridotite decrease of the *solidus*, experimentally determined at 2–2.5 GPa (Fig. 6a; Falloon and Green, 1990). When $P>2$ GPa, carbonates are stable phases and peridotite (±hydrous phases) *solidus* is considerably depressed: melting is supposed to commence with low fractions of carbonate-rich melts. When $P<2$ GPa, both carbonate-rich melts and carbonates decompose releasing CO_2 fluids (Canil, 1990; Frezzotti et al., 2002a,b).

These properties of CO_2 at depth are able to account for the variations of the physical properties of the mantle beneath the Western Mediterranean region. Carbonate melts have the lowest viscosity of any other magma type, and very low interfacial energies with respect to mantle minerals. Dihedral angles (θ) are in the range of 25–30° and depend only weakly on temperature or pressure (Watson and Brenan, 1987; Hunter and McKenzie, 1989; Watson et al., 1990). These properties allow very low fractions of carbonate melts to rise through an interconnected network at very low porosities (0.1%) and react with mantle minerals, which may well account for the low V_S detected at $P>2$ GPa (Dobson et al., 1996; Presnall and Gudfinnsson, 2005). Conversely, at $P<2$ GPa, the dihedral angles (θ) between CO_2 and matrix mantle minerals are greater than 60° and inhibit the formation of a porous fluid flow (Watson and Brenan, 1987): CO_2 pooling should occur associated to decarbonation in the mantle above 2 GPa, with cessation of V_S decrement (Canil, 1990; Frezzotti and Peccerillo, 2007).

Therefore, we propose that the low-velocity layer between 60 and 130 km of depth beneath the Western Mediterranean represents a low viscosity wedge induced by the presence of carbonate-rich melts. Starting from below, the onset of the V_S decrement at 130 km indicates the onset of mantle melting, while the level at about 60 km is the upward limit for the carbonate melt ascent. Such an interpretation does not signify that (hydrous) silicate melts are absent during mantle modifications at the considered pressures, but only that mantle processes are CO_2 mediated.

6.2. Carbonate-rich melts in the upper mantle beneath the Western Mediterranean

The generation of carbonate-rich melts or fluids via subduction is a two-step process. The first step consists in "removing" carbonates (e.g., by devolatilization or melting) from the subducting lithosphere, and introducing them into the overlying upper mantle. Once carbonates are expelled from the slab and fluxed into the overlying mantle, they might freeze in mantle rocks giving rise to carbonated peridotites. However, if temperatures are sufficiently high, they might be preserved at the liquid state and migrate through porous or reactive flow (Presnall and Gudfinnsson, 2005).

The addition of a carbonate component into the Western Mediterranean mantle may have been induced by two alternative processes: either decarbonation, or melting of sediment-bearing old oceanic and/or continental Adriatic–Ionian lithosphere. Carbonates, however, are stable to very high pressures and temperatures, and remain as refractory phases as lithosphere dehydrates. At depths between 90 and 150 km, marls do not undergo any devolatilization along subduction low-temperature geotherms (400–600 °C), and decarbonation commences only if temperatures exceed 700–950 °C (hot subduction; Kerrick and Connolly, 2001; Connolly, 2005). Further, decarbonation at high pressures requires fluxes of H_2O from the marl sediments and/or the underlying lithosphere (Kerrick and Connolly, 2001).

In order to free substantial amounts of CO_2, melting of carbonated crustal lithologies is necessary, which requires even higher temperatures (above 1000–1100 °C at 4 GPa; Dasgupta et al., 2004,2006; Thomsen and Schmidt, 2008; Fig. 6a). At $P>3.7$ GPa, melting of the assemblage phengite + quartz / coesite + clinopyroxene + kyanite + garnet + calcite (9–10 wt.%) generates immiscible silicate and carbonate liquids at 1100 °C, and, at higher temperatures, a homogeneous carbonate-rich hydrous-silicate melt (Thomsen and Schmidt, 2008). At these (P, T) conditions high-degrees of melt are produced: about 9 wt.% carbonate- and 30–47 wt.% silicate melt. The composition of the silicate melt varies from rhyolitic to phonolitic ($K_2O>10$ wt.%) at increasing pressures (Thomsen and Schmidt, 2008).

The foregoing processes call for temperatures that are too high for subduction zones with a convergence rate (about 3 cm/year) as the Adriatic–Ionian plate (van Keken et al., 2002; Carminati et al., 2005). Thus, it is improbable that decarbonation of crustal rocks at depth occurred during active subduction in the investigated region. Decarbonation or melting should have initiated successively, during a progressive rise of mantle temperatures, resulting from the combined effect of the strong extensional tectonics affecting this sector of the Tyrrhenian basin, and of the eastward mantle flow (Panza et al., 2007a) behind the retreating Adriatic–Ionian subducting plate. This implies that, in this area, crustal lithologies from the retreating Adriatic–Ionian lithosphere remained trapped in the mantle wedge at depths exceeding about 130 km before being melted as a consequence of back arc isotherm uprise. Present-day mantle temperatures beneath the Western Mediterranean, away from the active subducting Ionian plate, are estimated at 1260–1320 °C at depths greater than 105 km (Carminati et al., 2005), and such a thermal regime would favor melting of subducted crustal lithologies with respect to decarbonation reactions, generating carbonate and (hydrous) silicate melts (cf. Fig. 6a).

Possible mantle evolution can be evaluated by experimental models in the peridotite–CO_2 system, reported in Fig. 6, which indicate CO_2 as the most important controlling compound on both the temperature of melting of peridotite, and on the composition of the produced melt (Fig. 6a; Dalton and Presnall, 1998; Dasgupta and Hirschmann, 2006, 2007a,b; Dasgupta et al., 2007). Since nominally volatile-free mantle minerals can dissolve only a few ppm CO_2 (Keppler et al., 2003), carbonate phases may form at very low CO_2 concentrations, and abruptly induce a sharp decrease in peridotite partial melting temperatures (Fig. 6a); peridotite melting would commence with low fractions of carbonate-rich melts. At 3 GPa and 1300 °C, 0.1 wt.% of carbonate melt is in equilibrium with the peridotite mantle, while transition to carbonate-rich silicate melts (>2 wt.% of melt), requires temperature up to 1450 °C (Dasgupta et al., 2007).

Therefore, the amount and composition of mantle melts in the enriched mantle zone (i.e. low-velocity wedge) would depend, among other parameters, on temperature. Theoretically, on a further temperature increase, mantle melting enhancement might generate dominantly silicate-rich melts with a carbonate component, promote channeling, and ultimately volcanism. At the inferred present-day temperatures of 1260–1320 °C, the mantle beneath Western Mediterranean away from active orogenic volcanism can preserve low fractions of molten carbonates (Fig. 6a). Conversely, in those zones not far away or above the subducting plate, higher temperature fluxes might induce the highest degrees of partial melting, generating CO_2-rich magmas (i.e., the low-velocity ledge beneath the Campania volcanoes and the Aeolian arc; Fig. 4a and b).

6.3. Proposed regional evolution

According to our model, the tomographic images of the shallow low-velocity-layer represent carbonated partially molten, subducted crustal material mixed with mantle rocks at depths above 130 km (Fig. 6b). Metasomatic melts, would be constituted by a carbonate, and a hydrous silicate component, via melting of carbonated crustal

lithologies, as experimentally determined (see Section 6.2). The silicate component of this melt represents an important metasomatic agent adding SiO_2, LREE, and LILE to the mantle; progressive crystallization of silicate minerals from the metasomatic silicate component may result in an increasing carbonate-rich fraction in melts, which might induce extensive dissolution and oriented recrystallization of olivine (Dasgupta and Hirschmann, 2006). We might speculate that silicate and carbonate melts preserved as inclusions in spinel peridotites from Vulture illustrate the ongoing mantle refertilization, started more than 200,000 year ago.

Carbonate addition to the mantle via subduction should be considered a "one-shot" event, whose longevity depends on the timing of the geodynamic evolution in the investigated area. Mantle upwelling for low fractions of carbonate melt is "fast", and estimated between 100 and 1000 m in 0.1–1 M.y. (Hammouda and Laporte, 2000). Resulting ascent times are compatible with the timescale of the Adriatic–Ionian subduction retreat and may account for the persistence of the low-velocity layer also in those zones were subduction ceased around 30 M.y. ago (Balearic Sea).

While carbonate melts accumulate and persist in the shallow low-velocity mantle zone because of present day temperatures, part would outgas at 2 GPa (Fig. 6b). Degassing of CO_2 would result in stiffening of the more viscous silicate melt component, with consequent cessation of the processes, if temperatures are not further increased. Released CO_2 will temporarily halt (and tend to pool) above this pressure threshold to form diffuse and/or restricted gas-rich regions in the upper mantle (Fig. 6b). CO_2 could spread in the subcontinental lithosphere as isolated small bubbles confined at mineral grain boundaries, although we cannot exclude that CO_2 may coalesce to form larger (over pressurized?) reservoirs.

In Italy, non-volcanic high CO_2 flux is associated with the main crustal geological features, thus it is very likely that active tectonics represent the driving mechanism for mantle CO_2 release from crustal depths (Miller et al., 2004; Ventura et al., 2007). Deep strike-slip faults, such as the *41° N parallel line*, would constitute a possible fast way for upward CO_2 mantle rise and accumulation in the lower crust (see Mofete d'Ansanto, in Table 1). Upper mantle buoyancy could also allow mantle CO_2 upwelling towards the Moho and the lower crust. Aoudia et al. (2007) and Panza and Raykova (2008) investigated the role of buoyancy forces with respect to the ongoing slow and complex lithospheric deformations in the uppermost mantle along Central Italy, revealed by the very recent GPS measurements and by the unusual subcrustal seismicity distribution. These authors proposed that buoyancy forces, resulting from the heterogeneous density distribution in the lithosphere, govern the present-day deformation within Central Italy.

Upper mantle buoyancy may explain the upwelling towards the Moho and the lower crust, of otherwise inert CO_2. Deep CO_2 is indeed a fluid phase with peculiar characteristics: it is very compressible, and practically immobile (e.g., $\theta > 60°$), but at the same time it is highly volatile ($d = 1.15–1.2$ g/cm^3 in the depth range from 60 to 80 km). For these reasons, CO_2 could not migrate until the porosity reaches high values (>8%). It is then likely to ascend "explosively", facilitating earthquakes, not only at 4–8 km from the surface, but also at mantle depths, close to the Moho.

6.4. Aeolian arc and Etna CO_2 emission

In the Western Mediterranean, further massive CO_2 degassing occurs from active volcanoes, which contributes significantly to the total budget of geological emissions (Fig. 1; Table 1). Aeolian volcanoes, do not show any anomalous CO_2 flux with respect to typical magmas generated in a mantle modified by active subduction (see CO_2 output from Stromboli in Table 1). Conversely, Etna volcano alone constitutes an outstanding CO_2 emission anomaly in the centre of Mediterranean (Table 1). Etna is away from low-velocity mantle zones (Fig. 4; Panza et al., 2007b; Peccerillo et al., 2008) and, therefore, the explanation offered for the subduction-related volcanic areas of the Italian peninsula cannot be extended to this volcano.

In principle, CO_2 emission at Etna may reveal some interaction between magma and carbonate wall rocks, since the thick carbonate sequences of the Hyblean foreland are believed to be present beneath Etna (e.g. Grasso, 2001). Oxygen isotope data reported by Viccaro and Cristofolini (2008) are higher than mantle values ($\delta^{18}O \sim +6.1$ to $+7.1$), which would support magma contamination. However, Frezzotti et al. (1991) report evidence for deep CO_2 degassing at Etna volcano by mixed CO_2 + basaltic melt inclusions. Measured CO_2 densities indicate pressures of 0.7 GPa (about 25 km of depth) at 1300 °C, which correspond to more than 7000 ppm CO_2 in the magma (Armienti et al., 1996). Allard et al. (1997) determined even higher CO_2 contents in Etna magmas (1.23 wt.% CO_2, based on S/C ratios in the magma), consistent with deep degassing (50 km). According to Allard et al. (1997, 2006), CO_2 degassing from volatile-rich Etna basalts is related to the shallow mantle diapiring at the African–European plate boundary.

All these lines of evidence lead to the conclusion that the anomalous CO_2 emission appears to be a mantle-related process (Allard et al., 1997; D'Alessandro et al., 1997). We propose two possible models of carbonate recycling to explain the anomalous CO_2 emission at Etna. They both lean on the particular geodynamic setting of the Etna volcano. There is a growing evidence that Etna, although being a typical OIB-type volcano, bears geochemical evidence (e.g. enrichment in K and Rb, and B-isotopes) for the presence of subduction components, as discussed earlier (Condomines et al., 1995; Nakai et al., 1997; Schiano et al., 2001; Tonarini et al., 2001; Allard et al., 2006). Gvirtzman and Nur (1999) and Doglioni et al. (2001) highlight the particular position of Etna, which is located along a main lithospheric dextral transform fault system which runs from Lipari and Vulcano (Aeolian arc) to the Malta escarpment (the so-called Tindari–Letojanni fault; Fig. 3), and separates the foreland Hyblean block at the west from the subducting Ionian plate at the east. According to these Authors, the magmatism in this particular geodynamic setting is generated at a window along this fault, at the boundary between the foreland and a subducting slab. This would allow in the Etna magmatic system contemporaneous OIB-type mantle decompression and melting, and CO_2-rich fluids inflow from the undergoing slab. The Ionian subduction zone is very steep, almost vertical, which favors the channelling of slab-derived fluids along the subduction zone and their ascent from very high depth where decarbonation occurs, to shallow levels (Abers, 2005).

An alternative possibility is that the CO_2 source is provided by the carbonate sequences of the subducted Hyblean foreland. The low dipping angle of the Hyblean foreland (Doglioni et al., 2001 and references therein) and the absence of deep seismicity beneath the Western Aeolian arc (Caputo et al., 1970, 1972) suggest slab breakoff on the west of the Tindari–Letoianni fault. This implies detachment and foundering into the mantle of the Hyblean slab beneath the Etna volcanic zone. Sinking carbonate sequences of the foreland could release large amounts of CO_2 when conditions of decarbonation or melting are reached.

Therefore, present-day CO_2 degassing beneath the Western Mediterranean appears to be related to carbon-cycling from the crustal portion of subducted slabs into the upper mantle. However, whereas along zones directly affected by Oligocene to Present subduction, CO_2 emission is related to the temperature regimes and dynamic conditions that develop behind the retreating slab, at Etna the CO_2 emission would be generated either by fluid inflow from the Ionian subducting plate or from decarbonation of carbonate sequences of the detached foreland sinking into the upper mantle.

7. Concluding remarks

Present-day massive "cold" CO_2 soil degassing, occurring in tectonically active areas located above the subduction-enriched

mantle wedge (e.g. Tuscany, Northern Latium, Apennines, North Sardinia, *41° N parallel line*), supports efficient cycling of carbon and its return to the atmosphere in the western Mediterranean area.

We propose that the slab retreat during Oligocene to Present times left in front of itself a shallow layer, at a depth of 60–130 km, of very low-velocity mantle material that sits on top of a relatively faster low-velocity layer, which is standard for oceanic structures (e.g. Stixrude and Lithgow-Bertelloni, 2005). The very low velocities can be indeed associated to attenuation, but attenuation affects amplitudes rather than phases and we measure dispersion relations (phase and group velocities) at periods of 10 s and larger. The V_S values we get in the uppermost part (60–130 km of depth) of the mantle low-velocity zone remain very low with respect to the values reported for low-velocity zone of oceanic regions at global scale (Stixrude and Lithgow-Bertelloni, 2005), even when the upper bound of the V_S range is considered (see Panza et al., 2007a,b), and some increment is allowed to account for the attenuation effect through body-waves dispersion (Futterman, 1962; Panza, 1985).

This layer of very low-velocity mantle material was generated by melting of carbonated crustal lithologies, at temperature above 1100 °C. The result is a chemically and physically heterogeneous upper mantle beneath the Western Mediterranean. The anomalous non-volcanic CO_2 flux, which has been detected in Italy in those regions where volcanism is not active or absent, would derive from mantle degassing, providing a geological CO_2 source, additional to the rise of CO_2-rich magmas, in this active volcanic region.

Upper mantle carbonate Earth recycling via subduction and melting of crustal lithologies at depths >130 km, as observed In Western Mediterranean, represents a relevant process in the overall Earth deep carbon cycle. The flux of cycled CO_2 can be tentatively calculated based on the extension of the low-velocity wedge beneath the Western Mediterranean. Typical carbonate-rich melts in experimental melting of carbonated lherzolite (Dalton and Wood, 1993) contain about 45% CO_2 by weight. Accepting 0.1 wt.% of carbonate melt concentration (cf. Section 6.2), and assuming as convenient (but certainly high) 100% degassing, approximately 1.35 Mt of CO_2 (equal to 0.4 Mt carbon) could be released for each km^3 of metasomatized mantle. Assuming a time scale of 30 M.y., CO_2 degassing of the low-velocity wedge beneath the Western Mediterranean would conservatively lead to lithosphere–asthenosphere CO_2 flux of about 70 Mt/year, which exceeds yearly CO_2 degassing in Italy.

Acknowledgements

Perspective comments by two anonymous reviewers, and editorial handling by R. Dasgupta have considerably improved the manuscript. This research has been supported by the Italian MIUR PRIN 2004 project "Modelling of the mantle–crust system by petrological and geophysical methods", the Italian Space Agency project (SISMA), the Universities of Perugia and Siena, and the Italian Presidenza del Consiglio dei Ministri — Dipartimento della Protezione Civile (Project S1 of Convenzione DPC-INGV 2007-09).

References

Abers, G.A., 2005. Seismic low-velocity layer at the top of subducting slabs: observations, predictions, and systematics. Physics of the Earth and Planetary Interiors 149, 7.29.

Aiuppa, A., Bellomo, S., Bitetto, M., Brusca, L., Camarda, M., D'Alessandro, W., De Gregorio, S., Di Napoli, R., Gagliano Candela, E., Gurrieri, S., Longo, M., Pecoraino, G., Valenza, M., 2007. Soil and groundwater discharge of magmatic/hydrothermal CO_2 and He on south-western Ischia Island (Central Italy). Geophysical Research Abstracts 9, 02932.

Allard, P., Carbonnelle, J., Dajlevic, D., Le Bronec, J., Morel, P., Robe, M.C., Maurenas, J.M., Faivre-Pierret, R., Martin, D., Sabroux, J.C., Zettwoog, P., 1991. Eruptive and diffuse emissions of CO_2 from Mount Etna. Nature 351, 387–391.

Allard, P., Carbonelle, J., Metrich, N., Loyer, H., Zettwoog, P., 1994. Sulphur output and magma degassing budget of Stromboli volcano. Nature 368, 326–330.

Allard, P., Jean-Baptiste, P., D'Alessandro, W., Parello, F., Parisi, B., Flehoc, C., 1997. Mantle-derived helium and carbon in groundwaters and gases of Mount Etna, Italy. Earth and Planetary Science Letters 148, 501–516.

Allard, P., Metrich, N., Deloule, E., Belhadj, O., Mandeville, C., 2006. First ion microprobe determination of water and sulfur isotopic ratios in melt inclusions of olivines at Mount Etna. Eos, Transactions — American Geophysical Union 87 (52) Fall Meeting Supplement, Abstract V13D-08.

Aoudia, A., Ismail-Zadeh, A., Romanelli, F., 2007. Buoyancy-driven deformation and contemporary tectonic stress in the lithosphere beneath Central Italy. Terra Nova 19, 490–495.

Armienti, P., D'Orazio, M., Innocenti, F., Tonarini, S., Villari, L., 1996. October 1995–February 1996 Mt. Etna explosive activity: trace element and isotopic constraints on the feeding system. Acta Vulcanologica 8, 1–6.

Baubron, J.C., Allard, P., Toutain, J.P., 1990. Diffuse volcanic emissions of carbon dioxide from Volcano Island, Italy. Nature 344, 51–53.

Boyadzhiev, G., Brandmayr, E., Pinat, T., Panza, G.F., 2008. Optimization for nonlinear inverse problem. Rendiconti Lincei 19, 17–43.

Calanchi, N., Colantoni, P., Rossi, P.L., Saitta, M., Serri, G., 1989. The Strait of Sicily continental rift systems: phisiography and petro-chemistry of the submarine volcanic centres. Marine Geology 87, 55–83.

Caliro, S., Cardellini, C., Chiodini, G., Avino, R., Granieri, D., Smith, A., 2008. Carbon isotopic composition of soil CO_2 efflux at Solfatara (Plaegraean fields, Nales, Italy). Geophysical Research Abstracts 10, EGU2008–A-06568.

Cammarano, F., Goes, S., Vacher, P., Giardini, D., 2003. Inferring upper-mantle temperatures from seismic velocities. Physics of Earth Planetary Interiors 138, 197–222.

Canil, D., 1990. Experimental study bearing on the absence of carbonate in mantle-derived xenoliths. Geology 18, 1011–1013.

Caputo, M., Panza, G.F., Postpischl, D., 1970. Deep structure of the Mediterranean basin. Journal Geophysical Research 75, 4919–4923.

Caputo, M., Panza, G.F., Postpischl, D., 1972. New evidences about the deep structure of the Lipari Arc. Tectonophysics 15, 219–231.

Carapezza, M.L., Federico, C., 2000. The contribution of fluid geochemistry to the volcano monitoring of Stromboli. Journal of Volcanology and Geothermal Research 95, 227–245.

Carminati, E., Wortel, M.J.R., Spakman, W., Sabadini, R., 1998. The role of slab detachment processes in the opening of the western-central Mediterranean basins: some geological and geophysical evidence. Earth and Planetary Science Letters 160, 651–665.

Carminati, E., Negredo, A.M., Valera, J.L., Doglioni, C., 2005. Subduction-related intermediate-depth and deep seismicity in Italy: insights from thermal and rheological modelling. Physics of the Earth and Planetary Interiors 149, 65–79.

Chimera, G., Aoudia, A., Saraò, A., Panza, G.F., 2003. Active tectonics in Central Italy: constraints from surface wave tomography and source moment tensor inversion. Physics of the Earth and Planetary Interiors 138, 241–262.

Chiodini, G., Frondini, F., 2001. Carbon dioxide degassing from the Albani Hills volcanic region, central Italy. Chemical Geology 177, 67–83.

Chiodini, G., Frondini, F., Raco, B., 1996. Diffuse emission of CO_2 from the Fossa crater, Vulcano Island (Italy). Bulletin Volcanology 58, 41–50.

Chiodini, G., Cioni, R., Guidi, M., Raco, B., Marini, L., 1998. Soil CO_2 flux measurements in volcanic and geothermal areas. Applied Geochemistry 13, 543–552.

Chiodini, G., Frondini, F., Kerrick, D.M., Rogie, J.D., Parello, F., Peruzzi, L., Zanzari, A.R., 1999. Quantification of deep CO_2 fluxes from central Italy. Examples of carbon balance for regional aquifers and of soil diffuse degassing. Chemical Geology 159, 205–222.

Chiodini, G., Frondini, F., Cardellini, C., Parello, F., Peruzzi, L., 2000. Rate of diffuse carbon dioxide Earth degassing estimated from carbon balance of regional aquifers: the case of central Apennine, Italy. Journal of Geophysical Research 105 (B4), 8423–8434.

Chiodini, G., Cardellini, C., Amato, A., Boschi, E., Caliro, S., Frondini, F., Ventura, G., 2004. Carbon dioxide Earth degassing and seismogenesis in central and southern Italy. Geophysical Research Letter 31. doi:10.1029/2004GL019480.

Condomines, M., Tanguy, J.C., Michaud, V., 1995. Magma dynamics at Mt Etna: constraints from U–Th–Ra–Pb radioactive disequilibria and Sr isotopes in historical lavas. Earth Planetary Science Letters 132, 25–41.

Connolly, J.A.D., 2005. Computation of phase equilibria by linear programming: a tool for geodynamic modeling and its application to subduction zone decarbonation. Earth and Planetary Science Letters 236, 524–541.

Conticelli, S., 1998. The effect of crustal contamination on ultrapotassic magmas with lamproitic affinity: mineralogical, geochemical and isotope data from the Torre Alfina lavas and xenoliths, Central Italy. Chemical Geology 149, 51–81.

Conticelli, C., Peccerillo, A., 1990. Petrological significance of high-pressure ultramafic xenoliths from ultrapotassic rocks of Central Italy. Lithos 24, 305–322.

Conticelli, C., Peccerillo, A., 1992. Petrology and geochemistry of potassic and ultrapotassic volcanism in Central Italy: petrogenesis and inferences on the evolution of the mantle sources. Lithos 28, 221–240.

Conticelli, S., D'Antonio, M., Pinarelli, L., Civetta, L., 2002. Source contamination and mantle heterogeneity in the genesis of Italian potassic and ultrapotassic volcanic rocks: Sr–Nd–Pb isotope data from Roman Province and Southern Tuscany. Mineralogy and Petrology 74, 189–222.

Corti, G., Cuffaro, M., Doglioni, C., Innocenti, F., Manetti, P., 2006. Coexisting geodynamic processes in the Sicily Channel. In: Dilek, Y., Pavlides, S. (Eds.), Postcollisional Tectonics and Magmatism in the Mediterranean Region and Asia. Geological Society of America Special Paper, vol. 409, pp. 83–96.

D'Alessandro, W., Giammanco, S., Parello, F., Valenza, M., 1997. CO_2 output and $^{13}C(CO_2)$ from Mt Etna as indicators of degassing of shallow asthenosphere. Bulletin Volcanology 58, 455–458.

Dallai, L., Freda, C., Gaeta, M., 2004. Oxygen isotope geochemistry of pyroclastics clinopyroxene monitors carbonate contributions to Roman-type ultrapotassic magmas. Contributions to Mineralogy and Petrology 148, 247–263.

Dalton, J.A., Presnall, D.C., 1998. The continuum of primary carbonatitic–kimberlitic melt compositions in equilibrium with lherzolite: data from the system CaO–MgO–Al_2O_3–SiO_2–CO_2 at 6 GPa. Journal of Petrology 39, 1953–1964.

Dalton, J.A., Wood, B.J., 1993. The partitioning of Fe and Mg between olivine and carbonate and the stability of carbonate under mantle conditions. Contributions to Mineralogy and Petrology 114, 501–509.

Dasgupta, R., Hirschmann, M.M., 2006. Melting in the Earth's deep upper mantle caused by carbon dioxide. Nature 440, 659–662.

Dasgupta, R., Hirschmann, M.M., 2007a. Effect of variable carbonate concentration on the solidus of mantle peridotite. American Mineralogist 92, 370–379.

Dasgupta, R., Hirschmann, M.M., 2007b. A modified iterative sandwich method for determination of near-solidus partial melt compositions. II. Application to determination of near-solidus melt compositions of carbonated peridotite. Contributions to Mineralogy and Petrology 154, 647–661.

Dasgupta, R., Hirschmann, M.M., Withers, A.C., 2004. Deep global cycling of carbon constrained by the solidus of anhydrous, carbonated eclogite under upper mantle conditions. Earth and Planetary Science Letters 227, 73–85.

Dasgupta, R., Hirschmann, M.M., Stalker, K., 2006. Immiscible transition from carbonate-rich to silicate-rich melts in the 3 GPa melting interval of eclogite + CO_2 and genesis of silica-undersaturated ocean island lavas. Journal of Petrology 47, 647–671.

Dasgupta, R., Hirschmann, M.M., Smith, N.D., 2007. Water follows carbon: CO_2 incites deep silicate melting and dehydration beneath mid-ocean ridges. Geology 35, 135–138.

De Gregorio, S., Diliberto, I.S., Giammanco, S., Gurrieri, S., Valenza, M., 2002. Tectonic control over large-scale diffuse degassing in eastern Sicily (Italy). Geofluids 2, 273–284.

Della Vedova, B., Bellani, S., Pellis, G., Squarci, P., 2001. Deep temperatures and surface heat flow density distribution. In: Vai, G.B., Martini, P. (Eds.), Anatomy of an Orogen: The Apennines and Adjacent Mediterranean Basins. Kluwer Academic Publishers, Dordrecht, Netherlands, pp. 65–76.

Di Bella, M., Russo, S., Petrelli, M., Peccerillo, A., 2008. Origin and evolution of the Pleistocene magmatism of Linosa Island (Sicily Channel, Italy). European Journal of Mineralogy 20, 587–601. doi:10.1127/0935-1221/2008/0020-1832.

Dobson, D.P., Jones, A.P., Rabe, R., Sekine, T., Kurita, K., Taniguchi, T., Kondo, T., Kato, T., Shimomura, O., Urakawa, S., 1996. In-situ measurement of viscosity and density of carbonate melts at high pressure. Earth and Planetary Science Letters 143, 207–215.

Doglioni, C., Gueguen, E., Sabat, F., Fernandez, M., 1997. The western Mediterranean extensional basins and the Alpine orogen. Terra Nova 9, 109–112.

Doglioni, C., Harabaglia, P., Merlini, S., Mongelli, F., Peccerillo, A., Piromallo, C., 1999. Orogens and slabs vs. their direction of subduction. Earth Science Reviews 45, 167–208.

Doglioni, C., Innocenti, F., Mariotti, G., 2001. Why Mt Etna? Terra Nova 13, 25–31.

Downes, H., Kostoula, T., Jones, A., Beard, A., Thirlwall, M., Bodinier, J.-L., 2002. Geochemistry and Sr–Nd isotopic compositions of mantle xenoliths from the Monte Vulture carbonatite–melilitite volcano, central southern Italy. Contributions to Mineralogy and Petrology 144, 78–92.

Etiope, G., 1996. Migrazione e comportamento del "Geogas" in bacini argillosi. Ph.D. Thesis Extended abstract, Plinius 15, 90–94.

Etiope, G., 1999. Subsoil CO_2 and CH_4, and their advective transfer from faulted grassland to the atmosphere. Journal Geophysical Research 104 (D14), 16889–16894.

Faccenna, C., Becker, T.W., Lucente, F.P., Jolivet, L., Rossetti, F., 2001. History of subduction and back-arc extension in the Central Mediterranean. Geophysical Journal International 145, 809–820.

Falloon, T.J., Green, D.H., 1990. The solidus of carbonated fertile peridotite under fluid-saturated conditions. Geology 18, 195–199.

Federico, M., Peccerillo, A., 2002. Mineral chemistry and petrogenesis of granular ejecta from the Alban Hills volcano (Central Italy). Mineralogy and Petrology 74, 223–252.

Francalanci, L., Manetti, P., Peccerillo, A., Keller, J., 1993. Magmatological evolution of the Stromboli volcano (Aeolian Arc, Italy): inferences from major and trace element and Sr isotopic composition of the lavas and pyroclastic rocks. Acta Vulcanologica 3, 127–151.

Frezzotti, M.L., Peccerillo, A., 2007. Diamond-bearing C–O–H–S fluids in the mantle beneath Hawaii. Earth Planetary Science Letters 262, 273–283.

Frezzotti, M.L., De Vivo, B., Clocchiatti, R., 1991. Melt–mineral–fluid interactions in ultramafic nodules on alkaline lavas from M. Etna (Sicily, Italy) as recorded by melt and fluid inclusions. Journal of Volcanology and Geothermal Research 47, 209–219.

Frezzotti, M.L., Neumann, E.R., Touret, J.L.R., 2002a. Ephemeral carbonate melts in the upper mantle: carbonate–silicate immiscibility in microveins and inclusions within spinel peridotite xenoliths, La Gomera, Canary Islands. European Journal of Mineralogy 14, 891–904.

Frezzotti, M.L., Andersen, T., Neumann, E.-R., Simonsen, S.L., 2002b. Carbonatite melt-CO_2 fluid inclusions in mantle xenoliths from Tenerife, Canary Islands: a story of trapping, immiscibility and fluid–rock interaction in the upper mantle. Lithos 64, 77–96.

Frezzotti, M.L., De Astis, G., Dallai, L., Ghezzo, C., 2007. Coexisting calc-alkaline and ultrapotassic magmatism at Monti Ernici, Mid Latina Valley (Latium, Central Italy). European Journal of Mineralogy 19, 479–497.

Frondini, F., Chiodini, G., Caliro, S., Cardellini, C., Granieri, D., Ventura, G., 2004. Diffuse CO_2 degassing at Vesuvio, Italy. Bulletin of Volcanology 66, 642–651.

Frondini, F., Baldini, S., Balestra, R., Caliro, S., Cardellini, C., Chiodini, G., Donnini, M., Granieri, D., Morgantini, N., 2008. Interaction between deep and shallow fluids and carbon dioxide degassing at Mt Amiata region. Geophysical Research Abstracts 10, EGU2008–A-06343.

Futterman, W.I., 1962. Dispersive body waves. Journal of Geophysical Research 67, 5279–5291.

Gaetani, G.A., Grove, T.L., 1998. The influence of water on melting of mantle peridotite. Contributions to Mineralogy and Petrology 131, 323–346.

Gambardella, B., Marini, L., Ottonello, G., Vetuschi, M., Zuccolini, R., Cardellini, C., Chiodini, G., Frondini, F., 2004. Fluxes of deep CO_2 in the volcanic areas of central-southern Italy. Journal of Volcanology and Geothermal Research 136, 31–52.

Gerlach, T.M., 1991a. Present-day CO_2 emissions from volcanoes. EOS, Transactions — American Geophysical Union 72, 249, and 254–255.

Gerlach, T.M., 1991b. Etna's greenhouse pump. Nature 31, 352–353.

Gerlach, T.M., McGee, K.A., Elias, T., Sutton, A.J., Doukas, M.P., 2002. Carbon dioxide emission rate of Kilauea Volcano: implications for primary magma and the summit reservoir. Journal of Geophysical Research 107 (B9), 2189. doi:10.1029/2001JB000407.

Goes, S., van der Lee, S., 2002. Thermal structure of the North American uppermost mantle. Journal of Geophysical Research 107. doi:10.1029/2000JB000049.

Grasso, M., 2001. The Apenninic–Maghrebian orogen in Southern Italy, Sicily and adjacent areas. In: Vai, G.B., Martini, P.I. (Eds.), Anatomy of an Orogen. The Apennines and Adjacent Mediterranean Basins. Kluwer, Dordrecht, pp. 255–286.

Gudfinnsson, G.H., Presnall, D.C., 2005. Continuous gradations among primary carbonatitic, kimberlitic, melilititic, basaltic, picritic, and komatiitic melts in equilibrium with garnet lherzolite at 3–8 GPa. Journal of Petrology 46, 1645–1659.

Gvirtzman, Z., Nur, A., 1999. The formation of Mount Etna as the consequence of slab rollback. Nature 401, 782–785.

Hammouda, T., Laporte, D., 2000. Ultrafast mantle impregnation by carbonatite melts. Geology 28, 283–285.

Hunter, R.H., McKenzie, D., 1989. The equilibrium geometry of carbonate melts in rocks of mantle composition. Earth Planetary Science Letters 92, 347–356.

Hyndman, R.D., Shearer, P.M., 1989. Water in the lower continental crust: modelling magnetotelluric and seismic reflection results. Geophysical Journal International 98, 343–365.

Iacono Marziano, G., Gaillard, F., Pichavant, M., 2007a. Limestone assimilation and the origin of CO_2 emissions at the Alban Hills (Central Italy): constraints from experimental petrology. Journal of Volcanology and Geothermal Research 166, 91–105.

Iacono Marziano, G., Gaillard, F., Pichavant, M., 2007b. Limestone assimilation by basaltic magmas: an experimental re-assessment and application to Italian volcanoes. Contributions to Mineralogy and Petrology 155, 719–738.

Italiano, F., Nuccio, M., Pecoraino, G., 1998. Steam output from fumaroles of an active volcano: tectonic and magmatic hydrothermal controls on the degassing system at Vulcano (Aeolian arc). Journal Geophysical Research 103, 29829–29841.

Italiano, F., Martelli, M., Martinelli, G., Nuccio, P.M., 2000. Geochemical evidence of melt intrusions along lithospheric faults of the Southern Apennines, Italy: geodynamic and seismogenic implications. Journal of Geophysical Research 105 (B6), 13569–13578.

Italiano, F., Martinelli, G., Nuccio, P.M., 2001. Anomalies of mantle-derived helium during the 1997–1998 seismic swarm of Umbria–Marche, Italy. Geophysical Research Letters 28, 839–842.

Italiano, F., Martinelli, G., Pizzullo, S., Plescia, P., 2007. Greenhouse gases released from the Apennine Chain, Italy: mechanochemical production besides mantle-derived contribution ICGG9 Taiwan, 1–8 October 2007 Program Proceedings 84.

Jones, A.P., Kostoula, T., Stoppa, F., Wolley, A.R., 2000. Petrography and mineral chemistry of mantle xenoliths in a carbonate-rich melilititic tuff from Vulture volcano, Southern Italy. Mineralogical Magazine 64, 593–613.

Jung, H., Karato, S., 2001. Water-induced fabric transitions in olivine. Science 293, 1460–1463.

Keppler, H., Wiedenbeck, M., Shcheka, S.S., 2003. Carbon solubility in olivine and the mode of carbon storage in the Earth's mantle. Nature 424, 414–416.

Kerrick, D.M., 2001. Present and past non-anthropogenic CO_2 degassing from the solid Earth. Reviews in Geophysics 39, 565–585.

Kerrick, D.M., Connolly, J.A.D., 2001. Metamorphic devolatilization of subducted marine sediments and the transport of volatiles into the Earth's mantle. Nature 411, 293–296.

Knopoff, L., Panza, G.F., 1977. Resolution of upper mantle structure using higher modes of Rayleigh waves. Annali Geofisica, 30, 491–505.

Locardi, E., 1988. The origin of the Apenninic arc. Tectonophysics 146, 105–123.

Lustrino, M., Wilson, M., 2007. The circum-Mediterranean anorogenic Cenozoic Igneous Province. Earth Science Reviews 81, 1–65.

Lustrino, M., Morra, V., Melluso, L., Brotzu, P., D'Amelio, F., Fedele, L., Lonis, R., Franciosi, L., Petteruti, S., Liebercknect, A.M., 2004. The Cenozoic igneous activity in Sardinia. Periodico di Mineralogia 73, 105–134.

Lustrino, M., Melluso, L., Morra, V., 2007a. The geochemical peculiarity of "Plio-quaternary" volcanic rocks of Sardinia in the circum-Mediterranean area. In: Beccaluva, L., Bianchini, G., Wilson, M. (Eds.), Cenozoic Volcanism in the Mediterranean Area. Geological Society of America Special Paper, vol. 418, pp. 277–301.

Lustrino, M., Morra, V., Fedele, L., Serracino, M., 2007b. The transition between "orogenic" and "anorogenic" magmatism in the western Mediterranean area: the middle Miocene volcanic rocks of Isola del Toro (SW Sardinia, Italy). Terra Nova 19, 148–159.

Martelli, M., Nuccio, P.M., Stuart, F.M., Burgess, R., Ellam, R.M., Italiano, F., 2004. Helium–strontium isotope constraints on mantle evolution beneath the Roman Comagmatic Province Italy. Earth Planetary Science Letters 224, 295–308.

Martelli, M., Nuccio, P.M., Stuart, F.M., Di Liberto, V., Ellam, R.M., 2008. Constraints on mantle source and interactions from He–Sr isotope variation in Italian Plio-Quaternary volcanism. Geochemistry Geophysics Geosystems 9. doi:10.1029/2007GC001730.

Miller, S.A., Collettini, C., Chiaraluce, L., Cocco, M., Barchi, M., Kaus, B.J.P., 2004. Aftershocks driven by a high pressure CO_2 source at depth. Nature 427, 724–727.

Minissale, A., 2004. Origin, transport and discharge of CO_2 in central Italy. Earth Science Review 66, 89–141.
Minissale, A., Magro, G., Tassi, F., Frau, F., Vaselli, O., 1999. The origin of natural gas emissions from Sardinia island, Italy. Geochemical Journal 33, 1–12.
Mörner, N.A., Etiope, G., 2002. Carbon degassing from the lithosphere. Global Planetary Change 33, 185–203.
Nakai, S., Wakita, H., Nuccio, P.M., Italiano, F., 1997. MORB-type neon in an enriched mantle beneath Etna, Sicily. Earth Planetary Science Letters 153, 57–66.
Panza, G.F., 1981. The resolving power of seismic surface waves with respect to crust and upper mantle structural models. In: Cassinis, R. (Ed.), The Solution of the Inverse Problem in Geophysical Interpretation. Plenum Publication Corporation, pp. 39–77.
Panza, G.F., 1985. Synthetic seismograms: the Rayleigh waves modal summation. Journal of Geophysics 58, 125–145.
Panza, G.F., Calcagnile, G., 1979. The upper mantle structure in Balearic and Tyrrhenian bathyal plains and the Messinian salinity crisis. Palaeogeography Palaeoecology Palaeoclimatology 29, 3–14.
Panza, G.F., Raykova, R.B., 2008. Structure and rheology of lithosphere in Italy and surrounding. Terra Nova 20, 194–199.
Panza, G.F., Pontevivo, A., Chimera, G., Raykova, R., Aoudia, A., 2003. The lithosphere–asthenosphere: Italy and surroundings. Episodes 26, 169–174.
Panza, G.F., Raykova, R.B., Carminati, E., Doglioni, C., 2007a. Upper mantle flow in the western Mediterranean. Earth Planetary Science Letters 257, 200–214.
Panza, G.F., Peccerillo, A., Aoudia, A., Farina, B., 2007b. Geophysical and petrological modeling of the structure and composition of the crust and upper mantle in complex geodynamic settings: The Tyrrhenian Sea and surroundings. Earth Science Reviews 80, 1–46.
Pauselli, C., Barchi, M.R., Federico, C., Magnani, M.B., Minelli, G., 2006. The crustal structure of the northern Apennines (central Italy): an insight by the CROP03 seismic line. American Journal of Science 306, 428–450.
Peccerillo, A., 1985. Roman comagmatic province (Central Italy); evidence for subduction-related magma genesis. Geology 13, 103–106.
Peccerillo, A., 1999. Multiple mantle metasomatism in central-southern Italy: geochemical effects, timing and geodynamic implications. Geology 27, 315–318.
Peccerillo, A., 2003. Plio-Quaternary magmatism in Italy. Episodes 26, 222–226.
Peccerillo, A., 2005. Plio-Quaternary volcanism in Italy. Petrology, Geochemistry, Geodynamics. Springer, Heidelberg. 365 pp.
Peccerillo, A., Lustrino, M., 2005. Compositional variations of the Plio-Quaternary magmatism in the circum-Tyrrhenian area: deep- vs. shallow-mantle processes. In: Foulger, G.R., Nathland, J.H., Presnall, D.C., Anderson, D.L. (Eds.), Plates, Plumes and Paradigms. Geological Society of America Special Publication, vol. 388, pp. 421–434.
Peccerillo, A., Panza, G.F., 1999. Upper mantle domains beneath Central-Southern Italy: petrological, geochemical and geophysical constraints. Pure Applied Geophysics 156, 421–443.
Peccerillo, A., Poli, G., Serri, G., 1988. Petrogenesis of orenditic and kamafugitic rocks from Central Italy. Canadian Mineralogist 26, 45–65.
Peccerillo, A., Panza, G.F., Aoudia, A., Frezzotti, M.L., 2008. Relationships between magmatism and lithosphere asthenosphere structure beneath the western Mediterranean and implication for geodynamics. Randiconti Lincei 19, 291–309.
Peresan, A., Vorobieva, I., Soloviev, A., Panza, G.F., 2007. Simulation of seismicity in the block-structure model of Italy and its surroundings. Pure and Applied Geophysics 164, 2193–2234.
Pontevivo, A., Panza, G.F., 2006. The lithosphere–asthenosphere system in the Calabrian Arc and surrounding seas — Southern Italy. Pure Applied Geophysics 163, 1617–1659.
Presnall, D.C., Gudfinnsson, G.H., 2005. Carbonate-rich melts in the seismic low-velocity zone and deep mantle. In: Foulger, G.R., Natland, J.H., Presnall, D.C., Anderson, D.L. (Eds.), Plates, Plumes, and Paradigms. Geological Society of America Special Paper, vol. 388, pp. 207–216.
Rogers, N.W., Hawkesworth, C.J., Parker, R.J., Marsh, J.S., 1985. The geochemistry of potassic lavas from Vulsini, central Italy and implications for mantle enrichment processes beneath the Roman region. Contributions to Mineralogy and Petrology 90, 244–257.
Rogie, J.D., Kerrick, D.M., Chiodini, G., Frondini, F., 2000. Flux measurements of non-volcanic CO_2 emission from some vents in central Italy. Journal of Geophysical Research 105 (B4), 8435–8446.
Rosatelli, G., Wall, F., Stoppa, F., Rotolo, M., 2007. Calcio-carbonatite melts and metasomatism in the mantle beneath Mt. Vulture (Southern Italy). Lithos 99, 229–248.
Rosenbaum, G., Gasparon, M., Lucente, F.P., Peccerillo, A., Miller, M.S., 2008. Kinematics of slab tear faults during subduction segmentation and implications for Italian magmatism. Tectonics 27, TC2008. doi:10.1029/2007TC002143.
Rotolo, S.G., La Felice, S., Mangalaviti, A., Landi, P., 2007. Geology and petrochemistry of the recent (<25 ka) silicic volcanism at Pantelleria Island. Bollettino della Società Geologica Italiana 126, 191–208.
Sapienza, G., Scribano, V., 2000. Distribution and representative whole-rock chemistry of deep-seated xenoliths from Iblean Plateau, South-Eastern Sicily, Italy. Periodico di Mineralogia 69, 185–204.
Sapienza, G., Hilton, D.R., Scribano, V., 2005. Helium isotopes in peridotite mineral phases from Hyblean Plateau (south-eastern Sicily, Italy). Chemical Geology 219, 115–129.
Sartori, R., 2003. The Thyrrhenian backarc basin and subduction of the Ionian lithosphere. Episodes 26, 217–221.
Savelli, C., Gasparotto, G., 1994. Calc-alkaline magmatism and rifting of the deep-water volcano of Marsili (Aeolian back-arc, Tyrrhenian Sea). Marine Geology 119, 137–157.
Scambelluri, M., Hermann, J., Morten, L., Rampone, E., 2006. Melt- versus fluid-induced metasomatism in spinel to garnet wedge peridotites (Ulten Zone, Eastern Italian Alps): clues from trace element and Li abundance. Contributions to Mineralogy and Petrology 151, 372–394.
Schiano, P., Clocchiatti, R., Ottolini, L., Busà, T., 2001. Transition of Mount Etna lavas from a mantle-plume to an island-arc magmatic source. Nature 412, 900–904.
Schmidt, M.W., 2007. CO_2 and potassium in the mantle: carbonaceous pelite melts from the trailing edge of a detached slab hybridizing in the mantle to ultrapotassic kamafugite. Eos, Transactions — American Geophysical Union 88 (52) Fall Meet. Suppl., Abstract DI43A-01.
Schmidt, M.W., Poli, S., 1998. Experimentally based water budgets for dehydrating slabs and consequences for arc magma generation. Earth and Planetary Science Letters 163, 361–379.
Stixrude, L., Lithgow-Bertelloni, C., 2005. Mineralogy and elasticity of the upper mantle: origin of the low velocity zone. Journal of Geophysical Research 110, B03204. doi:10.1029/2004JB002965.
Stracke, A., Hofmann, A., Hart, S.R., 2005. FOZO, HIMU and the rest of the mantle zoo. Geochemistry Geophysics Geosystems 6. doi:10.1029/2004GC000824.
Thomsen, T.B., Schmidt, M.W., 2008. Melting of carbonated pelites at 2.5–5.0 GPa, silicate–carbonatite liquid immiscibility, and potassium–carbon metasomatism of the mantle. Earth and Planetary Science Letters 267, 17–31.
Tonarini, S., Armienti, P., D'Orazio, M., Innocenti, F., 2001. Subduction-like fluids in the genesis of Mt. Etna magmas: evidence from boron isotopes and fluid mobile elements. Earth and Planetary Science Letters 192, 471–483.
Turco, A., Zuppetta, A., 1998. Kinematic model for the Plio-Quaternary evolution of the Tyrrhenian–Apenninic system: implications for rifting processes and volcanism. Journal of Volcanology and Geothermal Research 82, 1–18.
van Keken, P.E., Hauri, E.H., Ballentine, C.J., 2002. Mantle mixing: the generation, preservation, and destruction of chemical heterogeneity. Annual Review of Earth Planetary Sciences 30, 493–525.
Varekamp, J.C., Thomas, E., 1998. Volcanic and anthropogenic contributions to global weathering budgets. Journal of Geochemical Exploration 62, 149–159.
Ventura, G., Cinti, F., Di Luccio, F., Pino, A., 2007. Mantle wedge dynamics versus crustal seismicity in the Apennines (Italy). Geochemistry Geophysics Geosystems 8. doi:10.1029/2006GC001421.
Viccaro, M., Cristofolini, R., 2008. Nature of mantle heterogeneity and its role in the short-term geochemical and volcanological evolution of Mt. Etna (Italy). Lithos 105, 272–288.
Watson, E.B., Brenan, J.M., 1987. Fluids in the lithosphere, 1. Experimentally-determined wetting characteristics of CO_2–H_2O fluids and their implications for fluid transport, host-rock physical properties, and fluid inclusion formation. Earth and Planetary Science Letters 85, 497–515.
Watson, E.B., Brenan, J.M., Baker, D.R., 1990. Distribution of fluids in the continental lithospheric mantle. In: Menzies, M.A. (Ed.), The Continental Lithospheric Mantle. Clarendon Press, Oxford, pp. 111–125.

Tectonophysics xxx (2009) xxx–xxx

Contents lists available at ScienceDirect

Tectonophysics

journal homepage: www.elsevier.com/locate/tecto

Can Earth's rotation and tidal despinning drive plate tectonics?

Federica Riguzzi [a,c,*], Giuliano Panza [b], Peter Varga [d], Carlo Doglioni [a,*]

[a] Dipartimento di Scienze della Terra, Università Sapienza, Roma, Italy
[b] Dipartimento di Scienze della Terra, Università di Trieste, and ICTP, Italy
[c] Istituto Nazionale di Geofisica e Vulcanologia, Roma, Italy
[d] Geodetic and Geophysical Research Institute, Seismological Observatory, Budapest, Hungary

ARTICLE INFO

Article history:
Received 9 January 2009
Accepted 10 June 2009
Available online xxxx

Keywords:
Plate tectonics
Earth's rotation
Tidal despinning
Earth's energy budget

ABSTRACT

We re-evaluate the possibility that Earth's rotation contributes to plate tectonics on the basis of the following observations: 1) plates move along a westerly polarized flow that forms an angle relative to the equator close to the revolution plane of the Moon; 2) plate boundaries are asymmetric, being their geographic polarity the first order controlling parameter; unlike recent analysis, the slab dip is confirmed to be steeper along W-directed subduction zones; 3) the global seismicity depends on latitude and correlates with the decadal oscillations of the excess length of day (LOD); 4) the Earth's deceleration supplies energy to plate tectonics comparable to the computed budget dissipated by the deformation processes; 5) the Gutenberg–Richter law supports that the whole lithosphere is a self-organized system in critical state, i.e., a force is acting contemporaneously on all the plates and distributes the energy over the whole lithospheric shell, a condition that can be satisfied by a force acting at the astronomical scale.
Assuming an ultra-low viscosity layer in the upper asthenosphere, the horizontal component of the tidal oscillation and torque would be able to slowly shift the lithosphere relative to the mantle.

1. Introduction

The energy budget of plate tectonics and the basic mechanisms that move plates are far to be entirely understood. A very large number of papers have suggested strong evidence for a system driven primarily by lateral density heterogeneities, controlled by the thermal cooling of the Earth, particularly with the cool slab pulling the attached plates (Conrad and Lithgow-Bertelloni, 2003). However, a number of issues contradict a simple thermal model capable to generate the Earth's geodynamics (Anderson, 1989). Large plates move coherently, being decoupled at the LVZ (Fig. 1). They show that the force acting on them is uniformly distributed and not concentrated to their margins. For example, the inferred slab pull would be stronger than the strength plates can sustain under extension (pull). Moreover, the geological and geophysical asymmetries of rift and subduction zones as a function of their polarity (Doglioni et al., 2007) may be interpreted as controlled by some astronomical mechanical shear (Scoppola et al., 2006).

The interest in the Earth's rotation as driving plate tectonics goes back to the theory of Wegener and to a number of papers in the early seventies (Bostrom, 1971; Knopoff and Leeds, 1972). This relation is based on the observation that plates have, for example, a westerly directed polarization relative to Antarctica (Le Pichon, 1968) or relative to the hotspot reference frame (Ricard et al., 1991; Gripp and Gordon, 2002; Crespi et al., 2007).

In this article we review a number of topics about the rotational contribution to plate tectonics, finally proposing a mechanical model to explain it.

2. Evidences for a worldwide asymmetry

It has been shown how plate motions followed and follow a mainstream (Fig. 2) that can be reconstructed from ocean magnetic anomalies and space geodesy data (Doglioni, 1990; Crespi et al., 2007). This flow is polarized toward the "west" relative to the mantle. The net rotation is only an average value in the deep hotspot reference frame, but it rises to a complete polarization in the shallow hotspot reference frame (Fig. 2). The latitude range of the net rotation equator is about the same of the Moon maximum declination range (±28°) during the nutation period (≈18.6 yr). Further indications come from the fact that the induced geopotential variations and the solid Earth tide modeling (McCarthy and Petit, 2004) generate maximum amplitudes of the Earth bulges (≈30 cm) propagating progressively within the same latitude range. In particular, the track of the semidiurnal bulge crest is about directed from E to W, as small circles moving from latitudes 28° to 18°, when the Moon moves from maximum to minimum declinations (the same happens at negative latitudes for the opposite bulge), thus suggesting a role of rotational and tidal drag effects (Bostrom, 2000; Crespi et al., 2007).

* Corresponding authors.
E-mail addresses: riguzzi@ingv.it (F. Riguzzi), carlo.doglioni@uniroma1.it (C. Doglioni).

0040-1951/$ – see front matter © 2009 Elsevier B.V. All rights reserved.
doi:10.1016/j.tecto.2009.06.012

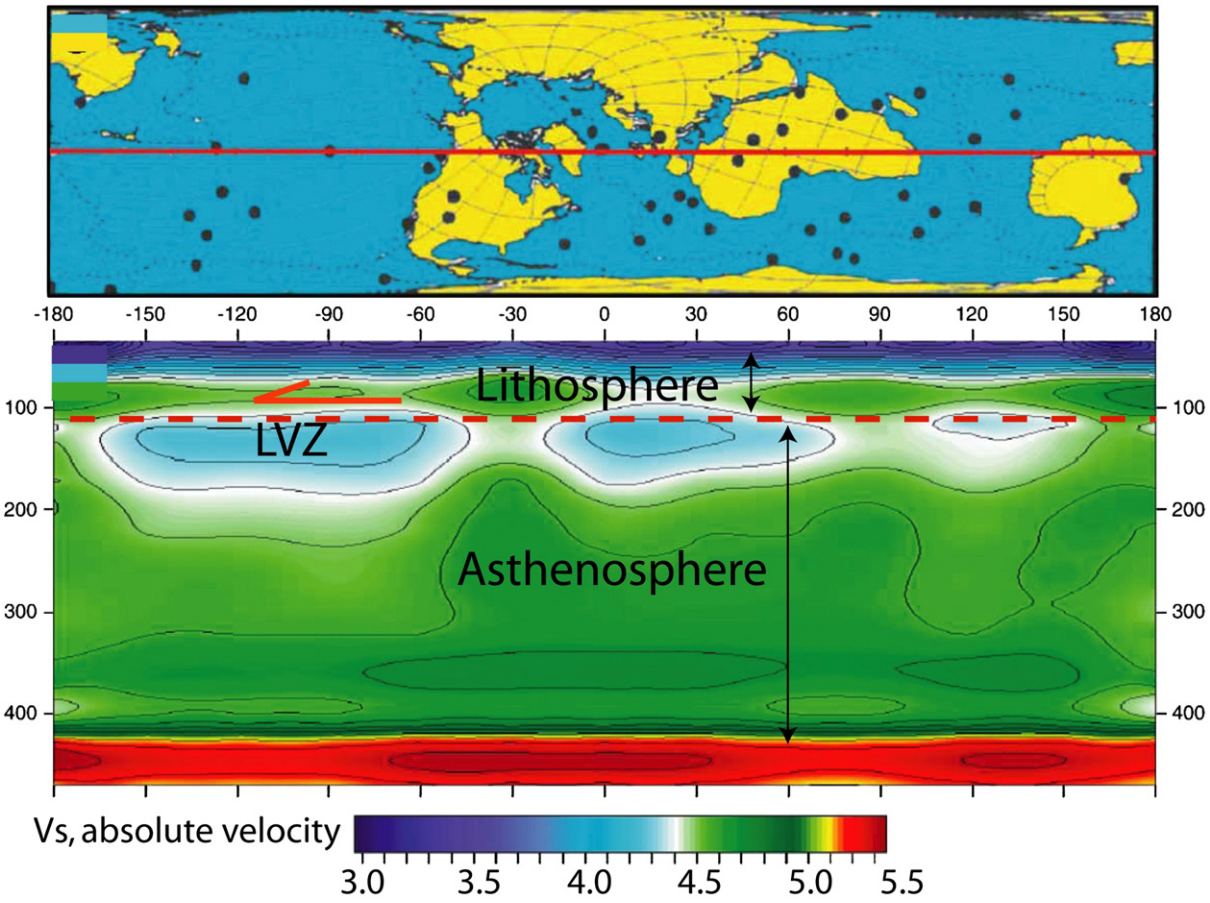

Fig. 1. Earth's cross section and related location map (red line, above), modified after Thybo (2006). Absolute shear wave velocity model includes a pronounced, global Low Velocity Zone (LVZ) at the top of the asthenosphere, which is strongest underneath the oceans, but also clearly identifiable underneath the continents. This level is here inferred as the main decoupling zone at the base of the lithosphere, possibly having an internal sub-layer with ultra-low viscosity, much lower than the average asthenosphere. (For interpretation of the references to color in this figure legend, the reader is referred to the web version of this article.)

Tectonic features on Earth show profound asymmetries as a function of their geographic polarity. A long list of signatures marks the distinction between orogens and related subduction zones and rift zones (Zhang and Tanimoto, 1993; Doglioni et al., 2003). These differences can be observed moving along the undulated flow of plate motions (Crespi et al., 2007; Doglioni et al., 2007) and diminish if east- versus west-facing structures are compared. The orogens associated with E- or NE-directed slabs (orogens of type A) are more elevated (>1000 m) with respect to what is observed at the steeper W-directed slabs, where the accretionary prisms (orogens of type B) have much lower average elevation (−1250 m), as shown in Fig. 3. The rocks outcropping along the orogens related to the E- or NE-directed subduction zones represent the entire crust and upper mantle section, whereas at the W-directed slab, the accretionary prisms are mostly composed by sedimentary and upper-crust rocks. Therefore orogens of type A have much deeper decoupling planes with respect to orogens of type B. The foredeep has lower subsidence rates (<0.2 mm/yr) along E- or NE-directed subduction zones with respect to the W-directed ones, where the foredeep-trench subsidence is much faster (>1 mm/yr). Along the E- or NE-directed subduction zones, the subduction hinge moves toward the upper plate, whereas it generally moves away from the upper plate along the W-directed subduction zones. This asymmetric behavior implies, on average, a three times faster lithospheric recycling into the mantle along W-directed subduction zones and provides evidence for polarized mantle convection. Gravity, heat flow anomalies, seismicity, etc. also support these differences, and along rift zones, the eastern flank is, on average, 100–300 m shallower than the western flank (Fig. 3).

Another critical issue is the dip of the subduction zones. The slab dip has been the topic of a number of researches (e.g., Jarrard, 1986). During the seventies it was noticed that the western Pacific slabs are steeper than the eastern side (Isacks and Barazangi, 1977). This asymmetry has been used (Nelson and Temple, 1972; Dickinson, 1978; Uyeda and Kanamori, 1979; Doglioni, 1990; 1993) to infer a mantle flow directed toward the "east", confirming the notion of the "westerly" drift of the lithosphere (Le Pichon, 1968; Bostrom, 1971; Shaw and Jackson, 1973; Moore, 1973). Recently, Lallemand et al. (2005), based on a study where they divided each slab into a shallower part (<125 km) and a deeper segment (>125 km), suggested that the dip difference between western- and eastern-directed subduction zones is not statistically significant, but they recognized that the slabs beneath the oceanic crust are steeper than beneath the continents. This slope difference confirms the presence of a large asymmetry in the Pacific, where the less steep slabs with continental lithosphere lie along the eastern margin, whereas the generally steeper slabs (apart Japan) with oceanic lithosphere in the overriding plate, prevail along the western Pacific margins.

The westward drift of the lithosphere implies a relative "eastward" mantle flow (e.g. Panza et al., 2007), the decoupling taking place in the asthenosphere whose top, generally, is deeper than 100 km. Therefore the shallow part of the slab may not show any relevant dip difference.

Cruciani et al. (2005) carefully measured the slab dip and they demonstrated that the slab age is not correlated to the dip of the slab, contrary to earlier observations (e.g., Wortel, 1984). The analysis of Cruciani et al. (2005) is deliberately limited to the uppermost 250 km of depth because in E- or NE-directed subduction zones, seismicity

Please cite this article as: Riguzzi, F., et al., Can Earth's rotation and tidal despinning drive plate tectonics? Tectonophysics (2009), doi:10.1016/j.tecto.2009.06.012

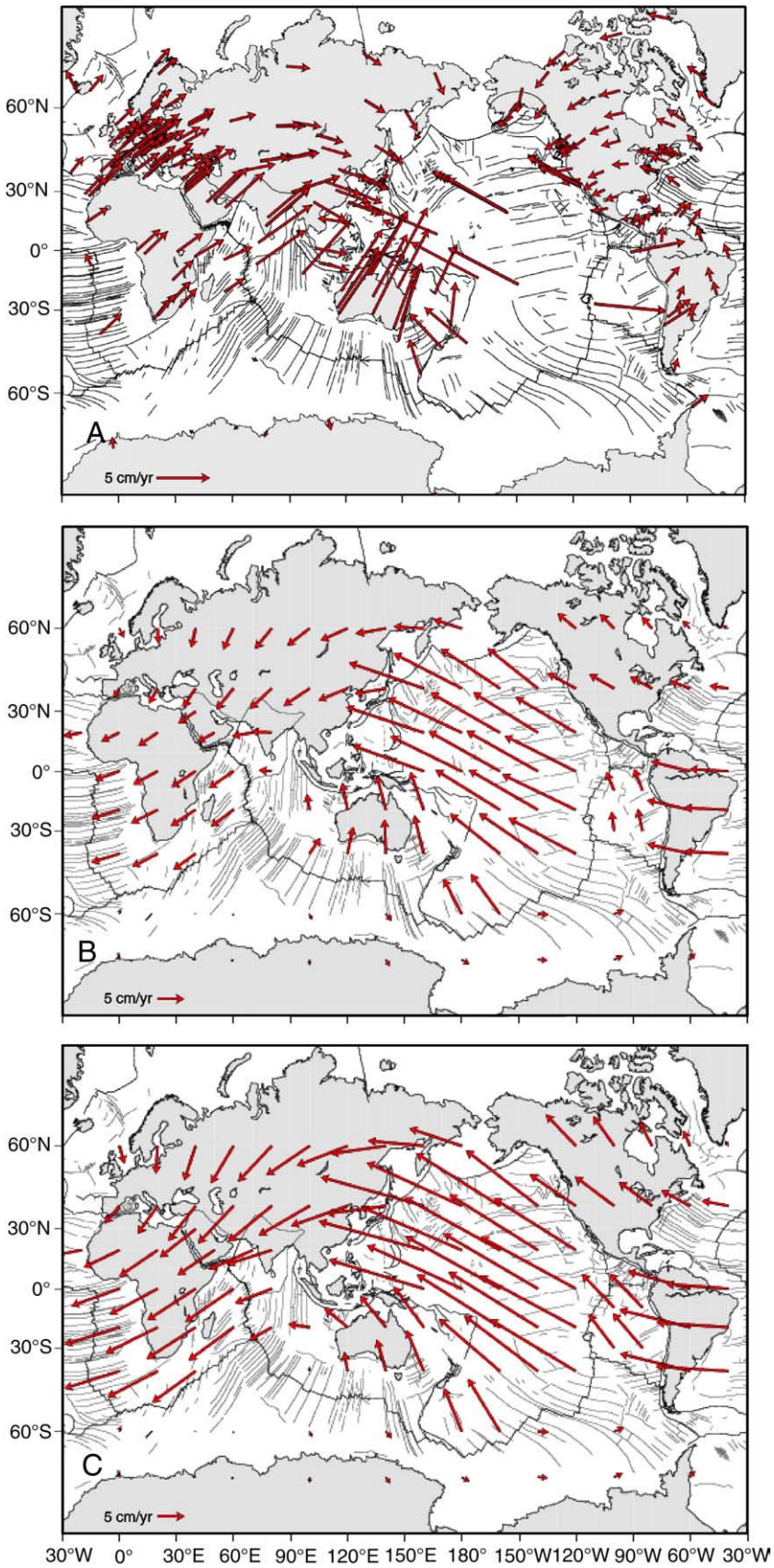

Fig. 2. Plate motions in the NNR reference frame (A, after Altamimi et al., 2007), in the deep (B) and shallow (C) hotspot reference frames (Crespi et al., 2007). In all reference frames plates follow an undulate mainstream. In case C, plates have a complete "westerly" directed polarization relative to the mantle.

Please cite this article as: Riguzzi, F., et al., Can Earth's rotation and tidal despinning drive plate tectonics? Tectonophysics (2009), doi:10.1016/j.tecto.2009.06.012

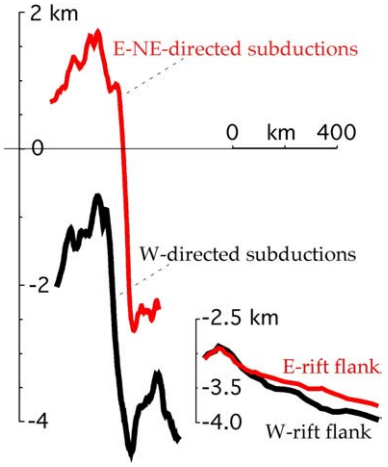

Fig. 3. Comparison between the average topography–bathymetry of subduction zones (left) and rift zones (right). The elevation is higher in the E- or NE-directed subduction zones and in the E-flank of rift zones.

does not extend systematically at greater depth, apart few areas where it appears concentrated between 550 and 670 km depth, close to the lower boundary of the upper mantle. The origin of these deep isolated earthquakes remains obscure: mineral phase change (Green and Houston, 1995), blob of detached slab, higher shear stress, shear affecting an uplifted lower mantle (Doglioni et al., 2009) and therefore they does not a priori represent the simple geometric prolongation of the shallow part of the slab.

When comparing the slab dip between 100 and 250 km of depth, and removing the subduction zones that are oblique with respect to the convergence direction, as Central America, the W-directed subduction zones show the larger (steeper) angles (Cruciani et al., 2005).

Moreover subduction zones, as a rule, juxtapose plates of different thickness and composition and this generates variation in the dip, e.g., a thicker plate with a stiff "vertical" margin will oblige the subducting slab to assume the shape of the overriding plate until it reaches its base, below the decoupling layer, at a depth of 100–150 km. The variability of the angle of obliquity of the subduction strike with respect to the convergence direction determines a further change in the dip of the slab, i.e., frontal subductions are steeper along the W-directed subduction zones than along E- or NE-directed ones. This is also evident from the foreland regional monocline that records the initial dip of the slab (Mariotti and Doglioni, 2000). In fact the dip is, on average, 6.1° along the W-directed subduction zones, while it is only 2.6° along the E- or NE-directed ones (Lenci and Doglioni, 2007).

In order to test the Lallemand et al. (2005) analysis, we recomputed the slab dip. In general, the W-directed subduction zones, when compared to E- or NE-directed slabs, show remarkable differences: (a) they are steeper, (b) they extend to greater depths and (c) they present a more coherent slab-related seismicity from the surface down to the 670 km discontinuity.

The dip of the slab perpendicular to the trench or strike of the subduction is given in Table 1 for W-directed and E- or NE-directed subduction zones. This measurement gives the maximum dip of the slab, regardless of the relative motion among upper and lower plates. In fact, the dip measured parallel to the convergence direction along a lateral ramp of a slab appears shallower. The measurements are based on geometries defined on the base of the seismicity (space distribution of hypocenters) alone, and not on images of inferred slabs based on tomography.

The selected subduction zones represent most of the world slabs. The analysis compares subduction polarity as a function of their strike with respect to the undulate mainstream of plate motion described by Crespi et al. (2007). The W-directed slabs are, on average, dipping 65.6°, whereas the E- or NE-directed slabs are dipping 27.1° (Fig. 4). These results that are fully in agreement with Isacks and Barazangi (1977) who showed that western Pacific slabs are generally steeper than the eastern ones for most of their strike, are significantly different from those of Lallemand et al. (2005). The reasons for this difference could be the smearing effect that cannot be excluded in any mantle tomography (Raykova and Panza, 2006; Anderson, 2007b), and the arbitrary connection of the shallow slab seismicity with the deep isolated clusters along the E- or NE-directed subduction zones, or a combination of both. In fact, high-velocity bodies suggesting the presence of slabs in tomographic images often do not match slab seismicity, and the inference of slabs deeper than 250 km based on tomographic images is velocity model dependent and the color palette can be significantly misleading (e.g., Trampert et al., 2004; Anderson, 2006; 2007a,b).

There are at least three zones in the world where the same plate with similar composition subducts contemporaneously along two opposite subduction zones. These are 1) the central Mediterranean where the Ionian (oceanic)–Adriatic (continental) lithosphere subducts both westward beneath the Apennines, and NE-ward beneath the Dinarides–Hellenides; 2) the northern Australia where the passive continental margins subduct westward along the Banda arc and NE-ward along the Papua-New-Guinea subduction zone; and 3) the Molucche area where again a narrow segment of lithosphere is sinking along opposite subduction zones. In all these cases the W-directed slab-related seismicity, regardless of the age and composition of the subducting lithosphere, is steeper and reaches deeper than the E- or NE-directed one. Moreover there are no sub-vertical slabs beneath E-directed subduction zones, neither sub-horizontal slabs along W-directed subduction zones, whereas the contrary is observed (e.g., Mexico, Andes from almost 0° to 15°, and Mariannas, 80–90°).

The steeper E-directed slabs are seen along the Nicaragua and New Hebrides subduction zones, whereas the least steep W-directed slab is along Japan. These cases that are used as arguments against the existence of a global asymmetry, may, in fact be an exception to the global trend explained by regional conditions. The Japan subduction is

Table 1
Dip of the slab of the W- and E- or NE- directed subduction zones.

W-directed	Slab dip >100 km	E- or NE-directed	Slab dip >70 km	Deep cluster
Tohoku-Japan	35°	Nicaragua	50°	
Kuriles-Kamchatka	45°	Cascadia	18°	
Molucche 3°N	50°	Molucche 3°N	45°	
Aleutians 55°N/160°W	50°	New Hebrides	50°	yes
N-New Zealand 39°S	65°	Zagros	18°	
Banda	55°	Himalaya	15°	
Tonga	58°	Perù 10°S	10°	
Cotabago	63°	Perù-Bolivia 15°S	18°	yes
Mariannas 22°N	84°	Chile 22°S	21°	yes
Izu-Bonin 32°N	72°	Chile 24°S	21°	
Izu-Bonin 27°N	83°	Ecuador 3°S	20°	
Apennines	72°	Costarica	50°	
Sandwich	69°	Colombia 5°N	25°	
Barbados	68°	Hellenides	23°	
Mariannas 12°N	85°	Mexico	10°	
Mariannas 19°N	84°	Sumatra 100°E	32°	
Vrancea	78°	Sumatra 115°E	35°	yes
Average	65.6°	Average	27.1	

Data after Ammon et al. (2008); Sacks and Okada (1974); Isacks and Barazangi (1977); Baranzangi and Isacks (1979); Pilger (1981); Vassiliou et al. (1984); McGeary et al. (1985); Jarrard (1986); Garfunkel et al. (1986); Oncescu and Trifu (1987); Bevis (1988); Cahill and Isacks (1992); Oncescu and Bonjer (1997); Engdahl et al. (1998); Gudmundsson and Sambridge (1998); Castle and Creager (1998); Gutscher et al. (1999); Chen et al. (2001); Karato et al. (2001); Engdahl and Villaseñor (2002); Rivera et al. (2002); Pardo et al. (2002); Billen et al. (2003); Hirth and Kohlstedt (2003); Das (2004); Lallemand et al. (2005); Milsom (2005); Syracuse and Abers (2006); Frepoli et al. (1996);Reyners et al. (2006); Billen and Hirth (2007); Vinnik et al. (2007); Chiarabba et al. (2008); Espurt et al. (2008); Pérez-Campos et al. (2008); and Scalera (2008).

Please cite this article as: Riguzzi, F., et al., Can Earth's rotation and tidal despinning drive plate tectonics? Tectonophysics (2009), doi:10.1016/j.tecto.2009.06.012

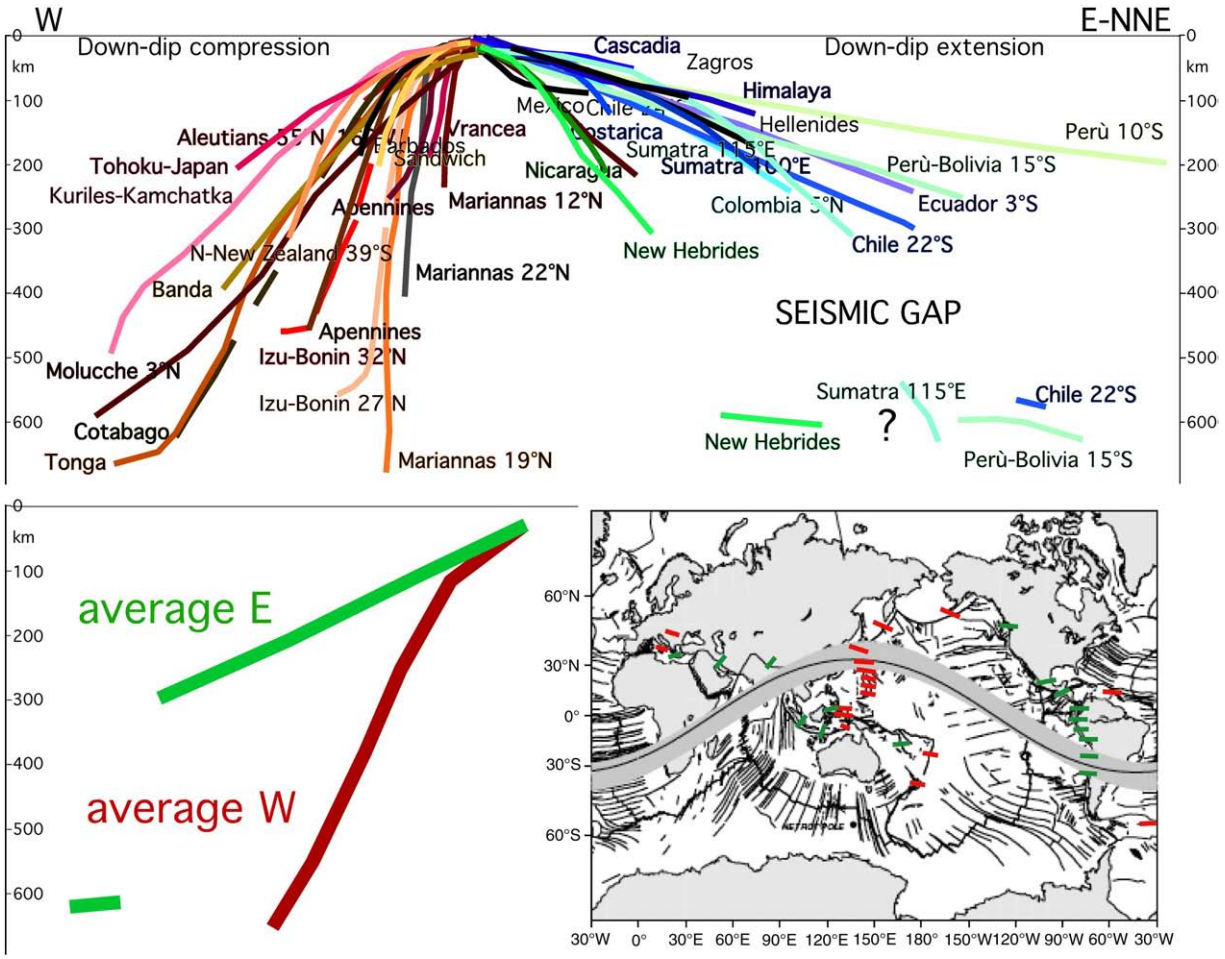

Fig. 4. Compilation of the slab dip measured along cross-sections perpendicular to the trench of most subduction zones. Each line represents the mean trace of the seismicity along every subduction. The asymmetry is also marked by the seismic gap between around 300–550 km occurring only along the E- or NE-directed subduction zones, that are, in general, shorter than the W-directed slabs. Some E- or NE-subduction zones present a deeper scattered cluster of hypocenters between 550–670 km which may be interpreted either as a detached fragment of the slab, or as a portion of lower mantle sucked from below, in the wake left by the slab in its anti-subduction (exumation) motion (Doglioni et al., 2009). The dominant down-dip compression occurs in the W-directed intraslab seismicity, whereas down-dip extension prevails along the opposed E- or NE-directed slabs. The W-directed slabs are, on average, dipping 65.6°, whereas the average dip of the E- or NE-directed slabs, to the right, is 27.1° (see Table 1).

presently not following the standard kinematics of W-directed subduction zones where the subduction hinge migrates away from the upper plate; the hinge moves toward Eurasia and in fact the Japan Sea is shrinking. On the other hand, New Hebrides and Central America subduction zones have a relevant transpressional component (oblique subduction), which could contribute to the steepness of the slab. Australia is moving NNE-ward in the NNR (No-Net-Rotation reference frame, DeMets et al., 1990), and the NNW strike of the Vanuatu-New Hebrides trench implies that the subduction has a strong right lateral component (lateral-oblique subduction). Moving along the southern tip of the New Hebrides trench, where the subduction is in a frontal geometry, the slab is much less inclined (<30°, Chatelain et al., 1993). The New Hebrides slab is quite short, with the typical seismic gap between 250–500 km. Similarly, the Central America slab has a left-lateral transpressive component, it is short, and becomes more flat along frontal segments of the subduction both to the south and to the north.

If the study of the slab dip is made based on mantle tomography images rather than on the space distribution of hypocenters a quite different picture can be drawn, e.g., the E-directed slabs appear longer and steeper. Thus this observation could be used to deny the asymmetry emerging from the analysis of the seismicity (the space distribution of hypocenters), but it must be kept in mind that the accuracy of the location of hypocenters clusters in the slabs (several tens of km) is comparable, if not much better, than the mantle tomography resolution (few hundreds of km) (e.g. Vasco et al., 2003). This is due to the information content of the travel time data used in tomography experiments and to the dependence, on the initial reference velocity model, of the tomographic images that are routinely obtained by means of linear inversion. Assuming that the high-velocity bodies inferred from tomography are real, an alternative interpretation of these faster velocities is given by Doglioni et al. (2009). Relative to the mantle, W-directed subduction zones provide larger volumes of lithosphere re-entering into the mantle than the opposite E- or NE-directed slabs, which have a low sinking angle and could have a net motion in a direction opposed to the one of the subduction. This kinematics is consistent with an upward suction of the underlying mantle, with the upraising at shallower levels of mantle rocks that are thus naturally detected as a body with velocity higher than that of the surrounding medium. This generates on tomographic images an inclined column, usually much broader than a lithospheric slab, of faster mantle, which generates the phantom of a slab. In this hypothesis, along the E- or NE-directed subduction zones, beneath 300 km, the mantle tomography would not depict the real slabs, possibly being misleading in the study of the subduction zones.

The seismic coupling indicates the friction at the interface between upper and lower plates along subduction zones. This is lower along subduction zones where backarc spreading forms (Ruff and Kanamori, 1980). Backarc extension is typical of W-directed subduction zones where the subduction hinge migrates away relative to the upper plate

Please cite this article as: Riguzzi, F., et al., Can Earth's rotation and tidal despinning drive plate tectonics? Tectonophysics (2009), doi:10.1016/j.tecto.2009.06.012

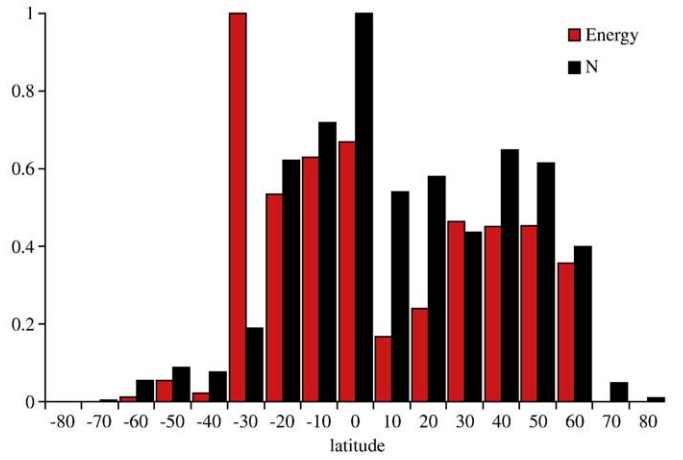

Fig. 5. Distribution of normalized N (number of earthquakes with $M_w \geq 7.0$) and E (elastic energy released by earthquakes with $M_w \geq 7.0$) grouped in 10° latitude bins, from the catalog — MGE7 global (earthquakes with $M_w \geq 7.0$ in the period 1900–2007). The outstanding energy release of the Chile earthquake (1960, $M_w = 9.5$) is well visible. Polar regions are silent whereas the seismic activity is maximum at low latitudes.

(Doglioni et al., 2007). High seismic coupling occurs where the subduction hinge converges relative to the upper plate, which is typical of E- or NE-directed subduction zones.

Another further asymmetry is the state of stress within slabs. W-directed subduction zones show predominantly down-dip compression of the intraslab seismicity, whereas E- or NE-directed slabs exhibit more frequently down-dip extension (Isacks and Molnar, 1971; Doglioni et al., 2007).

All these features have been interpreted as related to the "eastward" relative motion of the asthenosphere with respect to the lithosphere, which should determine not only different metamorphic and petrological evolutions (Peccerillo, 2005; Doglioni et al., 2007) but also different depths and behaviors of the basal decoupling planes. Moreover a relatively cooler mantle has been envisaged at the Earth's equator (Bonatti et al., 1993), favoring the idea of a rotational component in mantle differentiation.

3. Latitudinal distribution of global seismicity

We have analyzed the global distribution of seismic events for magnitudes $M \geq 7.0$, which release about 90% of the elastic energy of plate tectonics, using the Centennial Catalog (CC) updated with the USGS/NEIC global catalog. We call this new catalog MGE7 global.

The CC is a global catalog which contains the locations and magnitudes of instrumentally recorded large earthquakes (Engdahl and Villaseñor, 2002). In this catalog that extends from 1900 to April 2002 all available magnitudes for each earthquake have been reduced to a common, reliable value. Thus completeness is practically ensured for magnitudes $M_w \geq 7.0$. The CC has been updated to September 2007 by adding all the events with $M_w \geq 7.0$ extracted from the USGS/NEIC global catalog. The MGE7 global contains 1719 events with $M_w \geq 7.0$ and the locations clearly delineate the plate margins and the deformation areas. Nevertheless, the seismicity is latitude dependent and decreases with increasing latitude. The distribution of the normalized frequency of the events in 10° bins shows that polar regions are not affected by seismic activity with $M_w \geq 7.0$, and that most of the events fall in the range $-10° < \text{Lat} \leq 0°$ N (Fig. 5). The normalized energy computed by the classical relationship (Kanamori, 1977) shows that more than 73% of the elastic energy is radiated in the range $-30° < \text{Lat} \leq 30°$ N. These patterns support a rotational and astronomical tuning of plate tectonics: at low latitudes, plates tend to move faster, transform faults are longer, seismic activity is globally higher, etc.

4. Length of the day (LOD) versus seismicity

Varga et al. (2005) have shown the existence of a relationship between the number of events occurring per year (N) and LOD time series: as LOD increases, N is higher and vice versa. Similar relation exists between the energy released globally by large events ($M_w \geq 7.0$) per year, and LOD. We have analyzed the time series of LOD, detrended from secular drift, N and $\log_{10}E$ considering a time span of more than a century (1900–2007). The LOD time series is composed by the yearly averaged time series of JPL (1832–1997) completed with the combined C04 solutions up to 2007, provided by the International Earth Rotation and Reference System Service (IERS) (Bizouard and Gambis, 2008). The N time series consists of the yearly number of events occurred from 1900 to September 2007, the $\log_{10}E$ time series is the $\log_{10}$ of the global seismic energy yearly released. Since we are interested to identify long periods, the two time series are smoothed with a 5 yr moving average (a low-pass filter). To make an effective comparison, the two time series have been normalized. Fig. 6 shows the LOD, $\log_{10}E$ and N time series after the normalization.

The search for non-random processes in the normalized time series of LOD, $\log_{10}E$ and N is made, as a first step, by the Lomb normalized periodogram. LOD and N have significant peaks centered at 34 yr, corresponding respectively to normalized powers of 12.6 and 14.6, well beyond the value of 7.6, limit of the 95% level. The LOD and $\log_{10}E$ time series have significant periods at 51 yr, corresponding to normalized powers of 11.2 and 27.5 respectively.

The temporal interval common to the two time series is rather limited (102 yr), thus the detection of long periodicities is affected by a low resolution: the nearest peaks that can be really detected correspond to the frequency interval $f = 0.0294 \pm 0.0098$ yr^{-1}equivalent to the time interval of 25.5–51.0 yr. Therefore, we can conclude that the peaks identified in LOD, $\log_{10}E$ and N are significant but the time series are too short to detect with good resolution the real value of these periodicities.

The cross-correlation between the sequences has been computed in the frequency domain. The procedure is equivalent to the convolution with one of the two sequences reversed in time. At time lag 0, the cross-correlation between LOD and N is 0.79, and between LOD and $\log_{10}E$ is 0.81, both significant at the 95% confidence level. The magnitude squared spectral coherence is a positive normalized function of frequency and indicates how well one series corresponds to the other at each frequency. The spectral coherence of LOD and N approaches saturation at about 0.65 after about 20 yr; a higher level of coherence at low frequency is obtained between LOD and $\log_{10}E$, though it reaches the asymptotical value of about 0.78 after about 30 yr (Fig. 7).

It has been shown that seismicity is not able to significantly modify the LOD (Chao and Gross, 2005). Therefore the seismicity cannot be

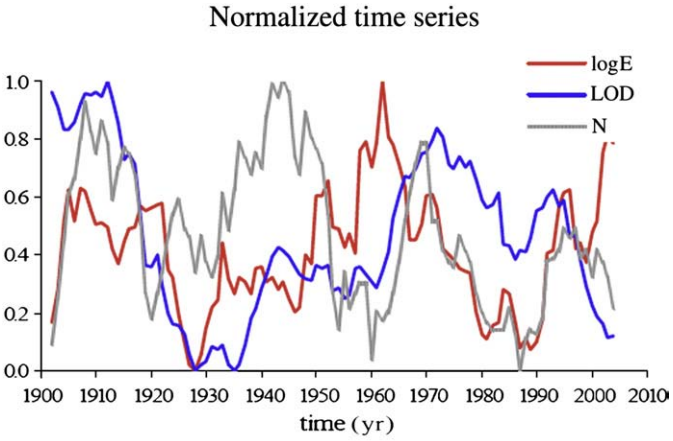

Fig. 6. Normalized time series of LOD (length of the day), N (number of earthquakes with $M_w \geq 7.0$), and $\log_{10}E$ (energy). The cross-correlation between LOD and N, and between LOD and $\log_{10}E$ is significant at 95% confidence level.

Please cite this article as: Riguzzi, F., et al., Can Earth's rotation and tidal despinning drive plate tectonics? Tectonophysics (2009), doi:10.1016/j.tecto.2009.06.012

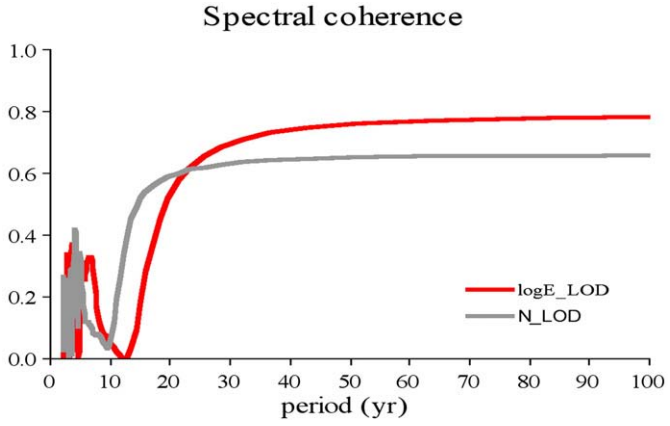

Fig. 7. Spectral coherence between LOD, N and LOD, $\log_{10}E$. The latter are more coherent at long periods than the first two. The saturation value of 0.65 is reached after 20 yr, when LOD and N are considered, while it reaches 0.78, after 30 yr, in the case of LOD and $\log_{10}E$.

responsible of the large and long-term LOD oscillations, and we argue that the process responsible for the LOD oscillation is the same as the one controlling the seismicity variation in time. Wang et al. (2000) have demonstrated a correlation between mounting stress and increase of the LOD along faults in China. The correlation appears most typically on decade time scales and seems to be direction-dependent.

The variability of the Earth's rotation vector relative to the body of the planet is caused by the gravitational torque exerted by the Moon, Sun and planets, displacements of matter in different parts of the planet and other possible excitation mechanisms. The solid Earth tides are deformations of the Earth that cause limited variations of the Earth's rotation vector and are not able to excite long period oscillations of LOD: the largest tidally induced LOD fluctuations are due to the fortnightly zonal tides, with amplitudes within 1 ms. Minor effects are due to monthly, semi-annual, and annual zonal tides (Yoder et al., 1981; Paquet et al., 1997), while the symmetric diurnal and semidiurnal tides cannot excite the LOD.

The secular linear decrease of the Earth rotation is mainly the consequence of a permanent phase lag in the deformation of the inelastic equatorial bulge due to the Moon attraction; its amplitude is estimated at 0.017 ms/yr (IERS Earth Orientation Center web site). To conserve the angular momentum of the system, the Earth's deceleration is mostly compensated by the enlarging of the Moon's orbit, at a rate of 38.2 ± 0.7 mm/yr (Dickey et al., 1994). The Earth spin has a variable rate now as in the past. The duration of day was about 19 h 2.5 Gyr ago, 21 h 0.5 Gyr ago, and it has been increasing during the last 500 Myr at a rate of about 1.79 ms/century (Denis et al., 2002).

The long-term variations of the Earth's angular velocity are mainly due to two different components with opposite effects: the tidal dissipation and the decrease of Earth oblateness, respectively acting to slow and to increase the Earth's angular velocity. The post-glacial rebound induces a net transfer of matter within the Earth toward higher latitudes, decreasing the Earth's moment of inertia and thereby decreasing LOD (Lambeck, 1980). There are shorter time scale variations of the LOD with wavelength of decades, or even seasonal and higher frequency oscillations (Jault et al., 1988; Kane and Trivedi, 1990; Marcus et al., 1998).

5. Solid Earth's energy budget and the plate tectonics expenditure

In plate tectonics it is assumed that the inertia and acceleration of the individual plates are nonexistent or negligible, and thus the plates are in dynamic equilibrium (Forsyth and Uyeda, 1975). At present, the solid Earth can be considered in energetic equilibrium: the energy sources that keep running its dynamical processes and the most significant phenomena consumers of terrestrial energy resources are equivalent in magnitude (see the Appendix). Thus it is natural to assume that the balance is in quasi equilibrium, i.e. there is no statistically meaningful difference between the total of income and expenditure energy rates. This circumstance allows for relatively small energy sources to influence global tectonic processes and we think the tidal despinning is able to influence plate tectonics through the westward lithospheric drift (Bostrom, 1971; Knopoff and Leeds, 1972). Small perturbations in the velocity of rotation trigger the release of a large amount of energy and seismicity (Press and Briggs, 1975). The energy rate necessary to move the Earth's shields, i.e. to move the thicker lithosphere relative to the underlying poorly developed low-velocity channel (as in the Baltic area), has been estimated at about $4 \cdot 10^{18}$ J/yr (Knopoff, 1972). Similar value is found by considering the energy of formation of tectonic dislocations that can be estimated as the consume of energy rate $\dot{E}$ necessary for lateral displacement of the lithosphere plates relative to the viscous mantle. Thus, it can be written as (Maslov, 1991).

$$\dot{E} = \chi \cdot \omega^2 \cdot \frac{a^4 \cdot \pi^2}{4 \cdot h} = \chi \cdot v^2 \cdot \frac{a^2 \cdot \pi^2}{4 \cdot h} = \chi \cdot v^2 \cdot \frac{D^2}{h}$$

One classical value of mantle viscosity is $\chi = 10^{22}$ Poise (1P = 0.1 Pa s), the plate angular (lateral) speed $\omega = 1.7\ ^\circ/\mathrm{yr} \cdot 10^{-6}$ ($v = 2$ cm/yr), $a = 6.371 \cdot 10^8$ cm the mean Earth's radius and the thickness of the crust $h = 100$ km one gets $\dot{E} = 1.27 \cdot 10^{19}$ J/yr. In the above equation $D = \pi \cdot a/2$ ($D = 1 \cdot 10^9$ cm) serves as horizontal scale of the plates.

If we consider the whole lithosphere this value has to be multiplied for $16/\pi$ obtaining $\dot{E} = 6.5 \cdot 10^{19}$ J/yr. Recent papers show a model of post-seismic relaxation indicating viscosity values of 10^{18} Poise (Aoudia et al., 2007; Melini et al., 2008). Consequently, the power needed to move the lithosphere could be significantly lowered, possibly to $\dot{E} = 6.5 \cdot 10^{15}$ J/yr.

The tidal friction in the Earth–Moon system can be determined on the basis of the temporal variation of the Earth's rotational energy plus the Moon orbital's energy

$$E_T = \frac{1}{2} C \omega^2 + \frac{1}{2} a_m^2 n_m^2 \cdot \left(\frac{M \cdot M_m}{M + M_m} \right) - G \frac{M \cdot M_m}{a_m}$$

where C, ω and M are the polar moment of inertia, the angular speed and the mass of the Earth, and a_m, n_m and M_m are the Earth–Moon distance, the Moon's orbital speed and the mass of the Moon, respectively, while G stands for the gravitational constant. Using Kepler's third law and conservation of momentum in the Earth–Moon system, $\dot{E} = C = (\omega - n_m)\,\dot{\omega}$; introducing the parameter's values provided by the IERS, we obtain $\dot{E} = 1.2 \cdot 10^{20}$ J/yr. Most of this dissipation occurs in the oceans and shallow seas and only a limited part in the mantle. According to Ray (2001) the tidal dissipation in the mantle amounts maximum to $0.42 \cdot 10^{19}$ J/yr, whereas the total oceanic and shallow seas dissipation is about $0.75 \cdot 10^{20}$ J/yr (Egbert and Ray, 2000). Therefore the residual available power, about $0.4 \cdot 10^{20}$ J/yr is larger than the one required to move the lithosphere with respect to the mantle, and we think that the Earth's rotation plays a key role in the generation of the relative shear.

6. The decoupling in the upper asthenosphere

The decoupling at the base of the lithosphere is suggested by a number of independent evidences, namely 1) the motion of the Pacific plate relative to the mantle source of the Hawaii volcanic track, as well as similar seamounts trails, needs a decoupling zone between lithosphere and the magmatic source; 2) the kinematic of plates indicates a migration of plate boundaries relative to each other and relative to the mantle (e.g., Garfunkel et al., 1986); 3) the shear wave splitting analysis points out for a shear between the lithosphere and the mantle,

Please cite this article as: Riguzzi, F., et al., Can Earth's rotation and tidal despinning drive plate tectonics? Tectonophysics (2009), doi:10.1016/j.tecto.2009.06.012

concentrated in the asthenosphere, where olivine crystals tend to align along the direction of motion of plates relative to the mantle (Gung et al., 2003; Debayle et al., 2005); 4) the notion of the net rotation or westward drift of the lithosphere computed in the hotspot reference frame (Gripp and Gordon, 2002), and supported by the asymmetry of tectonic features, requires a generalized decoupling between the lithosphere and the mantle, regardless of its nature (Doglioni, 1993); 5) the top of the asthenosphere (100–220 km) is marked by a pronounced decrease in velocity (the Low Velocity Zone, LVZ) of both P and S seismic waves, pointing for the occurrence of some melt (Panza, 1980); 6) most of the Earth's magmatism forms in the upper asthenosphere (e.g., Foulger and Jurdy, 2007), and the partial melting decreases the viscosity; and 7) the faster plate relative to the mantle has the lowest measured viscosity values (5×10^{17} Pa s, Pollitz et al., 1998).

The amount of decoupling in the asthenosphere is function of the viscosity of the layer. Moreover, the viscosity of the asthenosphere computed on the time scale of post-glacial rebound (10 ka) can be significantly different from the one related to long lasting processes (10 Ma). The viscosity quantifies the resistance of a fluid to flow, and it is the ratio between the shear stress and the strain rate. Some materials have a viscosity that depends on the time scale of an applied shear stress. The time scale of tidal drag can be considered as infinite. Studies of the mantle's mechanical properties during the last decades have repeatedly pointed out the non linear rheology of the mantle (e.g., Caputo, 1986; Kornig and Muller, 1989; Ranalli, 1995), which usually implies that viscosity in the asthenosphere decreases as the shear stress raises. The viscosity of the mantle based on the post-glacial rebound computation has four main limitations to our purpose: 1) it gives values at a much shorter time scale than the one of plate tectonic processes; 2) the viscosity is averaged on the mantle section loaded and unloaded by the ice cap, e.g., 2000 km, about 10 times thicker than the upper asthenosphere that may locally have much lower viscosity; 3) the viscosity is inferred by vertically loading and unloading the mantle, being 1 to 3 orders of magnitude higher than the viscosity measured under horizontal shear; and 4) a 50–100 km thick layer with low viscosity remains invisible to post-glacial rebound modeling.

Jordan (1974) recognized that the tidal despinning is supplying a relevant amount of energy sufficient to move plates, but he argued that the viscosity of the asthenosphere is too high in order to allow a decoupling of the overlying lithosphere induced by the Earth's rotation (Ranalli, 2000). However new evidences support the presence of an ultra-low seismic velocity at the top of the asthenosphere (Rychert et al., 2005), which might correspond to the presence, in the asthenospheric LVZ, of a layer with much lower viscosity than so far expected (Rychert et al., 2005; Aoudia et al., 2007). A justification for the existence of an ultra-thin viscosity anisotropy zone in the asthenosphere is supplied by Marone and Romanowicz (2007), even though so far limited to whole North America. Their Fig. 4c clearly shows the necessity of a thin decoupling zone at a depth of about 200 km where there is an abrupt shift of about 90° of the fast axis direction. Petrological and laboratory experiments also point for very low viscosity in the asthenosphere, particularly when intra-crystal pockets of melt occur (Hirth and Kohlstedt, 1995; Holtzman et al., 2003; Dingwell et al., 2004; Liebske et al., 2005). Water content in the asthenosphere can drastically lower its viscosity to 10^{15} Pa s (Korenaga and Karato, 2008). Moreover, the viscosity in the asthenospheric LVZ can be orders of magnitude lower when measured under horizontal shear with respect to the viscosity computed by vertical unloading due to post-glacial rebound (Scoppola et al., 2006).

It is important to remember that a thin ultra-low viscosity layer is invisible to post-glacial rebound viscosity computation due to the channel flow effect (Cathles, 1975) or to the geoid variation (Marquart et al., 2005). Therefore the occurrence of such a layer cannot be excluded a priori. The larger decrease in velocity of Vs than Vp in the low-velocity layer points for a significant amount of melt in the upper asthenosphere, accordingly to the fact that the geotherm is warmer than the solidus at 150–200 km depth. Electromagnetic studies seem to support the presence of an intra-asthenosphere layer with larger amount of fluids (Heinson, 1999) that would drop the LVZ viscosity.

Jin et al. (1994) have shown how the intra-crystalline melt in the asthenospheric peridotites under shear can generate a viscosity of about 10^{12} Pa s (Stevenson, 1994), a value compatible with the plate tectonics driven by the Earth's rotation (Scoppola et al., 2006).

Therefore the presence of an ultra-low viscosity layer in the upper asthenosphere (Fig. 1) can be considered as a possibility with the present available techniques of mantle sampling and laboratory experiment.

7. Model

The Earth system (solid Earth + hydrosphere + atmosphere) has an effective viscoelasticity which reacts with some delay with respect to the Earth and Moon alignment. The Earth would tend to move backward along this alignment (Fig. 8). The about 2–3° tidal lag angle between the tidal bulge and the gravitational alignment between the Earth and the Moon (e.g., Touma and Wisdom, 1994) determines a permanent torque toward the "west", opposite to the E-ward rotation of the planet. This torque is considered responsible for the secular deceleration of the Earth, and acts directly on the lithosphere.

In our model, the visco-elastic lithosphere (say 100 km thick) is dragged "westward" by the tidal torque, above a decoupling zone (50–100 km thick) with visco-plastic behavior, corresponding to the LVZ in the asthenosphere. The LVZ, where the mantle partly melts because the geotherm is higher than the mantle solidus, should correspond to a drastic decrease in viscosity of the upper asthenosphere, allowing the tidal torque to focus the dissipation of its energy in this layer (Fig. 9). It has to be noted that the mainstream of plate motion described by Crespi et al. (2007) has an angle of about 30° with respect to the equator, close to the revolution plane of the Moon about the Earth (28°), although this overlap is intermittent.

The solid Earth tide accompanies this translation provoking a semidiurnal oscillation of the lithosphere. The period 12 h25′

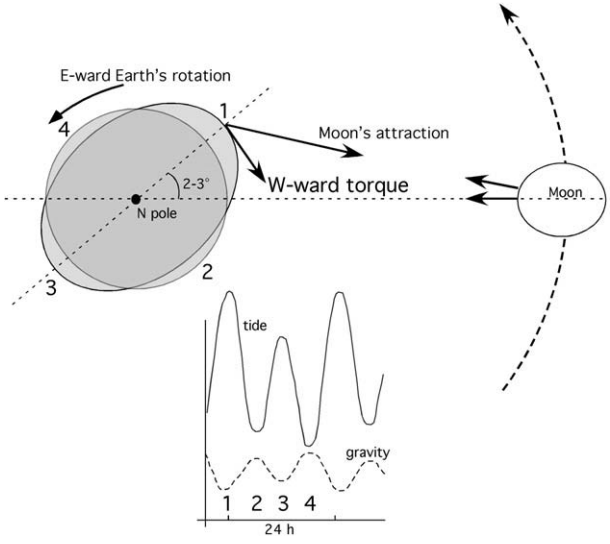

Fig. 8. Cartoon showing the Earth's bulge deviation (delay) from the (gravitational) Earth–Moon alignment of about 2–3° due to the visco-elastic nature of the Earth. This distribution of the mass tends to pull the planet along the gravitational alignment, acting permanently toward the "west", on the Moon's revolution plane. Since it acts in versus opposed to the E-ward rotation of the planet, this torque is considered responsible for the slow Earth's despinning. The torque can push the lithosphere horizontally, westward relative to the underlying mantle: tides generate waves that swing the lithosphere horizontally and vertically, and are accompanied by gravity variations of opposed sign. Therefore the lithosphere undergoes a permanent, isoriented oscillation.

Please cite this article as: Riguzzi, F., et al., Can Earth's rotation and tidal despinning drive plate tectonics? Tectonophysics (2009), doi:10.1016/j.tecto.2009.06.012

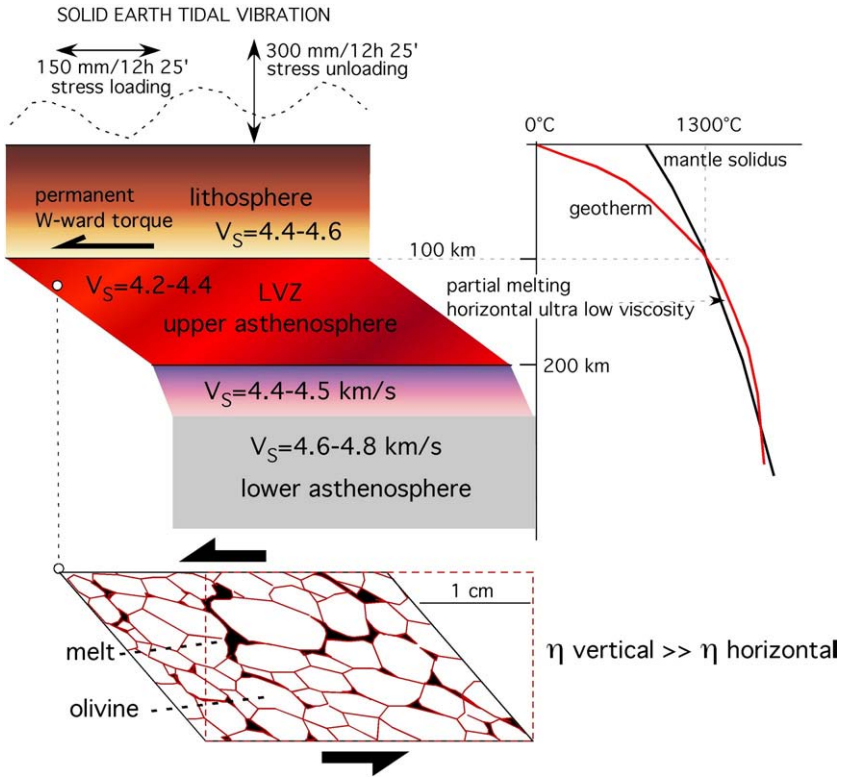

Fig. 9. Is focused in the asthenosphere, where the geotherm is above the temperature of mantle solidus, and small pockets of melt can induce a strong decrease of the viscosity in the upper part of the asthenosphere. The viscosity in this layer, the Low Velocity Zone of the asthenosphere, can be much lower than the present-day estimates of the asthenosphere viscosity based on the post-glacial rebound, because the horizontal viscosity under shear can be several orders of magnitude lower than the vertical viscosity computed averaging the whole asthenosphere. This should be the basic decoupling zone for plate tectonics, where the lithosphere moves relative to the underlying mantle. Tidal waves are too small to generate plate tectonics. However, their horizontal isoriented movement, might determine a fundamental consequence. The lithosphere, being swung horizontally by the solid tide of say 150 mm/semidiurnal, may, under a permanent torque, retain a small but permanent strain (e.g., a shift of 0.1 mm/semidiurnal). At the end of the year this slow restless deformation amounts to a cumulative effect of several centimeters which is consistent with the observed plate motion and thus could be what we consider the net rotation of the lithosphere.

corresponds to the mean semidiurnal lunar wave M_2, which is responsible first of all for the generation of tidal bulge; the solid Earth tides have a well-known vertical oscillation of 300–400 mm/12 h25′, but they also have a relevant 150–200 mm/12 h25′ horizontal swinging. Under a permanent torque, this oscillation may induce a tiny strain in the upper asthenosphere, say 0.1–0.2 mm. The cumulative effect of this small horizontal motion, which repeats twice a day, may well reach several centimeters (7–14) per year necessary to guarantee a lithosphere plate motion, at least partly decoupled from the deeper mantle, i.e., the net rotation or so-called W-ward drift of the lithosphere relative to the mantle (e.g., Crespi et al., 2007). In other words the horizontal shear determined by the persisting westward torque acting on an asthenosphere that undergoes the mechanical fatigue exerted by the semidiurnal tidal oscillation, might allow the relative motion of the overlying lithosphere. The advantage of this mechanism is to act contemporaneously all over the lithosphere.

A statistically significant correlation has been shown between seismicity ($M \geq 5.5$ global shallow thrust earthquakes) and higher peak tidal stresses at continent–ocean margins, where there is a large ocean-loading component of tidal stress (Ray, 2001). However, compressive earthquakes occur more frequently during the high tide (Cochran et al., 2004) whereas extensional earthquakes are more frequent during low tides (Wilcock, 2001). In compressional tectonic settings the vertical load is expressed by $\sigma 3$, whereas it is given by $\sigma 1$ in extensional tectonic settings. During a high tide (both solid and fluid) we could expect a thicker section of rocks and water and therefore an increase of the lithostatic load. However, during the high tide, the gravity is at the minimum, opposite to the sign of the tide. Therefore, the lithostatic load (ρgz, where ρ is density, g, gravity, and z, thickness) becomes smaller during the high tide, and larger during the low tide. This oscillating wave determines a decrease of $\sigma 3$ during the high tide, and an increase of $\sigma 1$ during the low tide. In the first case the Mohr circle enlarges to the left, while in the second case it enlarges to the right. Both opposite cases facilitate rupture in compressional and extensional settings respectively (Fig. 10).

In this view, the oscillating horizontal component of the tides load and pump the tectonic system, drop by drop, slowly but steadily, whereas the vertical component of the tides might be the unloading mechanism when enough energy has accumulated along fault zones. As an example, during the recent Apennines L'Aquila earthquake sequence (April 6, 2009), the main event ($M_w = 6.3$, extensional focal mechanism, NEIC) occurred very near to a gravity maximum (low solid tide), thus suggesting that the larger the lithostatic load, the larger is $\sigma 1$ and the activation of extensional stresses.

Since the lithosphere has been documented to be in a critical state, small variations of the lithostatic load even of few Pascal may trigger the rupture or the slow viscous flow of rocks (e.g., Twiss and Moores, 1992).

8. Discussion and conclusions

In this paper we describe in detail the asymmetry between W-directed and E- or NE-directed subduction zones, both in terms of morphology (Fig. 3), geology, and geophysical signatures (Fig. 4). The distribution in space and time of global seismicity ($M_w \geq 7$) is latitude dependent (Fig. 5), being very low in the polar regions. Moreover, the time series of LOD, $\log_{10}E$ and N (Fig. 6) have significant correlation and spectral coherence, particularly for periodicities longer than 25.5 yr (Fig. 7). The LOD decrease corresponds to an increase of the Earth's oblateness and to a polhody amplitude decrease (Lambeck, 1980; Bizouard and Gambis, 2008). Accordingly modulated are the occurrence of large seismic events and

Please cite this article as: Riguzzi, F., et al., Can Earth's rotation and tidal despinning drive plate tectonics? Tectonophysics (2009), doi:10.1016/j.tecto.2009.06.012

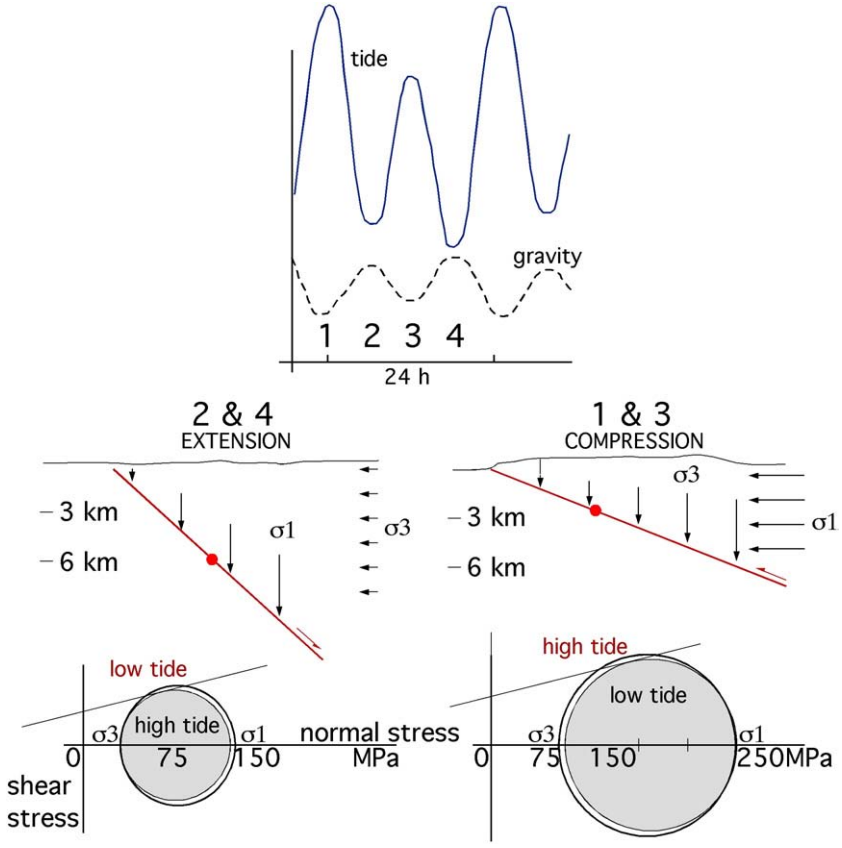

Fig. 10. During their passage, tidal waves determine very small variations of gravity. However these slight variations of the lithostatic load, acting on a lithosphere, which is slowly but persistently pumped westward, could determine the increase or decrease of σ1 in extensional environments, or σ3 in compressional tectonic settings. Therefore the same variation of the lithostatic load acts in an opposite way in the two different tectonic settings. In this model, the horizontal component of the solid Earth tide slowly accumulates the stress, whereas the vertical component could allow the downloading of the stress as a function of the tectonic setting and the orientation of the faults relative to the tidal waves.

the release of seismic energy: as the Earth slows down (increase of LOD) the seismicity (either *E* or *N*) increases and vice versa. We speculate that similar periodicities should affect also GPS velocities when sufficient time span of measurements will be covered, i.e., plates should move with similar periodicities, due to oscillating tidal torques and Earth's oblateness acting on the lithosphere.

The up and down of the solid Earth tides are too small to drive plates (e.g., Ray et al., 2001). However, the horizontal permanent torque exerted by the misalignment of the tidal bulge and the Earth–Moon gravitational trajectory rather provides a relevant amount of energy. We have reviewed the gross energy budget of the Earth, and the rotational-despinning energy dissipation can be considered sufficient to contribute significantly in moving plates, particularly if an ultra-low viscosity layer is present at the top of the asthenosphere, allowing the relative westward decoupling of the lithosphere.

The lithosphere and the underlying mantle represent a self-organized system in a critical state – SOC system (Stern, 2002) – open to external perturbations; plate tectonics is an example of a self-organizing complex system of hierarchical blocks in a critical state (Prigogine and Stengers, 1984). The Gutenberg–Richter law shows that large magnitude earthquakes are very rare events (Stein and Wysession, 2003), thus the energy released by one big earthquake seems to deplete temporally the energy budget of plate tectonics, i.e. a slab interacting with the surrounding mantle is not an isolated system, but it participates to a global expenditure of the stored energy.

Plate tectonics is an Earth's scale phenomenology, and the energy source for its activation is not concentrated in limited zones (e.g., subduction zones), but it acts contemporaneously all over the whole Earth's lithosphere, like the Earth's rotation. Romashkova (2009) has recently shown how the planet seismicity indicates that the Earth's lithosphere can be considered as a single whole. Only the global seismicity follows the Gutenberg–Richter law, while this simple SOC relation does not hold when considering smaller portions of the Earth (Molchan et al., 1997). All these evidences and models are in favor, even if not conclusive, of a significant contribution to plate tectonics by the Earth's rotation.

Our model supports an origin of plate tectonics in which the classic mantle convection is complemented and polarized by the steady-state torque provided by the tidal bulge misalignment. The horizontal component of the Earth's tide pumps the system; the vertical component of the tides excites gravity oscillations, which locally load and unload the tectonic features (Fig. 11). Low solid tide (larger gravity) favors extensional tectonics, whereas high solid tide (lower gravity) triggers compressional tectonics.

The differential velocity among plates would be controlled by the viscosity-related variable decoupling at the base of the lithosphere,

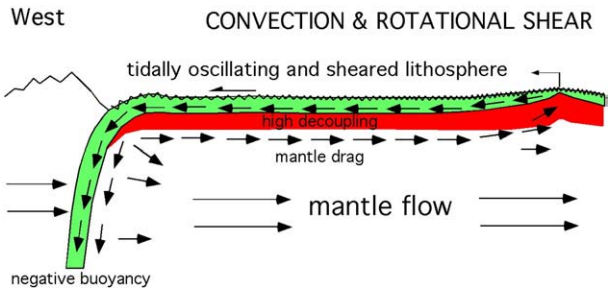

Fig. 11. Schematic flow patterns describing the coexistence of Earth's convection and the rotational shear. In this model, the cooling of the Earth, enhancing mantle convection, is added by the shear associated to the horizontal component of the solid Earth tide, thus triggering the westward drift of the lithosphere.

Please cite this article as: Riguzzi, F., et al., Can Earth's rotation and tidal despinning drive plate tectonics? Tectonophysics (2009), doi:10.1016/j.tecto.2009.06.012

combined with other forcing mechanisms of mantle convection such as mantle drag and slab pull. Numerical and analogue modeling should further test this model.

Acknowledgements

P. Varga acknowledges the support of the Hungarian Scientific Research Fund OTKA in the framework of project K 60394 ("Interaction of Earth rotation and geodynamical processes"). We are grateful to all the persons involved in the IERS-EOP database maintenance (http://hpiers.obspm.fr/eop-pc/). Discussions with E. Bonatti, E. Carminati, M. Cuffaro, R. Devoti and F. Innocenti were very stimulating. We thank L. Knopoff for helpful comments on an earlier version of this article. C. Bizouard and an anonymous referee reviewed the article.

Appendix A

Earth's energy budget and the plate tectonics expenditure

Table 2 shows the energy sources that keep running the dynamical processes of the Earth and the phenomena that are the most significant consumers of terrestrial energy resources.

According to Iriyama (1977), the most important sources of energy income rate are the accretion $\dot{E}_A$, the core formation (differentiation) $\dot{E}_C$, the radioactive decay (radiogenic heat production) $\dot{E}_R$ and the tidal friction $\dot{E}_T$. The main components of the energy expenditure rate of the Earth's planetary energy budget are represented by the heat flow $\dot{E}_{HF}$ and the global tectonic moment rate $\dot{E}_{TM}$, following the global estimation of Kreemer et al. (2002). The annual rate values here reported are the results of a compilation of the estimates available in the literature, here briefly discussed.

The real errors of the estimates reported in Table 2 cannot be determined so that we prefer to discuss their order of magnitude. Thus it is natural to assume that the balance is in quasi equilibrium, i.e. there is no statistically meaningful difference between the total of energy rate income and energy rate expenditure.

There are several attempts of estimation of solid Earth's energy rates; consequently we consider useful to report here the minimum and maximum values found in literature.

Energy income rate

Accretion

The birth and infancy of the Earth was a time of gravitational accumulation and profound differentiation. The total of our knowledge indicates that, in all probability, these events were comparatively rapid and took place very early and simultaneously with the formation of the Earth itself. The time span of accretion and differentiation (core formation) should be between 100 thousand to hundred million years (Monin, 1978; Walter and Trønes, 2004).

The energetics of the gravitational accumulation process has two different scenarios:

- the kinetic energy of the large number of small particles approaching the proto-planet is used for heating.
- the kinetic energy of falling bodies is used up for erosion of the globe (cratering and ejection of fragments of rocks from the planet).

Table 2
Energy budgets of the solid Earth.

Energy income $(J/yr)\times10^{21}$		Energy expenditure $(J/yr)\times10^{21}$	
Accretion $\dot{E}_A$	1.9–5.5	Heat flow $\dot{E}_{HF}$	1.4–1.5
Core formation $\dot{E}_C$	3.2–3.6		
Radioactive decay $\dot{E}_R$	0.2–2.1	Tectonic moment rate $\dot{E}_{TM}$	5.7–7.6
Tidal friction $\dot{E}_T$	0.04–0.1		
Total energy income	5–11	Total energy expenditure	7–9

The accretion energy rates $\dot{E}_A$ given by different authors, to characterize the accretion process, show a relatively significant scatter that depends upon the kind of assumptions made, namely:

- $1.9\cdot10^{21}$ J/yr (Sasaki and Nakazawa, 1986)
- $4.9\cdot10^{21}$ J/yr (Janle and Meissner, 1986)
- $4.9\cdot10^{21}$ J/yr (Verhoogen, 1980)
- $5.6\cdot10^{21}$ J/yr (Iriyama, 1977)

thus

$\dot{E}_A$ min $= 1.9 \cdot 10^{21}$ J/yr (Sasaki and Nakazawa, 1986)
$\dot{E}_A$ max $= 5.6 \cdot 10^{21}$ J/yr (Iriyama, 1977)

Core formation

The range of core formation energy rates $\dot{E}_C$ presented in different contributions is relatively small due to the use of more or less similar theoretical models:

- $3.2\cdot10^{21}$ J/yr (Flasar and Birch, 1973)
- $3.3\cdot10^{21}$ J/yr (Iriyama, 1977)
- $3.5\cdot10^{21}$ J/yr (Monin, 1978)
- $3.6\cdot10^{21}$ J/yr (Birch, 1965)

thus

$\dot{E}_C$ min $= 3.2 \cdot 10^{21}$ J/yr (Flasar and Birch, 1973)
$\dot{E}_C$ max $= 3.6 \cdot 10^{21}$ J/yr (Birch, 1965).

Radioactive decay

In the earliest stage of the Earth's history (4 billion years BP) the radiogenic heat production was about five times higher than at the Present Epoch (Rybach, 1976). Short-lived isotopes with half-lives of 10^5–10^7 yr, or even much shorter, may have had sufficient effect to melt the central parts of the forming proto-planet. Over the 4.6 Eon (Eon $= 10^9$ yr) lifetime of the Earth, four long-life isotopes ^{238}U, ^{235}U ^{232}Th and ^{40}K gave the most important contribution to the radiogenic heat production. The amount of radioactive heat in the crust is 8 TW, in the mantle 23 TW, while in the core it is about 9 TW (Anderson, 1989). More recently Lay et al. (2008) slightly increase these values to a total of 46 ± 3 TW, although a debate on the topic is still alive; for example Hofmeister and Criss (2005) suggest a lower value (31 ± 1 TW). The radioactive annual rates $\dot{E}_R$ published in different scientific contributions are:

- $2.1\cdot10^{20}$–$2.1\cdot10^{21}$ J/yr (Bott, 1982)
- $1.3\cdot10^{21}$ J/yr (Anderson, 1989)
- $2.1\cdot10^{21}$ J/yr (Iriyama, 1977)

thus

$\dot{E}_R$ min $= 0.2 \cdot 10^{21}$ J/yr (Bott, 1982)
$\dot{E}_R$ max $= 2.1 \cdot 10^{21}$ J/yr (Iriyama, 1977).

Tidal friction

The tidal friction energy rate $\dot{E}_T$ is $(0.04–0.12)\cdot10^{21}$ J/yr. The value of the despinning rate was five time smaller during Archean and Proterozoic than during the last 570 Ma (Phanerozoic) (Varga, 2006).

Thus,

$\dot{E}_T$ min $= 0.04 \cdot 10^{21}$ J/yr (Zschau, 1986)
$\dot{E}_T$ max $= 0.11 \cdot 10^{21}$ J/yr (Varga, 2006)

Please cite this article as: Riguzzi, F., et al., Can Earth's rotation and tidal despinning drive plate tectonics? Tectonophysics (2009), doi:10.1016/j.tecto.2009.06.012

Total energy income rate $\dot{E}_{IN} = (5 \div 11) \cdot 10^{21}$ J/yr. Then, the average value is

$$\dot{E}^{Av}{}_{IN} = (8 \pm 3) \cdot 10^{21} \text{ J/yr}$$

Energy expenditure

Heat flow
$\dot{E}_{HF}$ min $= 1.4 \cdot 10^{21}$ J/yr (Turcotte and Schubert, 2002; Lowrie, 2007).
$\dot{E}_{HF}$ max $= 1.5 \cdot 10^{21}$ J/yr (Lay et al., 2008).

Tectonic moment rate

Numerically, most of the energy expenditure goes into the global tectonic momentum $\dot{E}_{TM}$ and this shows that most of the energy loss is related to plate tectonic activities. The tectonic moment rate estimated by Kreemer et al. (2002) is $7.0 \cdot 10^{21}$ and is considered by the authors as a minimum value because it is estimated during a period of low seismic activity and on a short time span. Effectively, the tectonic moment rate strongly depends on the level of seismicity. Consequently we have recomputed this rate on our catalog (see the main manuscript) and applying the geometrical mean first on the same time span of Kreemer et al. (2002), obtaining the minimum value; then on the whole catalog, obtaining the maximum value.

$\dot{E}_{TM}$ max $= 5.7 \cdot 10^{21}$ J/yr
$\dot{E}_{TM}$ max $= 7.6 \cdot 10^{21}$ J/yr

Total energy expenditure $\dot{E}_{OUT} = (7 \div 9) \cdot 10^{21}$ J/yr. Then, the average value is

$$\dot{E}^{Av}{}_{OUT} = (8 \pm 3) \cdot 10^{21} \text{ J/yr}$$

Energy expenditure-income $\Delta\dot{E} = 0$ J/yr.

The balance is again in quasi equilibrium, i.e., there is no statistically meaningful difference between the total of energy rate income and expenditure.

References

Altamimi, Z., Collilieux, X., Legrand, J., Garayt, B., Boucher, C., 2007. ITRF2005. A new release of the International Terrestrial Reference Frame based on time series of station positions and Earth Orientation Parameters. J. Geophys. Res. 112, B09401. doi:10.1029/2007JB004949.

Ammon, C.J., Kanamori, H., Lay, T., 2008. A great earthquake doublet and seismic stress transfer cycle in the central Kuril islands. Nature 451. doi:10.1038/nature06521.

Anderson, D.L., 1989. Theory of the Earth. InBlackwell, pp. 1–366.

Anderson, D.L., 2006. Speculations on the nature and cause of mantle heterogeneity. Tectonophysics 416, 7–22.

Anderson, D.L., 2007a. New Theory of the Earth. Cambridge University Press. ISBN 978-0-521-84959-3, 0-521-84959-4.

Anderson, D.L., 2007b. Is There Convincing Tomographic Evidence for Whole Mantle Convection? http://www.mantleplumes.org/TomographyProblems.html.

Aoudia, A., Ismail-Zadeh, A.T., Romanelli, F., 2007. Buoyancy-driven deformation and contemporary tectonic stress in the lithosphere beneath Central Italy. Terra Nova 19, 490–495.

Baranzangi, M., Isacks, B.L., 1979. Subduction of the Nazca plate beneath Peru: evidence from spatial distribution of earthquakes. Geophys. J.R. Astron. Soc. 57, 537–555.

Bevis, M., 1988. Seismic slip and down-dip strain rates in Wadati–Benioff Zones. Science 240, 1317–1319.

Billen, M.I., Hirth, G., 2007. Rheologic controls on slab dynamics. Geochem. Geophys. Geosyst. 8, Q08012. doi:10.1029/2007GC001597.

Billen, M.I., Gurnis, M., Simons, M., 2003. Multiscale dynamic models of the Tonga–Kermadec subduction zone. Geophys. J. Int. 153, 359–388.

Birch, F., 1965. Energetics of core formation. J. Geophys. Res. 69, 4377–4388.

Bizouard, C., Gambis, D., 2008. The Combined Solution C04 for Earth Orientation Parameters, Recent Improvements. Springer Verlag series.

Bonatti, E., Seyler, M., Sushevskay, N., 1993. A cold suboceanic mantle belt at the Earth's equator. Science 261 (5119), 315–320. doi:10.1126/science.261.5119.315.

Bostrom, R.C., 1971. Westward displacement of the lithosphere. Nature 234, 356–538.

Bostrom, R.C., 2000. Tectonic Consequences of the Earth's Rotation. InOxford University Press, pp. 1–266.

Bott, M.P.H., 1982. The Interior of the Earth: Its Structure, Construction and Evolution. E. Arnold Publ. Ltd.

Cahill, T., Isacks, B.L., 1992. Seismicity and shape of the subducted Nazca plate. J. Geophys. Res. 97, 17,503–17,529. doi:10.1029/92JB00493.

Castle, J.C., Creager, K.C., 1998. NW Pacific slab rheology, the seismicity cutoff, and the olivine to spinel phase change. Earth Planets Space 50, 977–985.

Caputo, M., 1986. Linear and nonlinear inverse rheologies of rocks. Tectonophysicis 122, 53–71.

Cathles, L.M., 1975. The Viscosity of the Earth's Mantle. Princeton University Press. 386 pp.

Chen, P.-F., Bina, C.R., Okal, E.A., 2001. Variations in slab dip along the subducting Nazca Plate, as related to stress patterns and moment release of intermediate-depth seismicity and to surface volcanism. Geochem. Geophys. Geosyst. 2. doi:10.1029/2001GC000153.

Chatelain, J.L., Guillier, B., Gratier, J.P., 1993. Unfolding the subducting plate in the central new Hebrides island arc: geometrical argument for detachment of part of the downgoing slab. Geophys. Res. Lett. 20 (8), 655–658.

Chao, B.F., Gross, R.S., 2005. Did the 26 December 2004 Sumatra, Indonesia, earthquake disrupt the Earth's rotation as the mass media have said? EOS, 86, 1-2. Soc., 32, 203-217.

Chiarabba, C., De Gori, P., Speranza, F., 2008. The southern Tyrrhenian subduction zone: deep geometry, magmatism and Plio-Pleistocene evolution. Earth Planet. Sci. Lett. 268, 408–423.

Cochran, E.S., Vidale, J.E., Tanaka S., 2004. Earth tides can trigger shallow thrust fault earthquakes. Science 306, 1164–1166.

Conrad, C.P., Lithgow-Bertelloni, C., 2003. How mantle slabs drive plate tectonics. Science 298, 207–209.

Crespi, M., Cuffaro, M., Doglioni, C., Giannone, F., Riguzzi, F., 2007. Space geodesy validation of the global lithospheric flow. Geophys. J. Int. 168, 491–506.

Cruciani, C., Carminati, E., Doglioni, C., 2005. Slab dip vs. lithosphere age: no direct function. Earth Planet. Sci. Lett. 238, 298–310.

Das, S., 2004. Seismicity gaps and the shape of the seismic zone in the Band Sea region from relocated hypocenters. J. Geophys. Res. 109, B12303. doi:10.1029/2004JB003192.

Debayle, E., Kennett, B., Priestley, K., 2005. Global azimuthal seismic anisotropy and the unique plate-motion deformation of Australia. Nature 433, 509–512.

DeMets, C., Gordon, R.G., Argus, F., Stein, S., 1990. Current plate motions. Geophys. J. Int. 101, 425–478.

Denis, C., Schreider, A.A., Varga, P., Závoti, J., 2002. Despinning of the Earth rotation in the geological past and geomagnetic paleointensities. J. Geodyn. 34/5, 97–115.

Dickey, J.O., Bender, P.L., Faller, J.E., Newhall, X.X., Ricklefs, R.L., Ries, J.G., Shelus, P.J., Veillet, C., Whipple, A.L., Wiant, J.R., Williams, J.G., Yoder, C.F., 1994. Lunar laser ranging: a continual legacy of the Apollo program. Science 265, 482–490.

Dickinson, W.R., 1978. Plate tectonic evolution of North Pacific rim. J. Phys. Earth 26, 51–519 (Suppl.).

Dingwell, D.B., Courtial, P., Giordano, D., Nichols, A.R.L., 2004. Viscosity of peridotite liquid. Earth Planet. Sci. Lett. 226, 127–138.

Doglioni, C., 1990. The global tectonic pattern. J. Geodyn. 12, 21–38.

Doglioni, C., 1993. Geological evidence for a global tectonic polarity. J. Geol. Soc. Lond. 150, 991–1002.

Doglioni, C., Carminati, E., Bonatti, E., 2003. Rift asymmetry and continental uplift. Tectonics 22 (3), 1024. doi:10.1029/2002TC001459.

Doglioni, C., Carminati, E., Cuffaro, M., Scrocca, D., 2007. Subduction kinematics and dynamic constraints. Earth Sci. Rev. 83, 125–175. doi:10.1016/j.earscirev.2007.04.001.

Doglioni, C., Tonarini, S., Innocenti, F., 2009. Mantle wedge asymmetries along opposite subduction zones. Lithos. doi:10.1016/j.lithos.2009.01.012.

Egbert, G.D., Ray, R.D., 2000. Significant dissipation of tidal energy in the deep ocean inferred from satellite altimeter data. Nature 405, 775–778.

Engdahl, E.R., Villaseñor, A., 2002. Global Seismicity: 1900–1999. In: Lee, W.H.K., Kanamori, H., Jennings, P.C., Kisslinger, C. (Eds.), International Handbook of Earthquake and Engineering Seismology, 41. Academic Press, pp. 665–690.

Engdahl, E.R., van der Hilst, R.D., Buland, R., 1998. Global teleseismic earthquake relocation with improved travel times and procedures for depth determination. Bull. Seismol. Soc. Am. 88, 722–743.

Espurt, N., Funiciello, F., Martinod, J., Guillaume, B., Regard, V., Faccenna, C., Brusset, S., 2008. Flat subduction dynamics and deformation of the South American plate: insights from analog modeling. Tectonics 27, TC3011. doi:10.1029/2007TC002175.

Flasar, F., Birch, F., 1973. Energetics of core formation: a correction. J. Geophys. Res. 78, 6101–6103.

Forsyth, D., Uyeda, S., 1975. On the relative importance of driving forces of plate motion. Geophys. J.R. Astron. Soc. 43, 163–200.

Foulger, G.R., Jurdy, D.M., 2007. Plates, plumes, and planetary processes. Geol. Soc. Am. Spec. Pap. 430, 1–998.

Frepoli, A., Selvaggi, G., Chiarabba, C., Amato, A., 1996. State of stress in the Southern Tyrrhenian subduction zone from fault-plane solutions. Geophys. J. Int. 125, 879–891.

Garfunkel, Z., Anderson, C.A., Schubert, G., 1986. Mantle circulation and the lateral migration of subducted slabs. J. Geophys. Res. 91 (B7), 7205–7223.

Green II, H.W., Houston, H., 1995. The mechanics of deep earthquakes. Ann. Rev. Earth Planet. Sci. 23, 169–213.

Gripp, A.E., Gordon, R.G., 2002. Young tracks of hotspots and current plate velocities, Geophys. J. Int. 150, 321–361.

Gudmundsson, O., Sambridge, M., 1998. A regionalized upper mantle (RUM) seismic model. J. Geophys. Res. 103 (B4), 7121–7136.

Gung, Y., Panning, M., Romanowicz, B., 2003. Global anisotropy and the thickness of continents. Nature 422, 707–711.

Gutscher, M.-A., Malavieille, J., Lallemand, S., Collot, J.Y., 1999. Tectonic segmentation of the North Andean margin: impact of the Carnegie Ridge collision. Earth Planet. Sci. Lett. 168, 255–270. doi:10.1016/S0012-821X(99)00060-6.

Heinson, G., 1999. Electromagnetic studies of the lithosphere and asthenosphere. Surv. Geophys. 20 (4), 229–255.

Please cite this article as: Riguzzi, F., et al., Can Earth's rotation and tidal despinning drive plate tectonics? Tectonophysics (2009), doi:10.1016/j.tecto.2009.06.012

Hirth, G., Kohlstedt, D.L., 1995. Experimental constraints on the dynamics of the partially molten upper mantle, 2, Deformation in the dislocation creep regime. J. Geophys. Res. 100, 15441–15449.

Hirth, G., Kohlstedt, D., 2003. Rheology of the upper mantle and the mantle wedge: a view from the experimentalists. In: Eiler, J. (Ed.), Inside the Subduction Factory, Geophys. Monogr. Ser., vol. 138. AGU, Washington, D.C., pp. 83–105.

Hofmeister, A.M., Criss, R.E., 2005. Earth's heat flux revised and linked to chemistry. Tectonophysics 395, 159–177.

Holtzman, B.K., Groebner, N.J., Zimmerman, M.E., Ginsberg, S.B., Kohlstedt, D.L., 2003. Stress-driven melt segregation in partially molten rocks. G3 4, 8607. doi:10.1029/2001GC000258.

Iriyama, J., 1977. Energy balance in the Earth's interior. Tectonophysics 40, 243–249.

Isacks, B.L., Barazangi, M., 1977. Geometry of Benioff zones: lateral segmentation and downwards bending of the subducted lithosphere. In: Talwani, M., Pitman, W.C. (Eds.), Island Arc, Deep Sea Trenches and Back-Arc Basins, Maurice Ewing Series, vol. 1. AGU, Washington, D.C.

Isacks, B., Molnar, P., 1971. Distribution of stresses in the descending lithosphere from a global survey of focal-mechanism solutions of mantle earthquakes. Rev. Geophys. 9, 103–174.

Janle, P., Meissner, R., 1986. Structure and evolution of the terrestrial planets. Surv. Geophys. 8, 107–186.

Jarrard, R.D., 1986. Relations among subduction parameters. Rev. Geophys. 24, 217–284.

Jault, D., Gire, C., Le Mouel, J.J., 1988. Westward drift, core motions and exchanges of angular momentum between core and mantle. Nature 333, 353–356 1988.

Jin, Z.-M., Green, H.G., Zhou, Y., 1994. Melt topology in partially molten mantle peridotite during ductile deformation. Nature 372, 164–167.

Jordan, T.H., 1974. Some comments on tidal drag as a mechanism for driving plate motions. J. Geophys. Res. 79 (14), 2141–2142.

Kanamori, H., 1977. The energy release in great earthquakes. J. Geophys. Res. 82 (20), 2981–2987.

Kane, R.P., Trivedi, N.B., 1990. Decade fluctuations in the rotation rate of the Earth in the last 200 years. Pageoph 132 (4), 771–799.

Karato, S.-I., Riedel, M.R., Yuen, D.A., 2001. Rheological structure and deformation of subducted slabs in the mantle transition zone: implications for mantle circulation and deep earthquakes. Phys. Earth Planet. Inter. 127, 83–108.

Knopoff, L., 1972. Observation and inversion of surface-wave dispersion. Tectonophysics 13 (1–4), 497–519.

Knopoff, L., Leeds, A., 1972. Lithospheric momenta and the deceleration of the Earth. Nature 237 (12), 93–95.

Korenaga, J., Karato, S.-I., 2008. A new analysis of experimental data on olivine rheology. J. Geophys. Res. 113, B02403. doi:10.1029/2007JB005100.

Kornig, H., Muller, G., 1989. Rheological model and interpretation of postglacial uplift. Geophys. J. Int. 98, 243–253.

Kreemer, C., Holt, W.E., Haines, A.J., 2002. The global moment rate distribution within plate boundary zones. Geodyn. Ser. 30, 173–189.

Lallemand, S., Heuret, A., Boutelier, D., 2005. On the relationships between slab dip, back-arc stress, upper plate absolute motion, and crustal nature in subduction zones. Geochem. Geophys. Geosyst. 6, Q09006. doi:10.1029/2005GC000917.

Lambeck, K., 1980. In: Batchelor, G.K., Miles, J.W. (Eds.), The Earth's Variable Rotation: Geophysical Causes and Consequences. Cambridge University Press, Cambridge.

Lay, T., Hernlund, J., Buffet, B.A., 2008. Core–mantle boundary heat flow. Nature Geosci. 1, 25–32.

Lenci, F., Doglioni, C., 2007. On some geometric prism asymmetries. In: Lacombe, O., Lavé, J., Roure, F., Verges, J. (Eds.), Thrust Belts and Foreland Basins: From Fold Kinematics to Hydrocarbon Systems. Frontiers in Earth Sciences. Springer, pp. 41–60.

Le Pichon, X., 1968. Sea-floor spreading and continental drift. J. Geophys. Res. 73 (12), 3661–3697.

Liebske, C., Schmickler, B., Terasaki, H., Poe, B.T., Suzuki, A., Funakoshi, K., Ando, R., Rubie, D.C., 2005. Viscosity of peridotite liquid up to 13 GPa: implications for magma ocean viscosities. Earth Planet. Sci. Lett. 240, 589–604.

Lowrie, W., 2007. Fundamentals of Geophysics. Cambridge University Press.

McCarthy, D.D., Petit, G., 2004, IERS Conventions (2003), IERS Technical Note No.32, Verlag des Bundesamts für Kartographie uns Geodäsie, Frankfurt am Main.

Marcus, S.L., Chao, Y., Dickey, J.O., Gegout, P., 1998. Detection and modeling of nontidal oceanic effects on Earth's rotation rate. Science 281, 1656–1659.

Marone, F., Romanowicz, B., 2007. The depth distribution of azimuthal anisotropy in the continental upper mantle. Nature 447, 198–202. doi:10.1038/nature05742.

Mariotti, G., Doglioni, C., 2000. The dip of the foreland monocline in the Alps and Apennines. Earth Planet. Sci. Lett. 181, 191–202.

Marquart, G., Steinberger, B., Niehuus, K., 2005. On the effect of a low viscosity asthenosphere on the temporal change of the geoid — a challenge for future gravity missions. J. Geodyn. 39, 493–511. doi:10.1016/j.jog.2005.04.006.

Maslov, L.A., 1991. Geodynamics of the Pacific Segment of the Earth. Nauka, Moscow.

McGeary, S., Nur, A., Ben-Avraham, Z., 1985. Special gaps in arc volcanism: the effect of collision or subduction of oceanic plateaus. Tectonophysics 119, 195–221. doi:10.1016/0040-1951(85)90039-3.

Melini, D., Cannelli, V., Piersanti, A., Spada, G., 2008. Post-seismic rebound of a spherical Earth: new insights from the application of the Post-Widder inversion formula. Geophys. J. Int. 174 (4), 672–695.

Milsom, J., 2005. The Vrancea seismic zone and its analogue in the Banda Arc, eastern Indonesia. Tectonophysics 410, 325–336.

Molchan, G., Kronrod, T., Panza, G.F., 1997. Multi-scale seismicity model for seismic risk. BSSA 87 (5), 1220–1229.

Monin, A.S., 1978. On some problems of geophysical fluid dynamics. Proc. Natl. Acad. Sci. U.S.A. 75 (1), 34–39.

Moore, G.W., 1973. Westward tidal lag as the driving force of plate tectonics. Geology 1, 99–100.

Nelson, T.H., Temple, P.G., 1972. Mainstream mantle convection: a geologic analysis of plate motion. AAPG Bull. 56 (2), 226–246.

Oncescu, M.C., Bonjer, K.-P., 1997. A note on the depth recurrence and strain release of large Vrancea earthquakes. Tectonophysics 272, 291–302.

Oncescu, M.C., Trifu, C.-I., 1987. Depth variation of moment tensor principal axes in Vrancea (Romania) seismic region. Ann. Geophys. 5B, 149–154.

Panza, G.F., 1980. Evolution of the Earth's lithosphere. NATO Adv. Stud. Inst. Newcastle, 1979. In: Davies, P.A., Runcorn, S.K. (Eds.), Mechanisms of Continental Drift and Plate Tectonics. Academic Press, pp. 75–87.

Panza, G., Raykova, R.B., Carminati, E., Doglioni, C., 2007. Upper mantle flow in the western Mediterranean. Earth Planet. Sci. Lett. 257, 200–214.

Paquet, P., Dehant, V., Bruyninx, C., 1997. Earth rotation observations and their geophysical implications. Bull. Astron. Belgrade 156, 89–108.

Pardo, M., Comte, D., Monfret, T., 2002. Seismotectonic and stress distribution in the central Chile subduction zone. J. South Am. Earth Sci. 15, 11–22. doi:10.1016/S0895-9811(02)00003-2.

Peccerillo, A., 2005. Plio-Quaternary Volcanism in Italy. Petrology, Geochemistry, Geodynamics. Springer, Heidelberg. 365 pp.

Pérez-Campos, X., Kim, Y., Husker, A., Davis, P.M., Clayton, R.W., Iglesias, A., Pacheco, J.F., Singh, S.K., Manea, V.C., Gurnis, M., 2008. Horizontal subduction and truncation of the Cocos Plate beneath central Mexico. Geophys. Res. Lett. 35, L18303. doi:10.1029/2008GL035127.

Pilger, R.H., 1981. Plate reconstructions, aseismic ridges, and low-angle subduction beneath the Andes. Geol. Soc. Am. Bull. 92, 448–456. doi:10.1130/0016-7606(1981)92-448.

Pollitz, F.F., Buergmann, R., Romanowicz, B., 1998. Viscosity of oceanic asthenosphere inferred from remote triggering of earthquakes. Science 280, 1245–1249.

Press, F., Briggs, P., 1975. Chandler Wobble, earthquakes, rotation and geomagnetic changes. Nature 256, 270–273.

Prigogine, I., Stengers, I., 1984. Order Out of Chaos. Bantam, New York.

Ranalli, G., 1995. Rheology of the Earth. Chapman and Hall, pp. 1–413.

Ranalli, G., 2000. Westward drift of the lithosphere: not a result of rotational drag. Geophys. J. Int. 141, 535–537.

Ray, R., 2001. Tidal friction in the Earth and Ocean, Journées Luxembourgeoises de Géodynamique˙JLG 89th, Nov. 12–14, http://www.ecgs.lu/.

Ray, R.D., Eanes, R.J., Lemoine, F.G., 2001. Constraints on energy dissipation in the earth's body tide from satellite tracking and altimetry. Geophys. J. Int. 144, 471–480.

Raykova, R.B., Panza, G.F., 2006. Surface waves tomography and non-linear inversion in the southeast Carpathians. Phys. Earth Planet. Inter. 157, 164–180.

Reyners, M., Eberhart-Phillips, D., Stuart, G., Nishimura, Y., 2006. Imaging subduction from the trench to 300 km depth beneath the central North Island, New Zealand, with Vp and Vp/Vs. Geophys. J. Int. 165, 565–583. doi:10.1111/j.1365-246X.2006.02897.x.

Ricard, Y., Doglioni, C., Sabadini, R., 1991. Differential rotation between lithosphere and mantle: a consequence of lateral viscosity variations. J. Geophys. Res. 96, 8407–8415.

Rivera, L., Sieh, K., Helmberger, D., Natawidjaja, D., 2002. A comparative study of the Sumatran subduction-zone earthquakes of 1935 and 1984. BSSA 92 (5), 1721–1736.

Romashkova, L.L., 2009. Global-scale analysis of seismic activity prior to 2004 Sumatra-Andaman mega-earthquake. Tectonophysics 470, 329–344. doi:10.1016/j.tecto.2009.02.011.

Ruff, L., Kanamori, H., 1980. Seismicity and the subduction process. Phys. Earth Planet. Inter. 23, 240–252.

Rybach, L., 1976. Radioactive heat production in rocks and its relation to other petrophysical parameters. PAGEOPH 114, 309–317.

Rychert, C.A., Fischer, C.M., Rondenay, S., 2005. A sharp lithosphere–asthenosphere boundary imaged beneath eastern North America. Nature 436, 542–545.

Sacks, I.S., Okada, H., 1974. A comparison of the anelasticity structure beneath western South America and Japan. Phys. Earth Planet. Inter. 9, 211–219. doi:10.1016/0031-9201(74)90139-3.

Sasaki, S., Nakazawa, K., 1986. Metal-silicate fractionation in the growing Earth: energy source for the terrestrial magma ocean. J. Geophys. Res. 91, 9231–9238.

Scalera, G., 2008. Great and old earthquakes against great and old paradigms — paradoxes, historical roots, alternative answers. Adv. Geosci. Adv. Geosci. 14, 41–57.

Scoppola, B., Boccaletti, D., Bevis, M., Carminati, E., Doglioni, C., 2006. The westward drift of the lithosphere: a rotational drag? Bull. Geol. Soc. Am. 118 (1/2), 199–209. doi:10.1130/B25734.1.

Shaw, H.R., Jackson, E.D., 1973. Linear island chains in the Pacific: result of thermal plumes or gravitational anchors? J. Geophys. Res. 78 (35), 8634–8652.

Stein, S., Wysession, M., 2003. Introduction to Seismology, Earthquakes, and Earth Structure. Blackwell Publishing.

Stern, R.J., 2002. Subduction zones. Rev. Geophys. 40, 1012.

Stevenson, D.J., 1994. Weakening under stress. Nature 372, 129–130.

Syracuse, E.M., Abers, G.A., 2006. Global compilation of variations in slab depth beneath arc volcanoes and implications. Geochem. Geophys. Geosyst. 7, Q05017. doi:10.1029/2005GC001045.

Thybo, H., 2006. The heterogeneous upper mantle low velocity zone. Tectonophysics 416, 53–79.

Touma, J., Wisdom, J., 1994. Evolution of the Earth–Moon system. Astron. J. 108 (5), 1943–1961.

Trampert, J., Deschamps, F., Resovsky, J., Yuen, D., 2004. Probabilistic tomography maps chemical heterogeneities throughout the lower mantle. Science 306, 853–856.

Turcotte, D.L., Schubert, G., 2002. Geodynamics, Second ed. Cambridge University press.

Twiss, R.J., Moores, E.M., 1992. Structural Geology. W.H. Freeman and Compan, New York. 531 pp.

Uyeda, S., Kanamori, H., 1979. Back-arc opening and the mode of subduction. J. Geophys. Res. 84 (B3), 1049–1061.

Varga, P., 2006. Temporal variation of geodynamical properties due to tidal friction. J. Geodyn. 41, 140–146.

Please cite this article as: Riguzzi, F., et al., Can Earth's rotation and tidal despinning drive plate tectonics? Tectonophysics (2009), doi:10.1016/j.tecto.2009.06.012

Varga, P., Gambis, D., Bus, Z., Bizouard, C., 2005. The Relation Between the Global Seismicity and the Rotation of the Earth, Observatoire de Paris, Systémes de reference temps-espace UMR8630/CNRS, pp. 115–121.
Vasco, D.W., Johnson, L.R., Marques, O., 2003. Resolution, uncertainty, and whole Earth tomography. J. Geophys. Res. 108. doi:10.1029/2001JB000412.
Vassiliou, M.S., Hager, B.H., Raefsky, A., 1984. The distribution of earthquakes with depth and stress in subducting slabs. J. Geodyn. 1, 11–28.
Verhoogen, J., 1980. Energetics of the Earth, University of California, National Academy of Science.
Vinnik, L., Singh, A., Kiselev, S., Ravi Kumar, M., 2007. Upper mantle beneath foothills of the western Himalaya: subducted lithospheric slab or a keel of the Indian shield? Geophys. J. Int. 171, 1162–1171. doi:10.1111/j.1365-246X.2007.03577.x.
Wang, Q.-L., Chen, Y.-T., Cui, D.-X., Wang, W.-P., Liang, W.-F., 2000. Decadal correlation between crustal deformation and variation in length of day of the Earth. Earth Planets Space 52, 989–992.
Wortel, M.J.R., 1984. Spatial and temporal variations in the Andean subduction zone. J. Geol. Soc. 141 (5), 783–791.
Walter, M.J., Trønes, R.G., 2004. Early Earth differentiation. Earth Planet. Sci. Lett. 225, 253–269.
Wilcock, W.S.D., 2001. Tidal triggering of microearthquakes on the Juan de Fuca Ridge. Geophys. Res. Lett. 28 (20), 3999–4002.
Yoder, C.F., Williams, J.G., Parke, M.E., 1981. Tidal variations of Earth rotation. J. Geophys. Res. 86, 881–891.
Zhang, Y.-S., Tanimoto, T., 1993. High-resolution global upper mantle structure and plate tectonics. J. Geophys. Res. 98 (B6), 9793–9823.
Zschau, J., 1986. Tidal friction in the solid Earth: constraints from the Chandler wobble period. In: Anderson, A.J., et al. (Ed.), Space Geodesy and Geodynamics, pp. 315–344.

Please cite this article as: Riguzzi, F., et al., Can Earth's rotation and tidal despinning drive plate tectonics? Tectonophysics (2009), doi:10.1016/j.tecto.2009.06.012